CONTRIBUTIONS TO THE HYDRAULICS OF FLOW-THROUGH ROCKFILL STRUCTURES

by

Ali Roshanfekr

Submitted in partial fulfilment of the requirements
for the degree of Doctor of Philosophy

at

Dalhousie University
Halifax, Nova Scotia
September 2013

DEDICATION

To my devoted wife, Maliheh,

and my dearest parents, Shahnaz and Hedayatollah,

for their endless love and support.

TABLE OF CONTENTS

LIST OF TABLES vi
LIST OF FIGURES vii
ABSTRACT x
LIST OF ABBREVIATIONS USED xi
ACKNOWLEDGEMENTS xii
CHAPTER 1 INTRODUCTION 1
1.1. Flow-Through Rockfill Structures 1
1.2. Flow Taxonomy 4
1.3. Objectives 5
1.4. Research Overview 6
CHAPTER 2 ASSESSMENT OF POTENTIAL FOR SEEPAGE-INDUCED UNRAVELING FAILURE OF FLOW-THROUGH ROCKFILL DAMS 8
2.1. Abstract 8
2.2. Introduction 8
2.3. Theoretical Background 10
2.4. Geometries Considered and Boundary Conditions Used 19
2.5. Assessment of Magnitude of non-Darcy Effect 24
2.6. Grid Fineness (Nodal Density) Effect 26
2.7. Benefit of Using Specialized FD Molecules 27
2.8. Exit Gradient Magnitude and Direction 32
2.9. Initiation of Motion Threshold (Unraveling Potential) 35
2.10. Summary and Conclusions 41
CHAPTER 3 USE OF INDEX GRADIENTS AND DEFAULT TAILWATER DEPTH AS AIDS TO HYDRAULIC MODELING OF FLOW-THROUGH ROCKFILL DAMS 43
3.1. Abstract 43
3.2. Introduction 44
3.3. Estimating Height of Point of First Emergence 46
3.4. Isolation of Toe (Downstream of y_{exit} Vertical) 49
3.5. Estimating Default Tailwater Depth (h_{TW}) 58
3.6. Summary and Conclusions 69

CHAPTER 4 HYDRAULICS OF FLOW AT THE TOE OF NON-OVERTOPPING ROCKFILL STRUCTURES 70
4.1. Abstract 70
4.2. Introduction 71
4.3. Experimental Setup 73
4.4. Non-Darcy Flow and Exit Height Estimation 76
4.5. Modeling of Water Surface Profile of Seepage-face 79
4.5.1. Prerequisites 79
4.5.2. SVF Water Surface Profile 83
4.5.3. Linkage to Conventional Nodes 88
4.5.4. Linkage to Flux Nodes 91
4.5.5. Role of Roughness 94
4.5.6. Preliminary Results 95
4.5.7. Improved Model Verification 105
4.6. Use of Linear Variation(s) in Depth 107
4.6.1. Depth at Toe 111
4.7. Summary and Conclusions 111
CHAPTER 5 SUMMARY AND CONCLUSIONS 113
5.1. SUMMARY 113
5.2. CONCLUSIONS 114
5.3. FUTURE WORK 116
REFERENCES 118
APPENDIX A - DERIVATION OF THE NON-LINEAR HYDRAULIC CONDUCTIVITY EQUATION 124
A.1. THE RELATIONSHIP BETWEEN EMPIRICAL QUANTITIES: NON-LINEAR HYDRAULIC CONDUCTIVITY APPROACH 124
A.2. DERIVATION OF THE NON-LINEAR HYDRAULIC CONDUCTIVITY PARTIAL DIFFERENTIAL EQUATION 125
APPENDIX B - OBSERVED DATA 128
B.1. OVERVIEW 128
B.2. CHARACTERISTICS OF THE POROUS MEDIA 129
B.2.1. Porosity of the Model Embankments 129
B.2.2. Rock Particles: Dimensions and Shape 131

B.2.3. Grain Size Analysis 136
B.2.4. Hydraulic Mean Radius 137
B.2.5. Specific Gravity 138
B.3. Packed-Column Tests 139
B.4. Studies in the Dalhousie University Hydraulics Laboratory Glass-Walled Flume 141
APPENDIX C - COPYRIGHT PERMISSION LETTERS 146

LIST OF TABLES

Table 2.1. Previous investigations of flow-through rockfill structures. 15

Table 3.1. Values of 'b' for with h_{TW}/h_{us} = zero (24 embankments). 54

Table 3.2. Values of 'b' for with h_{TW}/h_{us} = 0.05 (24 embankments). 54

Table 3.3. Values of 'b' for with h_{TW}/h_{us} = 0.10 (24 embankments). 54

Table 3.4. Geometries of model flow-through dams considered for comparison of i_{DTW} and i_{eff}. 66

Table 3.5. Some experimental details (flume sizes and characteristics of gravel), see also Appendix B. 66

Table 3.6. Inferred C_{path} values and statistics of discharge comparisons. 67

Table 4.1. Some experimental details. 75

Table 4.2. Nature of the seepage-face problem and the parameters involved. 81

Table 4.3. Comparison of observed vs. computed seepage-wedge depths and ending flows (total discharge) for all eight models*. 98

Table 4.4. Effect of porosity on non-Darcy flow coefficient ω in equation [4.2d]. 102

Table 4.5. Exponential decay parameters in equations [4.18a] and [4.18b] for Strickler-based Manning's n calculation (all eight model embankments). 105

Table 4.6. Statistics for limited verification of modeling approach, using incremental discharges. 106

Table 4.7. Accuracy of mono vs. bilinear water surface profiles. 109

LIST OF FIGURES

Figure 1.1. Orthometric view and nomenclature for flow-through rockfill embankments.3

Figure 1.2. Flow taxonomy in open-channel hydraulics. 4

Figure 2.1. Nomenclature for rockfill dam of width B_w with constant flow Q passing through it. 9

Figure 2.2. FD molecule and associated areal coverage. 12

Figure 2.3. Example FD molecules next to impermeable surfaces. 17

Figure 2.4. FD star for nodes adjacent to phreatic surface or seepage-face. 18

Figure 2.5. Geometries used in parametric study; downstream slopes are (by row) 1V: mH. With 1V:1H upstream slope. 23

Figure 2.6. Convergence (grid relaxation) of model dam with 1800 nodes, using change in head at centrally-located interior node as indicator. 25

Figure 2.7. Ratios of hydraulic heads for two pairs of cases. 26

Figure 2.8. Nodal density effect on exit flow-line patterns; equation [2.12a] for special FD molecule used where needed. $H/B_C = 2.0$ and slope 1V:2H. 28

Figure 2.9. Example of integer slope with regular drop. 28

Figure 2.10. Nodal density effect on exit flow-lines for case of no special FD molecules at all; $H/B_C = 2.0$ and slope = 1V:2H. 30

Figure 2.11. Illustration of benefit of selective use of half-nodes on downstream face. 31

Figure 2.12. Minimal effect of using specialty node on direction of exit hydraulic gradient for $\Delta = 1$, $H/B_C = 2.0$ and slope = 1V:2H. 32

Figure 2.13. Mesh-size effect on exit hydraulic gradients with use of specialty node. Case of $H/B_C = 2.0$ and 1V:2H ($\theta = 26.6$ º). 33

Figure 2.14. Mesh size effect on exit hydraulic gradients, with no specialty node used. Case of $H/B_C = 2.0$ and 1V:2H. 34

Figure 2.15. Particle position and seepage force direction in the downstream face (adapted from Hansen *et al.* 2005). 36

Figure 2.16. Factor of safety as a function of exit gradient for dams with $H/B_C = 0.5$, for three velocities at toe of seepage-face. Particle diameter = 0.1 m. (See also Figure 2.19 for selected low-FS endpoints of 3 m/s cases.) 38

Figure 2.17. Factor of safety as a function of exit gradient for dams with $H/B_C = 0.5$, for three velocities at toe of seepage-face. Particle diameter = 0.3 m. (See also Figure 2.19 for selected low-FS endpoints of 3 m/s cases.)..... 39

Figure 2.18. Factor of safety as a function of exit gradient for dams in parametric study with $H/B_C = 0.5$, for three velocities at toe of seepage-face. Particle diameter = 0.6 m. (See also Figure 2.19 for selected low-FS endpoints of 3 m/s cases.)..... 40

Figure 2.19. Worst case factors of safety as a function of exit gradient for dams in parametric study with $H/B_C = 0.5$ (for three particle diameters and U = 3 m/s). 40

Figure 3.1. Nomenclature for rockfill dam of width B_w with constant flow Q passing through it. 44

Figure 3.2. Illustration of concept of angle of emergent flow-field, θ_{ff} 48

Figure 3.3. Schematic view of the parameters used for toe isolation in y_{exit} vertical. 51

Figure 3.4. Comparison and correlation between the calculated and observed 'b' values. 55

Figure 3.5. Effect of tailwater on the head variation in the y_{exit} vertical for isolation of the toe. 55

Figure 3.6. Effect of different slopes on the head variation in y_{exit} vertical for isolation of the toe. 56

Figure 3.7. Procedure for isolating the toe. 58

Figure 3.8. Definitions relating $h_{svft}\cos^2\theta$ to y_{exit}. 60

Figure 3.9. Behavior of tailwater with increasing flow. 62

Figure 3.10. Comparison of discharges. 68

Figure 3.11. Procedure for calculating default tailwater depth. 68

Figure 4.1. Nomenclature for non-overtopping rockfill embankments with constant flow (discharge Q passing through it). 71

Figure 4.2. Flume in the hydraulics laboratory of Dalhousie University and the experimental setup. 73

Figure 4.3. Representative water surface profile curvatures for three seepage-faces. 74

Figure 4.4. Illustration of concept of angle of emergent flow-field, θ_{ff} (adapted from Hansen *et al.* 2005). 79

Figure 4.5. Four point body-centered FD molecule used for modeling of hydraulic head inside model embankments. 83

Figure 4.6. Seepage-face in the toe of a rockfill embankment. 85

Figure 4.7. Conventional surficial nodes in toe of rockfill embankments (vector i_c is actually centered on node C)..... 89

Figure 4.8. Linkage of NLHC hydraulic head model to SVF algorithm via conventional head-based nodes..... 90

Figure 4.9. Flux nodes in toe of rockfill embankments. 92

Figure 4.10. Linkage of NLHC hydraulic head model to SVF algorithm via flux nodes. 93

Figure 4.11. Convergence study of NLHC FD scheme for full grid relaxation of Model # 6..... 96

Figure 4.12. Critical depth distance calculation from y_{exit} using Chow (1959) and Sharp and James (1963) for Models 1 to 6 (Q = 3.82 L/s)..... 97

Figure 4.13. Observed vs. computed local seepage-wedge depths along b_{ed} for all eight models (see Appendix B with respect to 'depth')..... 99

Figure 4.14. Manning's n variation in the seepage-face along ℓ_{SF} for all eight models. Exponential decay curves are Strickler based..... 104

Figure 4.15. Results of seepage-face flow wedge modeling..... 106

Figure 4.16. Linearized seepage-face depth variation using two straight lines. 108

Figure 4.17. Two straight line linearized seepage-face depths compared with seepage-face depth pattern calculated using SVF algorithm for Models 1 to 6, along b_{ed}... 110

ABSTRACT

Non-overflow flow-through rockfill structures are river engineering elements used to attenuate and delay inflow hydrographs. They represent expedient places to deposit rather enormous quantities of waste rock at mountainous mine sites. Their application has become so common that matters of safety regarding their design have been laid out in Section 8.5 of the Canadian Dam Safety Guidelines (CDA 2007). The research described herein was directed at investigating the different aspects of the hydraulics of these flow-through rockfill structures.

In order to assess the potential for an unraveling failure of flow-through rockfill dams, a systematic study of the hydraulic design of these structures was conducted and the non-linear nature of flow through these structures was dealt with using a *p*-LaPlacian-like partial differential equation. Subsequently, factors of safety against this type of failure are presented for a range of downstream slopes, thus showing the unsafe combinations of embankment slope and particle diameter.

Three different index gradients within the toe of such structures were investigated. In this regard, the gradient most suitable for independently computing the height of the point of first flow emergence on the downstream face is examined and a method for independently computing the variation in hydraulic head within that vertical (which allows for the toe of the structure to be isolated) is presented. An additional gradient that allows for the independent estimation of the default tailwater depth is proposed.

In order to provide better tools to assess the behavior of these embankments at the toe, laboratory and analytical studies were undertaken. In this regard, the hydraulics associated with the zone of the downstream toe were studied. The depth variation of the seepage-face was computationally modeled, and two approaches for solving the spatially varied flow (SVF) condition problem within the toe region undertaken. The results show that a dual linear variation in depth can be used to good accuracy, without inducing any unrealistic exit gradients in the zone of primary concern with respect to unraveling.

It is hoped that these techniques and computational tools provided herein will aid in facilitating the design and assessment of these flow-through rockfill structures.

LIST OF ABBREVIATIONS USED

1-D	One-Dimensional
2-D	Two-Dimensional
3-D	Three-Dimensional
BIEM	Boundary Integral-Equations Method
CDA	Canadian Dam Association
EPL	Equipotential Line
FEM	Finite Element Method
FD	Finite Difference
Fr	Froude Number
FS	Factor of Safety
FV	Finite Volume
GVF	Gradually-Varied Flow
HJ	Hydraulic Jump
IoM	Initiation of Motion
NLHC	Non-Linear Hydraulic Conductivity
ODE	Ordinary Differential Equation
PCL	Parkin *et al.* (1966) and Curtis and Lawson (1967)
PDE	Partial Differential Equation
Re	Reynolds Number
SVF	Spatially-Varied Flow
wsp	water surface profile

ACKNOWLEDGEMENTS

I would like to thank and acknowledge my supervisor, Dr. David Hansen, for all of his support and guidance throughout this research. I have learned a lot from his vast knowledge, insightful questions, ideas, and thoughts. I could not have wished for a better supervisor. I would also like to take this opportunity to thank Phoebe Hansen for all her kindness and hospitality.

I would like to thank my committee members, Dr. Mysore Satish and Dr. Guy Kember, for their inputs and suggestions and guidance. I thank Dr. James Kells for acting as my external examiner and for his valuable feedback.

I am grateful to Blair Nickerson for helping with the experimental setup in the Hydraulics lab. Without his help it would not have been possible for me to complete my experiments in time. I would also like to thank the faculty and staff of the Department of Civil and Resource Engineering which have helped me in many ways. A special thanks to all of my friends at Dalhousie University for all of their support.

Finally, I would like to express my deepest gratitude to my wife, Maliheh and my appreciation to my family and in-laws, Shahnaz, Hedayatollah, Meghdad, Mohammad, Malak, Marzieh, Sina and Zahra, for encouraging me from kilometers away.

I would also like to remember my father-in-law Mohammad Ali whose memory gave me and my wife strength along the way.

CHAPTER 1 INTRODUCTION

1.1. FLOW-THROUGH ROCKFILL STRUCTURES

The focus of this thesis is on the hydraulics of flow-through rockfill structures; it is therefore necessary to begin with the definition of rockfill hydraulics. A rockfill may be defined as a coarse-grained and free-draining material composed of large, loosely-placed particles (Parkin 1991). The above definition might vary from author to author, based on different standpoints and technical evolutions. From a hydraulic point of view, very small particles cannot be considered part of a rockfill (Martin 1991). In regards to friction head losses (open-channel flow), stability and permeability, the behavior of these particles under flow action is a subject belonging to classical hydraulics and soil mechanics, and does not represent the specific behavior of rockfills. Martins (1991) defines rockfill hydraulics as the "study of the interaction between flow and irregular, loose particles, with a characteristic dimension larger than 1 cm". Naturally, rockfill hydraulics has an interface with the hydraulics of porous media with smaller particles.

Flow-through rockfill structures are river engineering elements that are often used to attenuate and delay inflow hydrographs. They also represent expedient places to deposit rather enormous quantities of waste rock at mountainous mine sites. These embankments are not barrages in the ordinary sense but are rather similar to hydraulic structures (spillways) constructed out of very coarse porous media. They have become sufficiently common that matters of safety regarding their design have been laid out in Section 8.5 of the Canadian Dam Safety Guidelines (CDA 2007).

The quantity of flow passing through these 'structures' is much greater than that of any true dam and consequently, there are two different kinds of failure corresponding to these structures: massive failure and unraveling failure. In order to analyze the potential for a massive failure, a limit-equilibrium stability analysis (*e.g.* Bishop's Method) can be used (Garga *et al.* 1995). For unraveling failure on the other hand a moment-based analysis of the stability of individual particle(s) under the seepage-face can be performed (Hansen *et al.* 2005). The most common mechanism of failure for

these kinds of structures is often a progressive 'unraveling' of the downstream toe (Wilkins 1956, Parkin *et al.* 1966). This phenomenon process is partly caused by the large amounts of seepage exiting under high hydraulic gradients. Unraveling failure results from the initiation-of-motion (IoM) of one or perhaps a few stone particles, which in turn impacts particles further down the seepage-face (Figure 1.1), destabilizing them into motion, and so on (Wilkins 1956, Parkin 1963, Gerodetti 1981). This implied 'domino effect' may be overstated because the simultaneous movement of many particles at the toe may be just as disastrous (*i.e.* downstream limit of B_d, see Figure 1.1), especially since there may be nothing to prevent the last 'row' of particles from moving downstream. The variation and the pattern of the hydraulic head within the entire structure is of interest because the rapidity of the variation in this head affects the strength of the exit gradient. The flow or seepage in question is a non-Darcy flow of the high-Reynolds-number type. Figure 1.1 shows an orthometric view and the nomenclatures used in this study for a flow-through rockfill embankment.

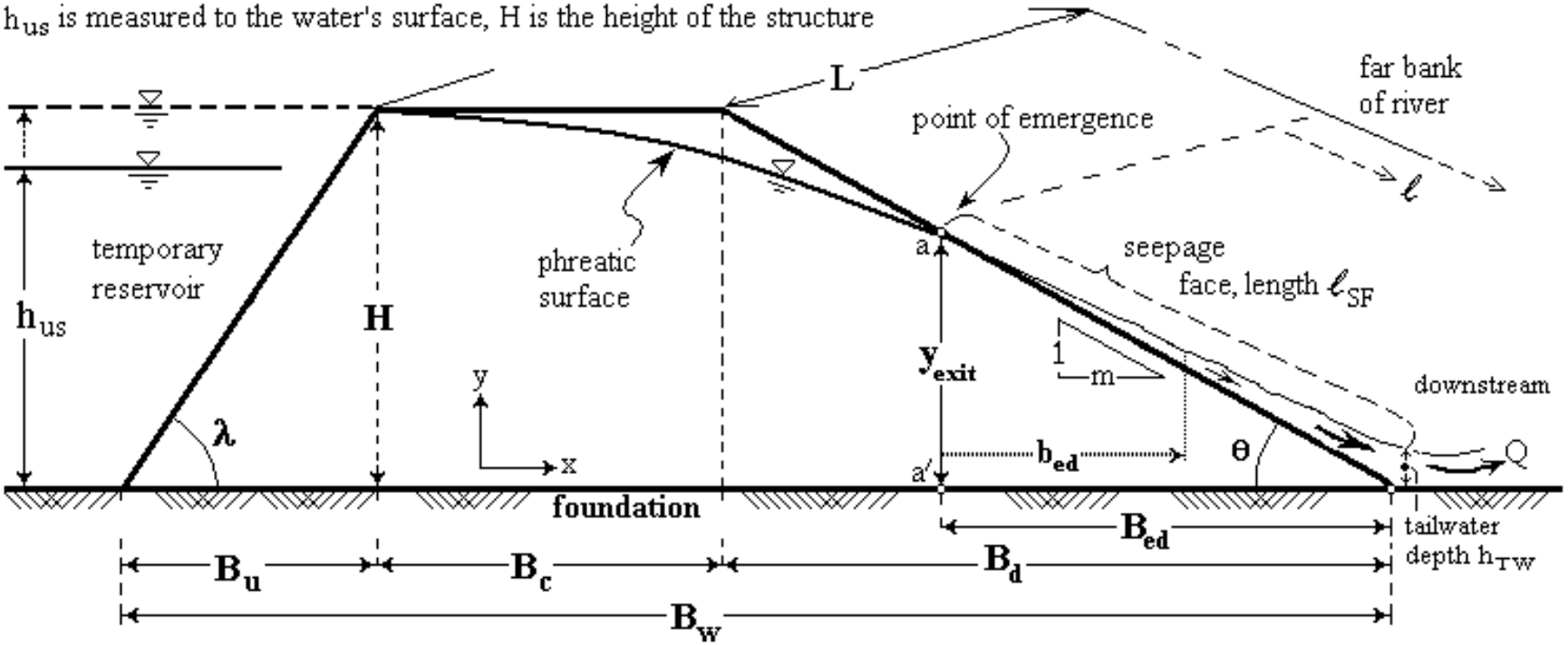

Figure 1.1. Orthometric view and nomenclature for flow-through rockfill embankments.

1.2. FLOW TAXONOMY

It is known that flow through porous media is analogous to flow in open-channels and can be described using open-channel flow equations if the right parameters are used (Bari and Hansen 2002). In order to study rockfill hydraulics, understanding the classification and nature of flow will result in a better understanding of the behavior of the flow within rockfill structures. Figure 1.2 shows the flow classification and the open-channel flow taxonomy.

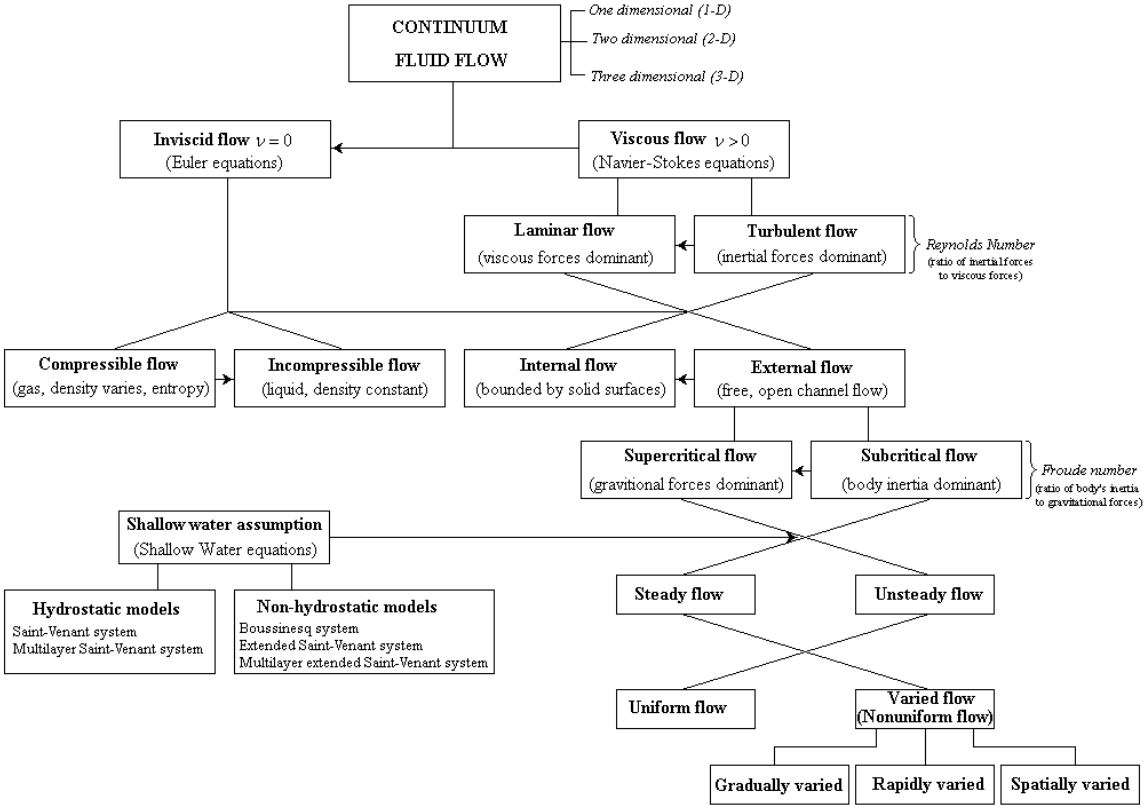

Figure 1.2. Flow taxonomy in open-channel hydraulics.

Due to the turbulent nature and high flow rate within these structures, the above flow taxonomy can also be adapted to rockfill structures (Freeze and Cherry 1979). For example in flow-through rockfill structures, the phreatic surface can be described by a gradually-varied flow equation (Harr 1962, Dake 1972, Sturm 2001) and the seepage-face is described by a spatially-varied flow equation (Sharp and James 1963, Hansen 1992, Hansen and Roshanfekr 2012b).

1.3. OBJECTIVES

Various studies have covered different aspects of the safety and design of flow-through rockfill structures, but it appears that little attention has been paid to simplifying the design of the internal and downstream face hydraulics of these barrages. The main purpose of this thesis is therefore to study the hydraulics of flow-through rockfill embankments and to give additional guidance on the safety and design of these structures.

The research described herein aims to investigate and study the hydraulics, 'seepage' characteristics[1] and safety of rockfill embankments, as well as to quantify their resistance to hydraulically-induced deterioration. This will concern both the flow inside and 'outside' of the structure. In the latter case, the downstream toe of the structure poses interesting challenges. The detailed study of the sediment effect, flow in the river reach and of the turbulence/eddies around these structures however is not within the scope of this research. In this research six main aspects were investigated:

1) The variation and pattern of the hydraulic head within the entire structure. In order for an accurate and efficient head determination, two non-linear finite-difference (FD) techniques for steady-flow analysis were compared with one another as well as to the ordinary Darcian case, and recommendations made. The relative intensity of the non-linear effect were also quantified using the preferred numerical modeling technique.

2) The parametric investigation of the strength and spatial variations in the surficial exit gradient directly under the seepage-face. Outcomes were used to demonstrate how a particle-based Factor of Safety (FS) varies according to hydraulic conditions, down to the toe of a given structure with a given geometry.

[1] High velocity flows through porous media(s) are not generally thought of as 'seepage' even though engineering literature on it sometimes appears in volumes that also deal with ordinary seepage.

3) The effects of grid density on smoothness in exit-flowline patterns and the marginal benefits of using specialized finite-difference molecules (two ancillary contributions).

4) The use of representative hydraulic gradients in the context of the hydraulics of the toe. In this regard three different gradients were studied:

   a. The gradient most useful in independently computing the height of the point of first emergence relative to the foundation.

   b. The gradient appropriate to independently computing the variations in the hydraulic head within the point of first flow emergence vertical for isolating the toe.

   c. The gradient that will allow the independent estimation of the default tailwater depth.

5) The modeling of the seepage-face over the toe of these structures; specifically, the spatial rate of change in depth ($dd/d\ell$) and discharge ($dQ/d\ell$), and the spatial variations in hydraulic resistance.

6) The simplification of the downstream boundary conditions of these structures.

1.4. RESEARCH OVERVIEW

This thesis consists of five chapters and references, including three papers, either published or under second review for publication, and appendices. The present chapter gives an overview of the overall project, and an introduction to the main topics included in the subsequent chapters. Chapters Two to Four represent journal papers, each consisting of an introduction, a literature review, a main body and summary/conclusions. The main body of each paper explains the experimental investigations, the results obtained from the models, and the semi-empirical equations developed to predict the behavior of flow-through rockfill embankments. Chapter Two presents a *p*-LaPlacian-like equation and estimates the factor of safety within the flow-through rockfill

structures. In Chapter Three, the use of three index gradients within the toe of rockfill embankments is presented. In this regard, the applicability of the flow-field angle theory is verified. In Chapter Four, the hydraulics of flow within the toe of the rockfill embankments is presented. Chapter Five includes the summary, conclusions, and recommendations for future work. A complete list of references, followed by appendices showing derivations, observations and some supplementary data conclude this thesis.

CHAPTER 2 ASSESSMENT OF POTENTIAL FOR SEEPAGE-INDUCED UNRAVELING FAILURE OF FLOW-THROUGH ROCKFILL DAMS[1]

2.1. ABSTRACT

A purely numerical parametric study of 24 flow-through rockfill dam geometries was conducted. The non-linear nature of the *p*-LaPlacian-like partial differential equation was dealt with using a finite-difference scheme which directly incorporated the exponent of a power law that replaced Darcy's Law. Convergence, use of specialty nodes, nodal density, and boundary condition effects were quantitatively investigated. The flow-field angle of the toe was found to be a useful starting point in studying the potential for unraveling failure. Factors of safety (FS) against this type of failure are presented for a range of downstream slopes, thus showing which combinations of slope and particle diameter are unsafe. It is shown that the FS tends to drop below unity under the seepage-face primarily because of the strength of the exit gradient near the toe of the structure, and secondarily because of the overflow velocity. It is hoped that the techniques and results presented will facilitate the design and assessment of flow-through rockfill structures.

Keywords: seepage modeling, coarse rockfill, unraveling failure, initiation of motion, flow-through embankments.

2.2. INTRODUCTION

Flow-through rockfill dams and drains have various physical manifestations. As the former, they can serve to attenuate and delay inflow hydrographs; in the latter, they

---

[1] With Permission from ASCE (see Appendix C).
Hansen D., and Roshanfekr A. 2012a. Assessment of potential for seepage-induced unraveling failure of flow-through rockfill dams. ASCE International Journal of Geomechanics, 12(5):560-573.
Note: Numerical modeling works presented in this chapter were carried out by the second author.

may simply represent expedient places to deposit rather enormous quantities of waste rock at mountainous mine sites. These embankments are not barrages in the ordinary sense, acting more as hydraulic structures (spillways) constructed out of very coarse porous media. They have become sufficiently common that matters of safety to be considered in their design are laid out in Section 8.5 of the Canadian Dam Safety Guidelines (CDA 2007). They are embankments only in a loose sense because the quantity of water passing through them is far larger than for any true dam, and the mechanism of failure is most commonly a progressive erosion or unraveling of the downstream toe (Wilkins 1956, Parkin *et al.* 1966) rather than a pseudo-rotational failure. This process is due to the large amount of seepage that exits under relatively high hydraulic gradients, although deep-seated failure is also possible (Garga *et al.* 1995).

The idea of unraveling failure is that the initiation-of-motion (IoM) of a few stones results in impacts on particles further down the seepage-face (Figure 2.1), destabilizing them into motion, and so on (Wilkins 1963, Gerodetti 1981). The implied domino effect may be overstated because the simultaneous movement of many particles at the terminus of the toe may be at least as disastrous (*i.e.* downstream limit of B_d in Figure 2.1), especially since there may be nothing to prevent this last 'row' of particles from moving downstream. In any case, the toe of such structures (that above B_{ed}) is the primary zone of engineering concern (Hansen *et al.* 2005).

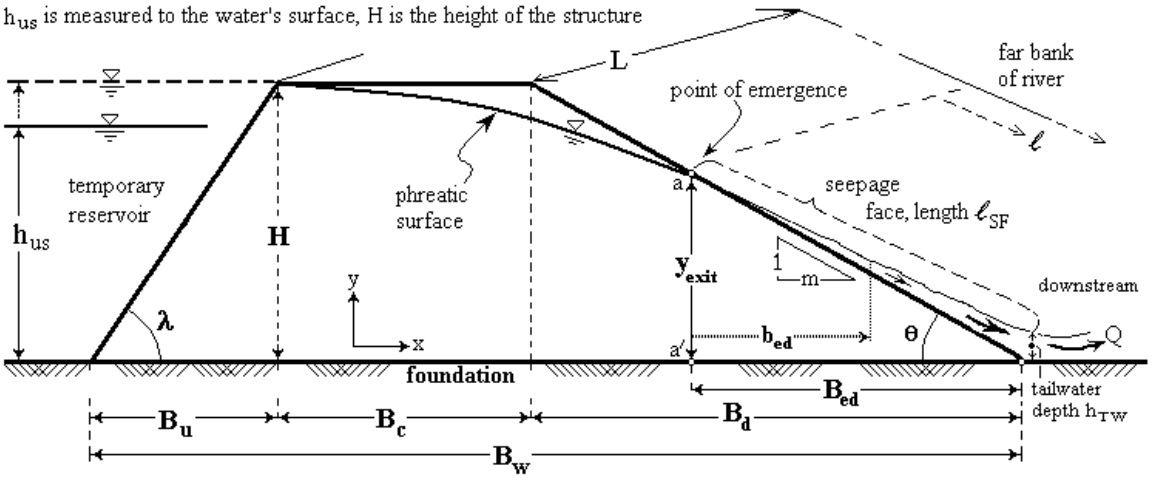

Figure 2.1. Nomenclature for rockfill dam of width B_w with constant flow Q passing through it.

The variation in and pattern of hydraulic head[1] within the entire structure is of interest because the rapidity of the variation in this head affects the strength of the exit gradient. The flow or seepage in question is non-Darcy flow of the high-Reynolds-number type. In the interests of accurate and efficient head determination, two existing non-linear finite-difference (FD) techniques for steady-flow analysis are compared to each other and to the ordinary Darcian case, and recommendations are made. The relative intensity of the non-linear effect is quantified using the preferred numerical modeling technique.

The most important outcome presented herein is of a parametric investigation of the strength and spatial variation in the surficial exit gradient that is directly under the seepage-face. It is used to show how a particle-based Factor of Safety (FS) varies according to hydraulic conditions, down to the toe of a given structure with a given geometry. Finally, two ancillary contributions are made: the outcomes of studies of the effect of grid density on smoothness in exit-flowline patterns and the marginal benefit accrued by using specialized finite-difference molecules. It is hoped that these various numerical tools and computational aids will facilitate the efficient assessment and design of flow-through rockfill structures, as a particular class of geo-hydraulic structure.

2.3. THEORETICAL BACKGROUND

The ability to determine the internal pattern of, or spatial variation in, the hydraulic head for a given set of external boundary conditions is fundamental to the analysis of flow-through rockfill structures. Through a parametric study of a range of geometries, knowledge of this pattern was used in three ways (described in the following sections):

(i) to compare outcomes from two different FD models, **(ii)** to assess the degree of 'non-Darcy-ness' *via* comparison with head patterns found for ordinary (Darcian) seepage

[1] $h = z + p/\gamma$, sometimes called piezometric head, often called total head (see complete review of the semantics in Hansen 2003). The scalar of interest herein is h.

scenarios, and **(iii)** to study subtleties in the exit-face gradients and associated flow-lines, shown to dominate unraveling potential by Hansen *et al.* (2005).

Apart from the choice of numerical method (FD, FEM, FV, or BIEM) there are two primary methods for modeling high-Reynolds-number non-Darcy flows, if the widely-used FD method is selected[1]. Parkin *et al.* (1966) and Curtis and Lawson (1967) did the seminal work for this class of boundary-value problem. A detailed derivation of their expressions (referred to herein as the PCL expressions) with corrections to the original work, can be found in Hansen (1992). The PCL partial differential equation is:

$$\left[\left(\frac{\partial h}{\partial x}\right)^2+\left(\frac{\partial h}{\partial y}\right)^2\right]\left(\frac{\partial^2 h}{\partial x^2}+\frac{\partial^2 h}{\partial y^2}\right)+\left(N'-1\right)\left[\left(\frac{\partial h}{\partial x}\right)^2\frac{\partial^2 h}{\partial x^2}+2\frac{\partial h}{\partial x}\frac{\partial h}{\partial y}\frac{\partial^2 h}{\partial x\partial y}+\left(\frac{\partial h}{\partial y}\right)^2\frac{\partial^2 h}{\partial y^2}\right]=0 \quad [2.1]$$

Equations of the form of equation [2.1] are often referred to as *p*-LaPlacian partial differential equations (*cf.* Vazquez 2007). The associated 9-point PCL FD form is (*cf.* Figure 2.2):

$$h_C = T_1\left(h_1+h_3+h_5+h_7\right)+T_2\cdot T_3 \quad [2.2a]$$

where:

$$T_1=\frac{1}{2\left(N'+1\right)} \quad [2.2b]$$

$$T_2=\frac{\left(N'-1\right)}{2\left(N'+1\right)} \quad [2.2c]$$

$$T_3=\left[(h_1+h_5)(h_1-h_5)^2+0.5(h_1-h_5)(h_3-h_7)(h_2+h_6-h_4-h_8)+(h_3+h_7)(h_3-h_7)^2\right] /\left[(h_1-h_5)^2+(h_3-h_7)^2\right] \quad [2.2d]$$

As expected, setting $N^{/} = 1.0$ (= 1/N, see equation [2.5]) causes the PCL expressions to revert to the familiar expressions used to model 2-D Darcian flow through isotropic homogeneous media (*e.g.* Freeze and Cherry 1979):

---

[1] Spreadsheets have been shown by a number of investigators, to be a highly efficient way to perform the 2-D steady-flow analysis in question (*e.g.* Kleiner 1985, Olsthoorn 1985, Townsend *et al.* 1991).

$$\frac{\partial^2 h}{\partial x^2} + \frac{\partial^2 h}{\partial y^2} = 0 \qquad [2.3]$$

$$h_C = \frac{1}{4}\left(h_1 + h_3 + h_5 + h_7\right) \qquad [2.4]$$

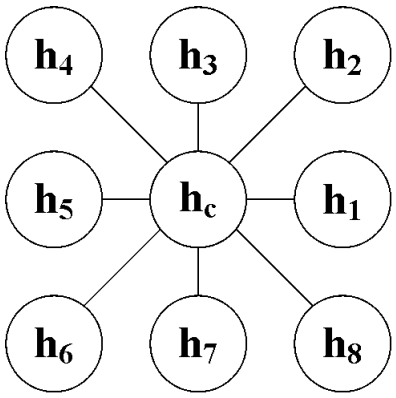

a) 'molecule' style schematic of nine-point scheme.

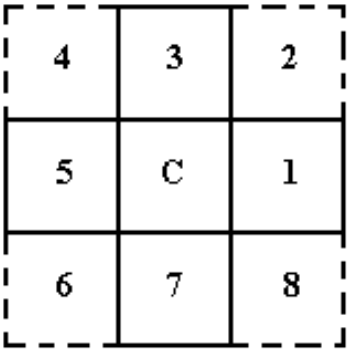

b) corresponding body-centered coverage.

Figure 2.2. FD molecule and associated areal coverage.

Townsend *et al.* (1991) compared experimentally measured heads with heads modeled using equation [2.2], and obtained good results. However, a disadvantage of the PCL FD expression is that it is only good for internal nodes[1]. Another way of handling this class of steady-flow problem has been described by Kells (1995). It represents an adaptation of a modification to Darcy's Law suggested by Cedergren (1989). One way to make Darcy's linear law into a non-linear law is simply to use a non-linear hydraulic

[1] Neither the Australian researchers nor Townsend *et al.* 1991 presented any non-Darcy expressions for non-internal nodes, the derivation of which may be intractable, given the complexity of the simple internal-node case.

conductivity (NLHC). It can be readily shown that if this non-linearity is controlled by the local hydraulic gradient, outcomes are identical to the non-linear (power function) version, for simple cases. One non-linear power function used for non-Darcy flow (Parkin *et al.* 1966) is:

$$i = \alpha V^N \qquad [2.5]$$

where:

α = coefficient,
N= exponent with value between 1 (laminar flow) and 2 (fully turbulent flow),
i= hydraulic gradient (dimensionless),
V= bulk velocity (L/T).

Darcy's Law may be stated as $V = K \cdot i$. The apparent hydraulic conductivity (K) is accounted for using (see Appendix A):

$$K = \omega i^{\psi} \qquad [2.6]$$

then from equation [2.5] it follows that:

$$\omega = \left(\frac{1}{\alpha}\right)^{\frac{1}{N}} \qquad [2.7]$$

and that:

$$\psi = \frac{1}{N} - 1 \qquad [2.8]$$

As a matter of fundamental fluid mechanics (and that not restricted to flow through porous media) it is worth noting that fully-developed turbulence (FDT) is associated with N = 2. This implies that ψ = -0.5 for FDT, from equation [2.8].

Some researchers have used a gradient-dependent hydraulic conductivity (*e.g.* Cedergren 1989, Kells 1995) for high-Reynolds-number flows, and this normally necessitates a separate but head-linked matrix or grid in which the hydraulic conductivity is updated iteratively. However, if equation [2.5] is incorporated into the continuity equation, the following expression results (referred to herein as the NLHC expression, the derivation of this *p*-LaPlacian-like PDE can be found in Appendix A):

$$\left|\frac{\partial h}{\partial x}\right|^{\psi} \frac{\partial^2 h}{\partial x^2} + \left|\frac{\partial h}{\partial y}\right|^{\psi} \frac{\partial^2 h}{\partial y^2} = 0 \qquad [2.9]$$

Equation [2.9] is a specific simplification of equation [2.1]. In the development of equation [2.9] it is assumed that the hydraulic conductivity is a function of the magnitude of the gradient in each orthogonal direction, not the magnitude of the hydraulic gradient as a vector, as in equation [2.1] (Curtis and Lawson 1967, Kells 1995). Table 2.1 summarizes prior numerical work on steady non-linear flow through rockfill banks and embankments.

Temperature and heat conduction represent direct analogues of hydraulic head and seepage. Various investigators have used the idea of non-linear heat conduction and have come up with expressions similar to equation [2.9]. Polyanin and Zaitsev (2004) classified heat flow problems as being governed by linear and non-linear PDE's, with the non-linear problems having either a power-law non-linearity (as above) or an exponential non-linearity. Gao and Li (1996) successfully examined non-linear thermal conduction in granular composite materials using a conductivity equation of the form $K=a+bi^2$ (where a and b are constants). Tanigawa *et al.* (1996) studied transient heat conduction and thermal stress problems in a non-homogeneous plate with temperature-dependent material properties, also with good success.

Table 2.1. Previous investigations of flow-through rockfill structures.

Investigator(s)	**No. of Reported Dam Geometries, 2-D Shape, and Flow Condition(s)**	**Numerical Method**	**Notes**
Curtis and Lawson (1967)	one, long rectangular, partial overflows	finite-difference	no sloping seepage-face
Volker (1969)	one, trapezoidal, h≈¾H non-overflowing	finite element	heads modeled with and without internal wall[1]
Parkin (1971)	one, trapezoidal, h=H non-overflowing	finite element[1]	one-third of downstream side submerged by imposed tailwater
Townsend *et al*. (1991)	one, trapezoidal, h=H non-overflowing	finite-difference	heads modeled with and without impermeable facing[2]
Kells (1995)	one, long rectangular, complete overflow	finite element	no sloping seepage-face; full SVF analysis of increasing and decreasing dQ/dx (over long crest)[3]

1. Phreatic surface found automatically. Some seepage-face flow but no details on its modeling.
2. Seepage-face present, modeled as a triangular overflow (as herein). Phreatic surface independently determined and modeled.
3. With some of the behavior being opposite to the seepage-face problem presented herein.

Jardin *et al.* (2008) studied 1-D diffusion problems at temperatures that necessitated a gradient-dependent diffusion coefficient. The work was done in polar coordinates and used $K = a(|i| - i_{crit})^{0.5}$ plus a constant to describe the gradient-dependent conduction component of this coefficient. The magnitude of the gradient was taken to be in the orthogonal directions in said study. Several investigators have used a temperature dependent thermal conductivity (*e.g.* Munier *et al.* 1981, Budd and Collins 1998, DeLillo *et al.* 2006) and in doing so some used the absolute value of the temperature within a non-linear power-law heat equation (*e.g*. Souplet and Weissler 2003, Vazquez 2007). The range of the ψ exponent in equations of the form of [2.9] for which some solution exists is $-1 < \psi$ (or p-2) $< +\infty$ (where p is the power constant in the *p*-LaPlacian PDE, Esteban *et al.* 1988). This range contains $\psi = -0.5$. In principle, there is no difficulty in applying finite-difference methods to such non-linear systems but the resulting FD equation also becomes non-linear and can be difficult to solve (Özisik 1993 and Smith 1978).

Various finite-difference approximations or schemes are available for non-linear problems. These include the lagging of scalar-dependent properties by one time step, the use of three-time-level finite-differentiation, and various linearization procedures. A simple FD scheme may be developed using central differences in order to solve equation [2.9] based on only the orthogonal neighbors of h_C (*i.e.* a scheme in which the corner locations in Figure 2.2 are omitted). Estimating the gradients and gradients-of-gradients in equation [2.9] as follows:

$$\left|\frac{h_5 - h_1}{2\Delta x}\right|^{\psi} \frac{h_1 - 2h_C + h_5}{\Delta x^2} + \left|\frac{h_3 - h_7}{2\Delta y}\right|^{\psi} \frac{h_3 - 2h_C + h_7}{\Delta y^2} = 0 \qquad [2.10a]$$

and assuming that the nodes in the grid are of equal size ($\Delta x = \Delta y$, Δ herein),

$$|h_5 - h_1|^{\psi}(h_1 - 2h_C + h_5) + |h_3 - h_7|^{\psi}(h_3 - 2h_C + h_7) = 0 \qquad [2.10b]$$

the following expression arises:

$$h_C = \frac{h_1|h_5 - h_1|^{\psi} + h_3|h_3 - h_7|^{\psi} + h_5|h_5 - h_1|^{\psi} + h_7|h_3 - h_7|^{\psi}}{2|h_5 - h_1|^{\psi} + 2|h_3 - h_7|^{\psi}} \qquad [2.10c]$$

The merits of the NLHC approach are that: **(i)** both theoretical literature and experimental data exist on the empirical quantities α and N and hence ω and ψ (*e.g.* flow quantity Wilkins 1956, phreatic surface Basak 1977), **(ii)** the quantities α and N can be formally determined from the two coefficients used in an alternate non-linear form commonly adopted by chemical and mechanical engineers– a zero intercept 2nd order polynomial – the so-called Forchheimer equation or form (George and Hansen 1992), and **(iii)** it can be readily adapted to the various kinds of non-internal nodes that are needed in most civil engineering applications. Such adaptations are needed at irregular boundaries (of both the impermeable and phreatic-surface type) and in order to carefully follow upstream and downstream slopes, especially those that represent non-integer rates of decline for the slope of interest (*e.g.* not 1V:2H, 1V:3H, etc.). Furthermore, the lower two-thirds of the downstream slope will usually have the complication of being under the seepage-face, in which case the imposed bounding condition is the sum of the exterior head implied by the thickness of the seepage-face (which increases down the face) and

the elevation head (which decreases down the face). Finally, **(iv)** a 3-D version of equation [2.10] can be readily written, if desired.

Expressions for the various special cases will now be presented. Figure 2.3 shows two cases of contiguous proximity to impermeable boundaries.

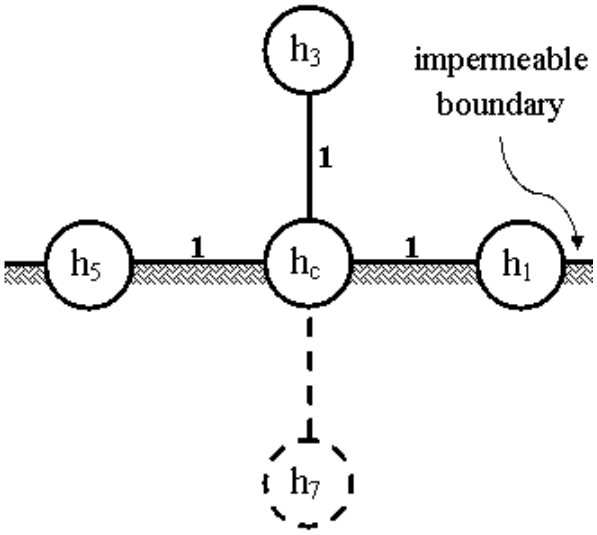

a) node adjacent to impermeable surface.

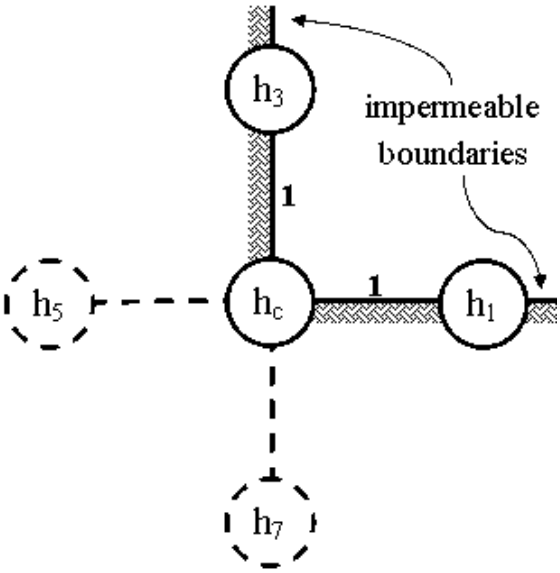

b) node at intersection of impermeable surfaces[1].

Figure 2.3. Example FD molecules next to impermeable surfaces.

[1] The corner FD molecule shown in Figure 2.3b was not needed in this research because this 'corner case' did not exist for the 2-D cases studied herein.

The expression used herein for cases/positions associated with Figure 2.3a is:

$$h_C = \frac{h_1|h_5 - h_1|^{\psi} + 2h_3|2h_3|^{\psi} + h_5|h_5 - h_1|^{\psi}}{2|h_5 - h_1|^{\psi} + 2|2h_3|^{\psi}} \qquad [2.11a]$$

and with Figure 2.3b is:

$$h_C = \frac{2h_1|2h_1|^{\psi} + 2h_3|2h_3|^{\psi}}{2|2h_1|^{\psi} + 2|2h_3|^{\psi}} = \frac{h_1^{(1+\psi)} + h_3^{(1+\psi)}}{h_1^{\psi} + h_3^{\psi}} \qquad [2.11b]$$

The case of positions adjacent to the phreatic surface (the slope of which changes continuously), or of positions adjacent to the seepage-face, can be handled as follows.

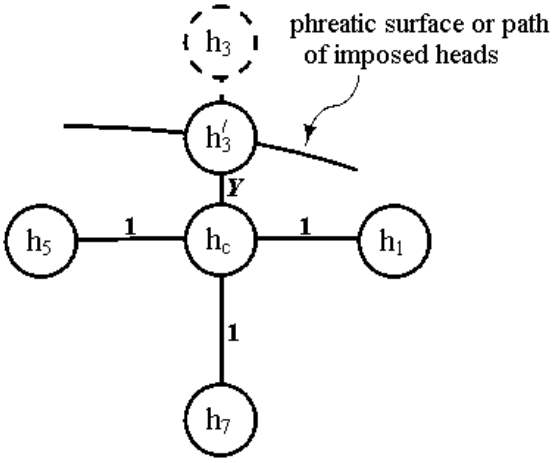

a) one intra-nodal cut.

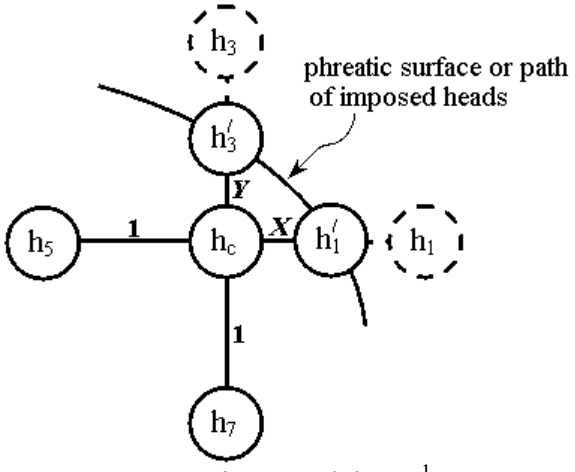

b) two intra-nodal cuts[1].

Figure 2.4. FD star for nodes adjacent to phreatic surface or seepage-face.

[1] The corner FD molecule shown in Figure 2.4b was not needed in this research because this 'corner case' did not exist for the 2-D cases studied herein.

The expression associated with Figure 2.4a used in the analysis described herein is:

$$h_C = \left[\left|h_5 - h_1\right|^{\Psi} + \frac{\left|h_3' - h_7\right|^{\Psi}}{Y} + \left|h_5 - h_1\right|^{\Psi} + \left|h_3' - h_7\right|^{\Psi} \right]^{-1} \cdot \left[h_1\left|h_5 - h_1\right|^{\Psi} + \frac{h_3'\left|h_3' - h_7\right|^{\Psi}}{Y} + h_5\left|h_5 - h_1\right|^{\Psi} + h_7\left|h_3' - h_7\right|^{\Psi} \right] \quad [2.12a]$$

and with Figure 2.4b is:

$$h_C = \left[\frac{\left|h_5 - h_1'\right|^{\Psi}}{X} + \frac{\left|h_3' - h_7\right|^{\Psi}}{Y} + \left|h_5 - h_1'\right|^{\Psi} + \left|h_3' - h_7\right|^{\Psi} \right]^{-1} \cdot \left[\frac{h_1'\left|h_5 - h_1'\right|^{\Psi}}{X} + \frac{h_3'\left|h_3' - h_7\right|^{\Psi}}{Y} + h_5\left|h_5 - h_1'\right|^{\Psi} + h_7\left|h_3' - h_7\right|^{\Psi} \right] \quad [2.12b]$$

where:

X = centre-to-centre distance between h_C and h_1' in y direction, divided by global Δx, *i.e.* X=(distance from h_C to h_1')/global Δx,

Y = centre-to-centre distance between h_3' and h_C in x direction, divided by the global Δy, *i.e.* Y=(distance from h_C to h_1')/global Δy (not needed herein).

The phreatic surface case is a sub-set of the case of having a series of imposed hydraulic heads, only that said heads consist entirely of elevation head. Equations [2.12a and b] are modifications of the linear flow versions presented by others (*e.g*. Southwell 1946, Kleiner 1985).

2.4. GEOMETRIES CONSIDERED AND BOUNDARY CONDITIONS USED

Twenty four hypothetical flow-through dams were modeled (Figure 2.5). These had the following characteristics: **(i)** An upstream slope of 1V:1H in all cases. **(ii)** Heights defined in terms of crest-width, namely, as H = 0.5 B_C, 1.0 B_C, 2.0 B_C, and 3.0 B_C. **(iii)** A crest-width that could be easily set to a coarse and integer nodal density. If the crest of the structure is used as a means for vehicles to cross the stream or river, a value of 15 m would be a common width for the total right-of-way. Therefore, making a

node 1 m by 1 m would result in a suitably coarse yet simple density, with 15 nodes making up the crest. (Much higher nodal densities were, however, also investigated.) **(iv)** A range of downstream slopes, from 1V:1H to 1V:6H. From the point of view of unraveling failure and based on prior experience, it was expected that this would encompass a suitable range of factors-of-safety, from below unity to above unity.

With regard to boundary conditions, three different relative magnitudes of h_{TW} were imposed *a priori* at the downstream toe, namely: $h_{TW}/H = 0.05$, 0.10, and 0.20. The variation in the seepage-face 'thickness' was then assumed to vary linearly from zero to the implied h_{TW} value. This is usually an acceptable approximation (Hansen 1992) but is the subject of on-going research, as an interesting spatially-varied flow (SVF) problem first investigated by Sharp and James (1963). The values of the bounding nodes making up the seepage-face and directly beside the porous media nodes of the downstream face were therefore set at:

$$h_{SF} = z_{SF}(\ell) + \frac{p_{SF}(\ell)}{\gamma_w} \qquad [2.13]$$

where:

h_{SF} = local seepage-face head (L),
$z_{SF}(\ell)$ = elevation of seepage-face; varies from zero at $\ell = \ell_{SF}$ to $\ell = 0$ at y_{exit} (L),
$p_{SF}(\ell)/\gamma_w$ = pressure head[1] (also a function of position on face), magnitude varies from zero at $\ell = 0$ to h_{TW} at $\ell = \ell_{SF}$ (L),
γ_w = unit weight of water (F/L^3).

Finally, the maximum upstream water-level (h_{us}) allowed in any given case was made equal to the height of the dam (H). Overflow is imminent beyond this upstream depth; being a highly undesirable condition (CDA 2007) it was not considered.

The envelope defining the entire flow-through zone is incomplete without knowledge of the elevation of the point of emergence as well as of the path of the phreatic surface behind it. The y_{exit} of the model dams was determined using the concept of the angle of the emergent flow field, θ_{ff} (Hansen *et al.* 2005), together with the equation of Stephenson (1979) - as per earlier findings on the performance of various 1-D

[1] $p_{SF}(\ell)/\gamma_w = y\cos^2\theta$ where y is measure orthogonally to the foundation, also see Figure 4.16.

non-Darcy flow equations (Hansen *et al.* 1995). Since y = q/V is an identity for open-channel flow and q was uni-valued (= Q/L), then $y_{exit} = q/V$. For:

Stephenson (1979) $$V = n\sqrt{\frac{gd}{K_{steph}}i} \quad [2.14a]$$

where: $$K_{Steph} = \frac{800}{Re} + \kappa_{ang} \quad [2.14b]$$

so: $$i = \frac{K_{steph}}{gdn^2}V^2 \text{ (}i.e.\text{ a form of equation [2.5])} \quad [2.14c]$$

It follows that: $$y_{exit} = \frac{q}{n\sqrt{\frac{gd}{K_{steph}}i_{exit}}} \quad [2.15]$$

where:

κ_{ang} = empirical constant ranging from 1 for spheres to 4 for angular stone (L/T),
Re = Stephenson's particle Reynolds number (=Vd/nν),
n = porosity (dimensionless),
d = particle diameter (L)[1],
i_{exit} = hydraulic gradient most suitable for use in finding y_{exit} (dimensionless).

In Leps' (1973) summary of various geo-hydraulic design methods extant for this class of structure, it was re-presented that a practitioner's approximation of the representative hydraulic gradient acting within the toe and for use in equation [2.15], or similar, is simply tanθ. Hansen *et al.* (2005) introduced the idea of a variable angle θ_{ff} for this emergent flow field and showed that the following equation performs better than tanθ, when used to estimate y_{exit}:

[1] It is possible to dramatically change the apparent permeability of a porous medium without changing D_{50}. This can be done by making the particle gradation well graded (poorly sorted), so that both much smaller (and much larger) particles are present. This has the effect of decreasing permeability because a given void space created by some large(r) particles is filled in with small(er) particles. However, the more efficient packing of mass that is implied by this kind of gradation results in a decreased porosity (and porosity is a part of the Stephenson equation). Theoretically and according to the so-called capillary model of flow through porous media, it can be shown (Hansen 2004) that the representative pore size, known as the hydraulic mean radius (Taylor 1948), is m=ed/6 for spherical particles. Since e=n/(1-n), m=nd/6(1-n), indicating that accounting of this effect in the Stephenson (1979) equation is imperfect. Regardless, if D_{50} is used in the equation, the medium should be "poorly graded" (nearly uni-sized), as it was herein.

$$\frac{\theta_{ff}}{\theta} = 1.41\frac{y_{exit}}{H} + 0.17 \qquad [2.16]$$

where:

y_{exit}= exit height (L),
H= height of dam (L),
θ_{ff}= angle of emergent flow field (see Figure 3.2),
θ= angle of downstream toe (see Figure 2.1).

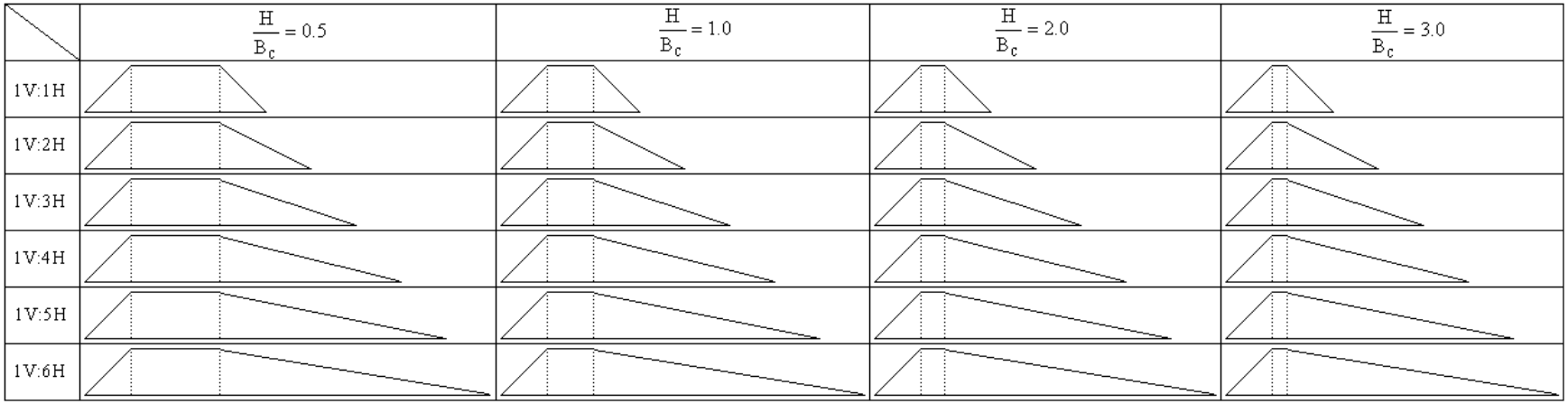

Figure 2.5. Geometries used in parametric study; downstream slopes are (by row) 1V: mH. With 1V:1H upstream slope.

Equation [2.16] was so used in equation [2.15] to obtain y_{exit} and was the starting point for calculation of the phreatic surface in the upstream direction. The existence of the phreatic surface makes this a so-called free-boundary problem. If the Finite Element Method (FEM) is used to solve this class of boundary value problem, an initial position for the phreatic surface is provided to the mesh and then various options may be used to 'home in' on the correct position of the free boundary. Desai (1972) used the FEM to solve the unsteady Darcian embankment-seepage problem. The initial position of the moving surface was imposed and an increase in the head at the upstream end propagated downstream through the problem, with the position of the moving surface found by using a combination of the previous surface and an updated field velocity component. Desai (1973) used the FEM to solve the steady-state Darcian embankment seepage problem. The free surface that satisfied the zero normal-velocity condition, while minimizing the overall flow-field energy, was found. Volker (1969) used the same method to locate the free surface, but for a trapezoidal embankment of prismatic cross-section. Desai and Sherman (1971) used the FD method to study transient seepage. The initial position of the moving surface was imposed and an increase in the head at the upstream end propagated downstream through the problem, with the position of the moving surface found using a combination of the previous surface and the updated field-velocity component. In this study the position was independently and easily determined using the porous media analogue of gradually-varied open-channel flow theory (*cf*. Hansen *et al*. 2005), *a priori*, and then simply imposed on the FD grid. The details of the analytical expression applicable to prismatic sections, and of the numerical approach needed when the valley in which the dam resides is non-prismatic, are also presented in Hansen *et al.* (2005).

2.5. ASSESSMENT OF MAGNITUDE OF NON-DARCY EFFECT

It was found that the effect in question could be masked by insufficient convergence of the numerical outcomes. Figure 2.6 shows the outcome of a representative study of the convergence of one of the numerical solutions, a process sometimes referred to as ‘grid relaxation’ (Southwell 1946). All 24 grids were similarly

relaxed to a high degree of convergence. In Figure 2.7a the outcomes for the PCL and NLHC methods of modeling are compared. In Figure 2.7b the outcomes for laminar and fully-developed turbulent flow modeling are compared. Figure 2.7a shows that there is very little difference between hydraulic heads found using the PCL approach and the NLHC method of modeling using equations [2.10] through [2.12], where both are cases of completely non-Darcy flow (N=2). Figure 2.7b shows that there is also little difference between hydraulic heads found using equation [2.4] for flow governed by Darcy's Law (in concert with its various special cases) compared to that modeled via equations [2.10] through [2.12] for completely non-Darcy flow. Figure 2.7b also shows that: **(i)** non-Darcy hydraulic heads are higher than those found using the assumption of linear Darcian flow, **(ii)** that the difference between these heads is not large, and that **(iii)** it always increases toward the toe of the structure (the part of the dam most prone to unraveling failure). Finally, due to the fact that the non-Darcy free surface is always slightly higher than the free surface associated with laminar flow, there is a narrow zone in which the ratio cannot be computed. The imposed non-Darcy free surface found using methods described in Hansen *et al.* (2005) and was indeed higher than the upper limit of the shaded areas in Figure 2.7b, but imperceptibly so as presented.

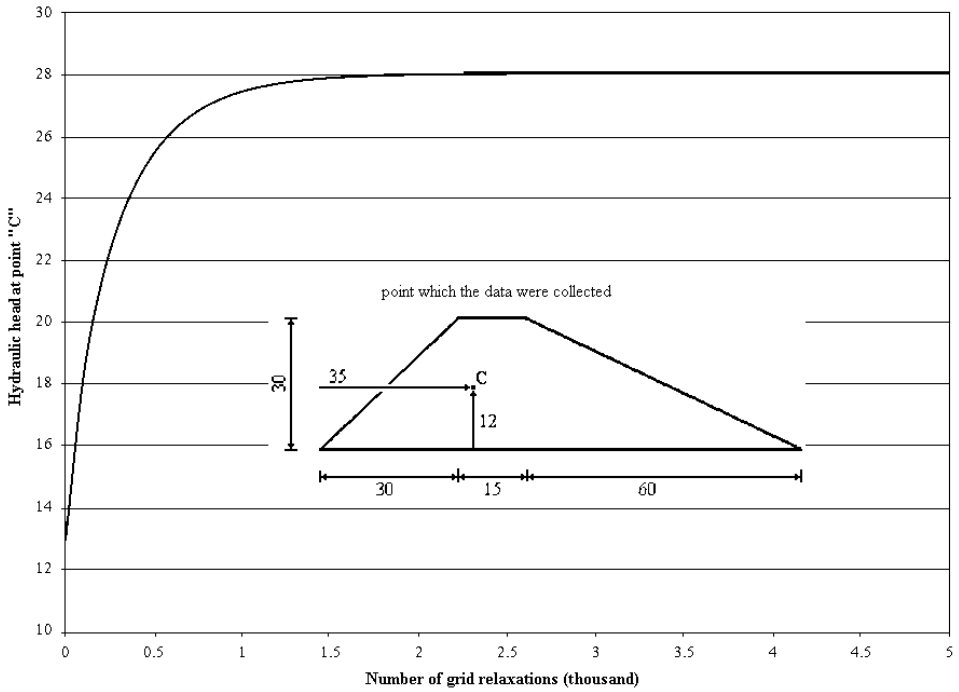

Figure 2.6. Convergence (grid relaxation) of model dam with 1800 nodes, using change in head at centrally-located interior node as indicator.

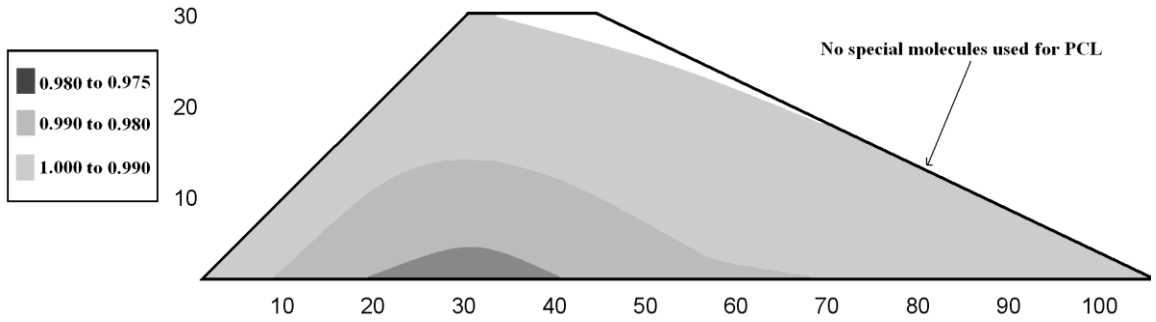

a) comparison of PCL and NLHC methods of modeling hydraulic head (ratio of NLHC results to PCL results for mid-size dam, $H/B_C = 2.0$, 1V:2H).

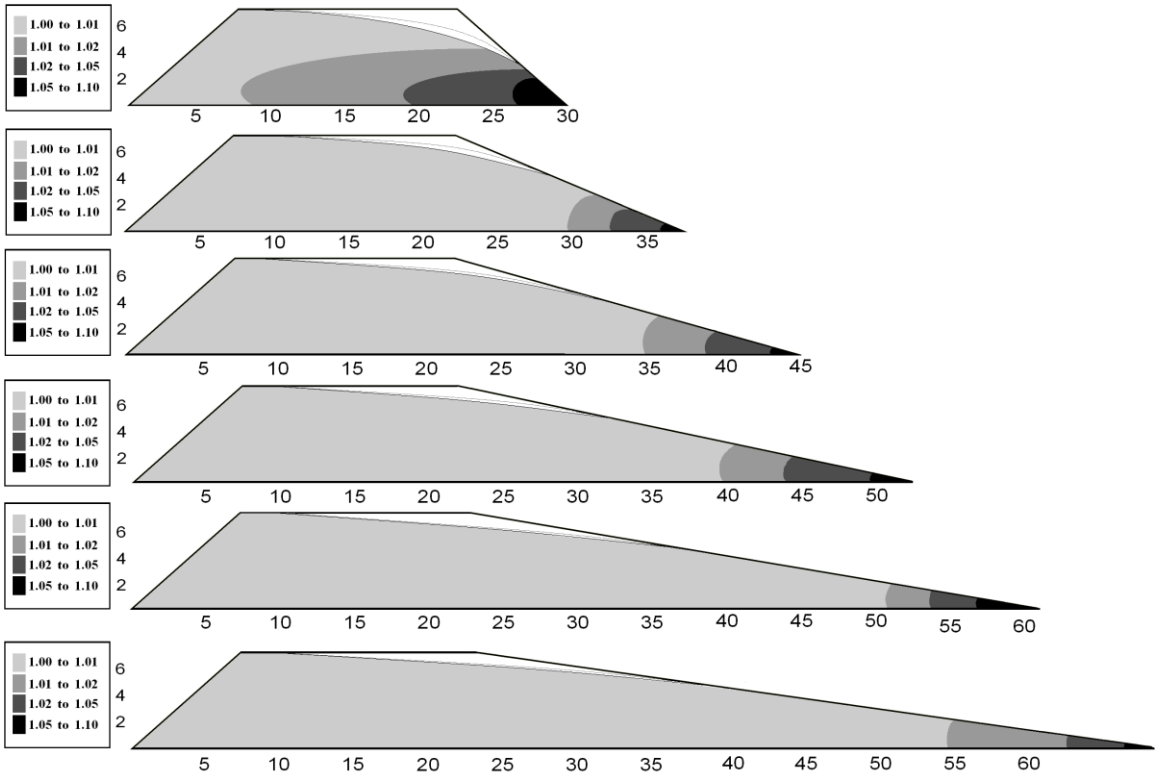

b) comparison of modeling outcomes for two extremes of turbulent intensity; none (laminar, N=1 in equation [2.5]) and fully-developed turbulent flow (N=2). Ratios shown in legends were found using ratio of heads from N=2 case to heads from N=1 case.

Figure 2.7. Ratios of hydraulic heads for two pairs of cases.

2.6. GRID FINENESS (NODAL DENSITY) EFFECT

A given finite area of porous medium, typically considered in 2-D, can be represented by few nodes or by many. The effect of this density was of interest because a

coarse representation of the problem numerically will result in a low level of detail and even in rather erratic outcomes. The latter are manifested by flow-lines that undulate and by spatially-fluctuating hydraulic gradients. The density can be defined by how many nodes correspond to, or are used to construct, a unit dimension. In this study and as was shown in Figure 2.5, the nominal dimension of B_C in Figure 2.1 was 15 units, in all cases. Three densities were tested. Using B_C as the reference quantity, these corresponded to 15 nodes, 30 nodes, and 75 nodes being used to construct B_C. (If the nominal dimension of 15 is intended to represent 15 physical meters, the associated sizes considered for a single node were $\Delta = 1$ m, $\Delta = 0.5$ m, and $\Delta = 0.2$ m.)

Figure 2.8 shows qualitatively that making the mesh finer reduces undulations in the flow-line pattern near the seepage-face, especially near the point of emergence. The benefit of increasing nodal density was smaller than expected. However, the upper-most example in Figure 2.8 shows inward flow, which is physically unrealistic.

2.7. BENEFIT OF USING SPECIALIZED FD MOLECULES

Figure 2.4 illustrates the situations wherein certain irregular 'permeable' boundaries are present, such as at the phreatic surface and the seepage-face. Although slopes with integer regularity in the manner in which the elevation drops can be easily set up in a step-like manner (1V:1H corresponding to 45°, 1V:3H corresponding to 18.4°, etc), even this kind of regular stepping can be handled more carefully. The example in Figure 2.9 shows where the minor discrepancy exists between a truly continuous 1V:2H slope and a slope simply modeled using one vertical drop in Δx for every two horizontal shifts via Δy. This minor discrepancy can be remedied through the intermittent use of the special FD molecules (Figure 2.4) and the associated expressions (equations [2.12a and b]), but it was considered of interest to see how much difference this additional attention to detail would make, and for a range of nodal densities. The study of this discrepancy was considered to be representative of the question of how much benefit might be accrued by using any one of the special molecules shown in Figure 2.4.

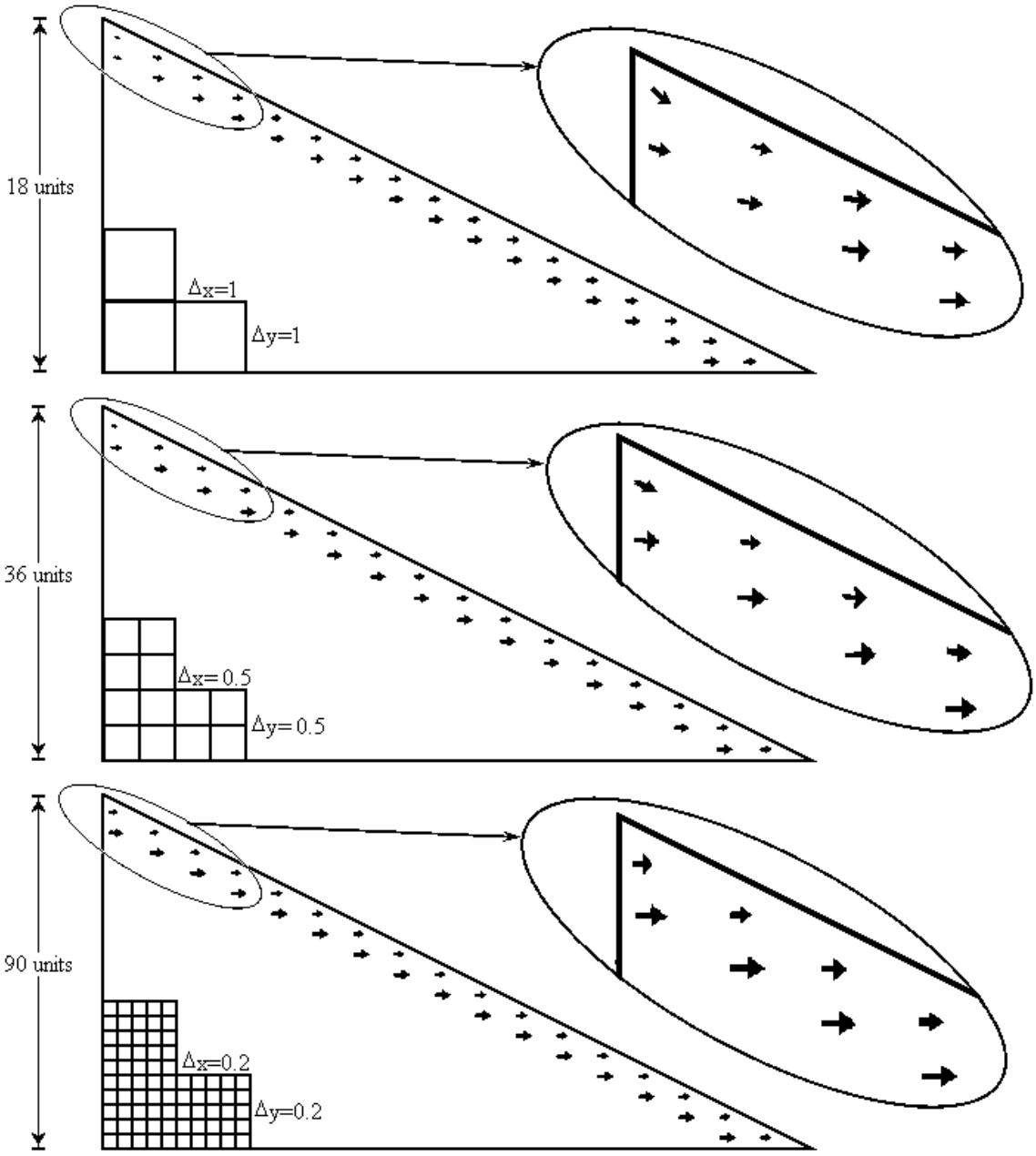

Figure 2.8. Nodal density effect on exit flow-line patterns; equation [2.12a] for special FD molecule used where needed. $H/B_C = 2.0$ and slope 1V:2H.

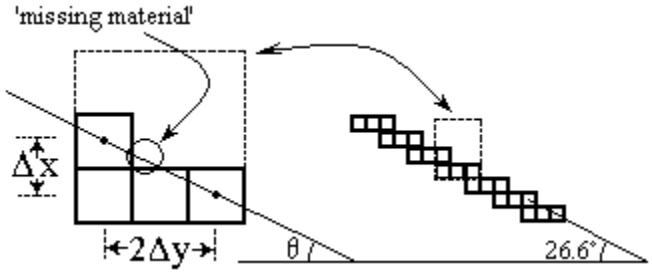

Figure 2.9. Example of integer slope with regular drop.

In comparing the top of Figure 2.10 with the top case of Figure 2.8 (and correspondingly for the middle and bottom cases), it qualitatively appears that the use of specialized FD molecules under the seepage-face does not obviate the undesirable effects of using a coarsely-defined grid. Conversely, it qualitatively appears that the benefit accrued from using a fine grid make it unnecessary to use specialized FD molecules under the seepage-face.

In the current study, block-centered nodes were used. Although use of special computational molecules can help to get a better representation of the slope of the downstream face of the phreatic surface, these will not completely resolve the issue. Figure 2.11 shows that the special nodes reduce the jaggedness of the line representing the downstream face of embankment, but do not eliminate it.

As can be seen from Figure 2.12 the curve describing the exit angle of the local seepage vector is smoother for the truncated-arm case[1]. However, the difference in the two exit angles is everywhere small.

[1] Truncared-arm is when special molecules are used for the downstream toe (also see Figures 2.11)

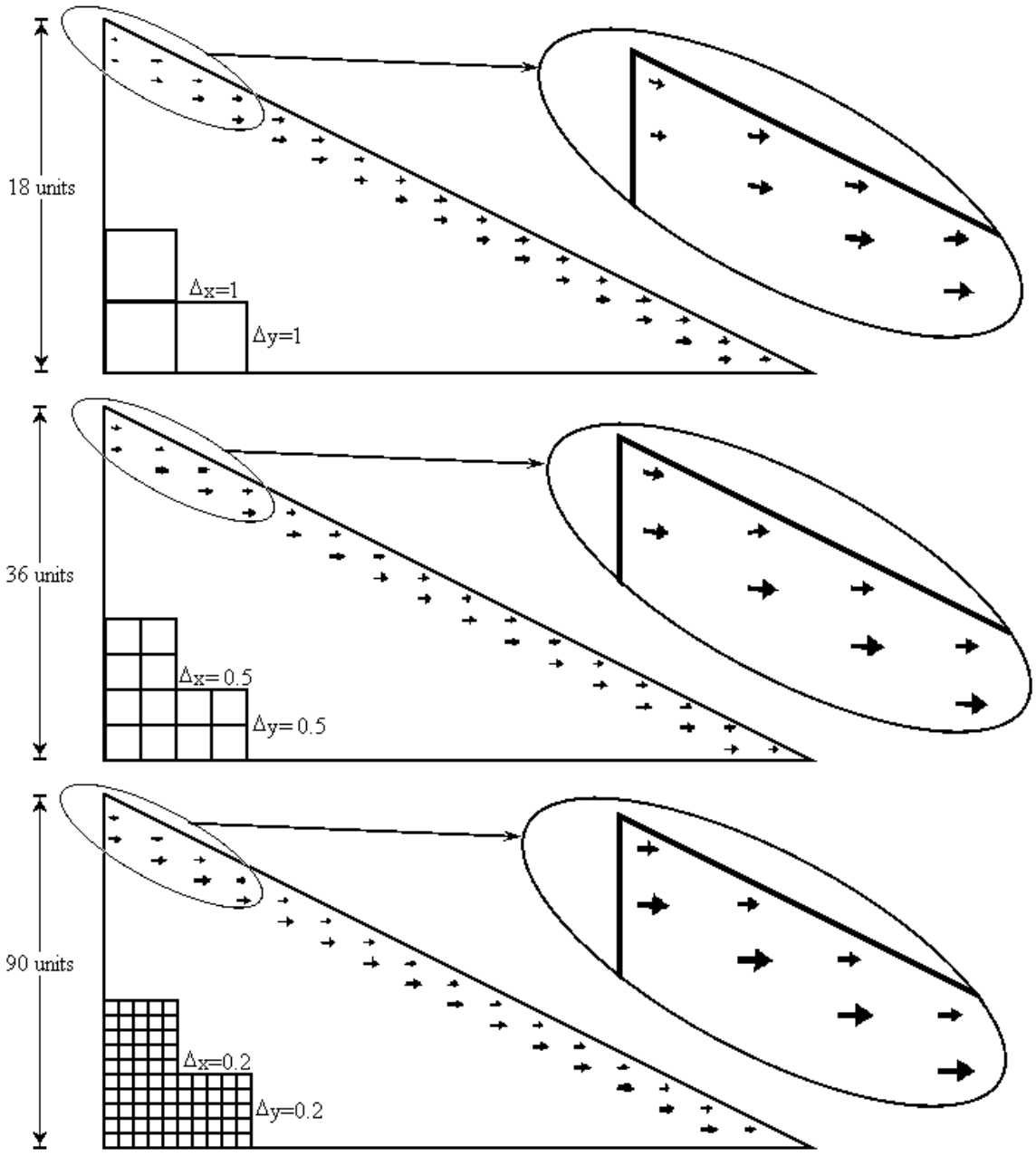

Figure 2.10. Nodal density effect on exit flow-lines for case of no special FD molecules at all; $H/B_C = 2.0$ and slope = 1V:2H.

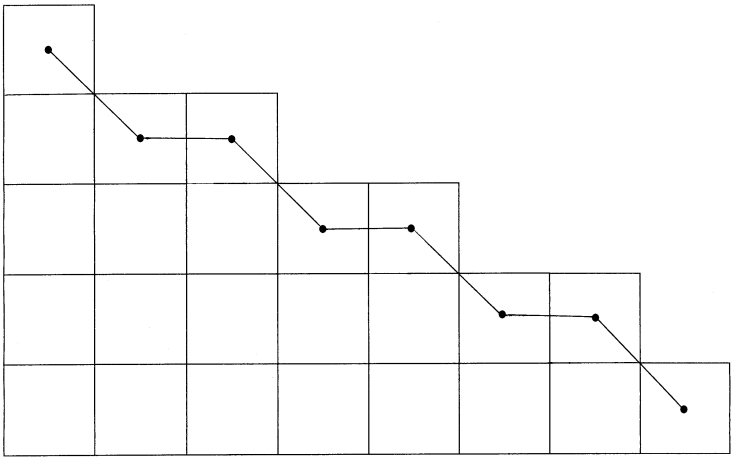

a) no specialty nodes used in downstream face.

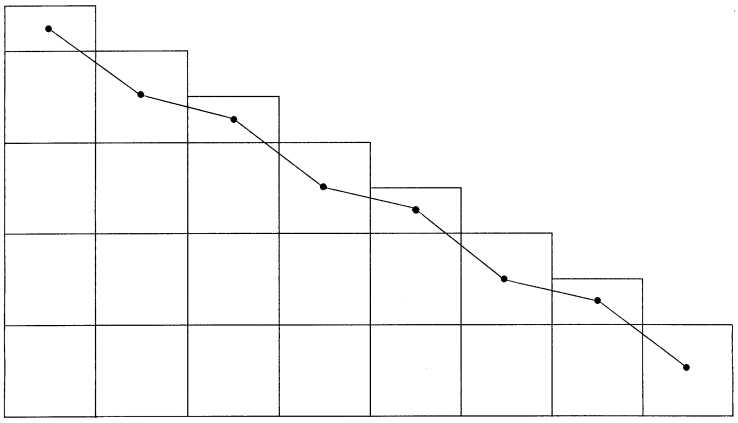

b) 0.5Δx (≡0.5Δy) specialty nodes used in downstream face.

Figure 2.11. Illustration of benefit of selective use of half-nodes on downstream face.

Figure 2.12 shows a comparison of the exit gradient directions for a grid in which no specialty nodes are used and one in which 0.5Δx (≡0.5Δy) nodes are incorporated.

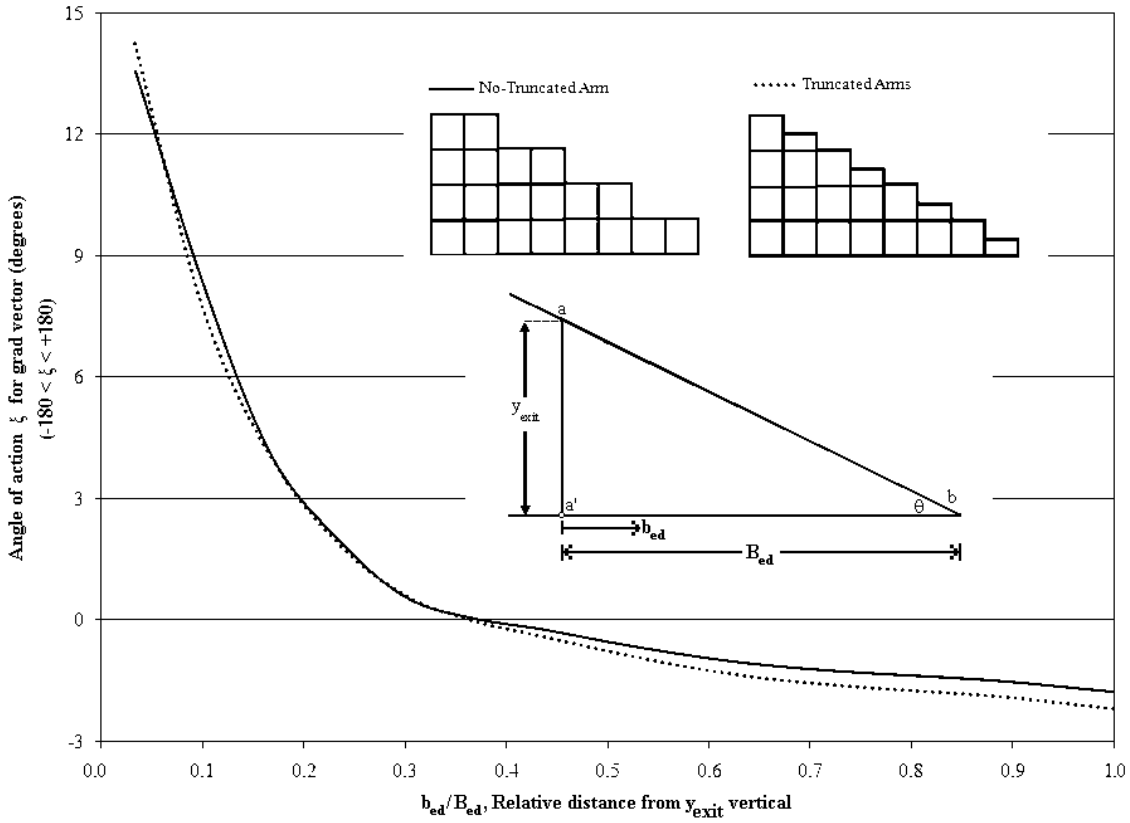

Figure 2.12. Minimal effect of using specialty node on direction of exit hydraulic gradient for Δ =1, H/B_C = 2.0 and slope = 1V:2H.

2.8. EXIT GRADIENT MAGNITUDE AND DIRECTION

A more quantitative study of the magnitude and direction of the exit gradient next to the seepage-face was undertaken. This gradient has previously been found to play a powerful destabilizing role with respect to the initiation-of-motion (IoM) of particles residing on the surface of the downstream toe (Hansen *et al.* 2005). Using central differences, the general expression for the absolute magnitude of this gradient is:

$$i = \sqrt{\left(\frac{h_3 - h_7}{2\Delta y}\right)^2 + \left(\frac{h_5 - h_1}{2\Delta x}\right)^2} \qquad [2.17]$$

and its direction, as $+\xi$ degrees below the horizontal, is:

$$\xi = \frac{180}{\pi}\arctan\left(\frac{h_3 - h_7}{h_5 - h_1}\right) \qquad [2.18]$$

Figures 2.13 and 2.14 show the effects of mesh size on the strength and direction of the exit gradient.

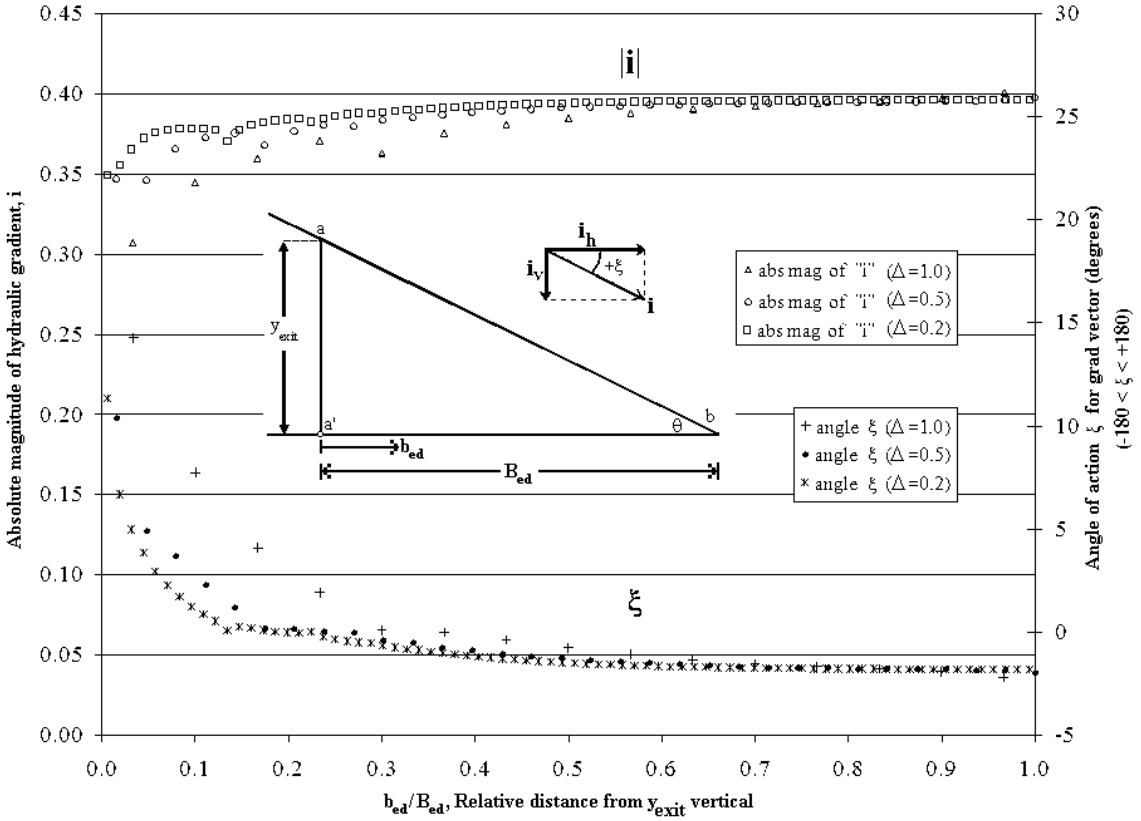

Figure 2.13. Mesh-size effect on exit hydraulic gradients with use of specialty node. Case of $H/B_C = 2.0$ and 1V:2H ($\theta = 26.6$ º).

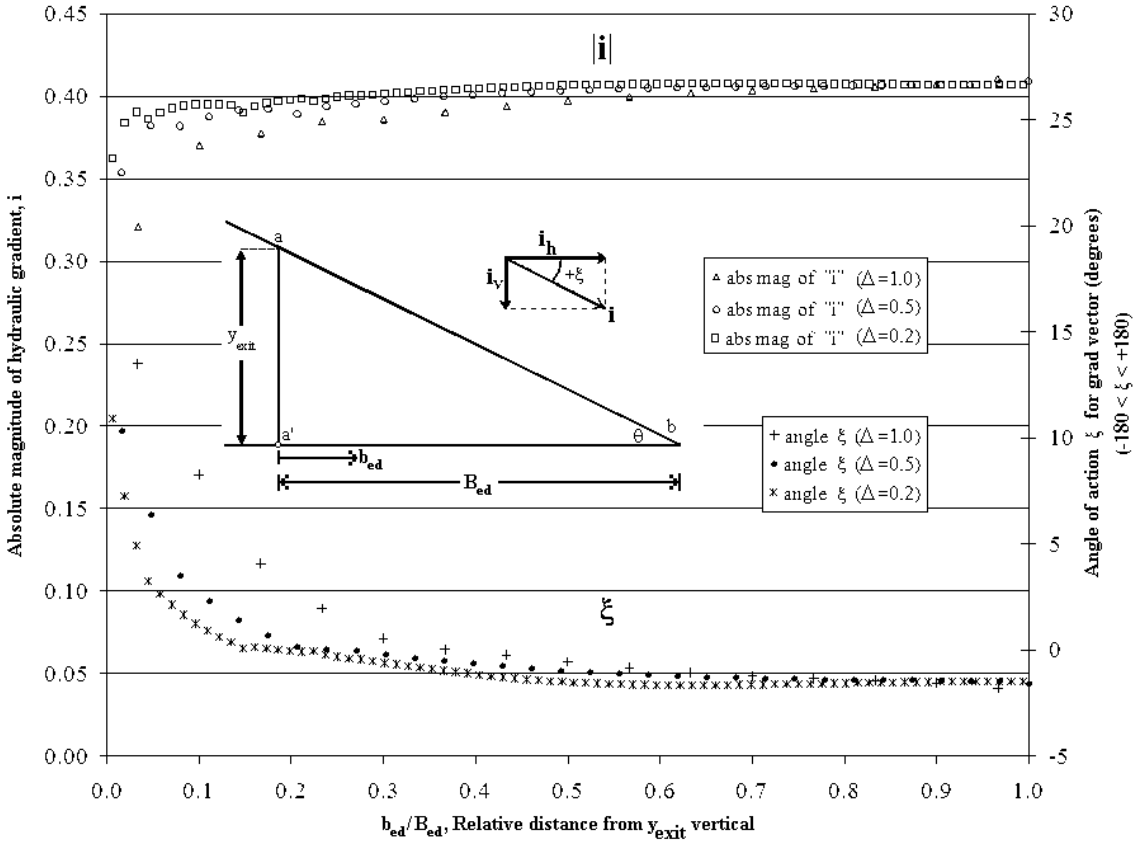

Figure 2.14. Mesh size effect on exit hydraulic gradients, with no specialty node used. Case of $H/B_C = 2.0$ and 1V:2H.

Figures 2.13 and 2.14 imply that seepage exits outwardly, at an angle of between 12° and 29°, relative to the plane of the downstream toe (see angle of F_{seep} in Figure 2.15). Figures 2.13 and 2.14 also show that on the upper one-third of the face, the hydraulic gradient vector is more inward, relative to the plane of the face, and lower in absolute magnitude. This is significant because any gradient vector which is more outward as well as higher in magnitude is more important as a destabilizing force causing IoM and unraveling. Figures 2.13 and 2.14 also show that **(i)** using a coarse grid results in some unreliable point-value outcomes for the magnitude of the local hydraulic-gradient vector, as well as for the associated direction of this vector, on the upper one-third of the seepage-face, **(ii)** using a fine grid does not necessarily result in reliable point outcomes for said magnitude and direction even if specialized nodal definitions (equation [2.12]) are used throughout, and **(iii)** if accurate exit gradient vectors are needed for the entire seepage-face, both a fine grid and specialized nodal definitions should be used.

2.9. INITIATION OF MOTION THRESHOLD (UNRAVELING POTENTIAL)

The initiation of motion (IoM) of a single rock particle under the seepage-face is the beginning of so-called unraveling failure. This initial disruption is driven by the same forces that bring about the continued movement and rapid disaggregation of the entire surface, as part of an artificial deposit of porous media – the force associated with the exiting seepage, and the force caused by the flow moving down over it, of length ℓ_{SF} (Figure 2.1). The former may be quantified using the fundamental principle describing seepage forces that $F_{seep}/\forall_{unit} = \gamma_w.i$, and the latter using the well-known equation for the drag exerted by a fluid that is moving past a bluff body. With various qualifications these forces can be applied through moment-arms that depend partly on the particle size. The only stabilizing moment is that associated with the submerged weight of the particle (see Figure 2.15 and Hansen *et al*. 2005 for further details).

Using the first six previously-mentioned 24 geometric configurations (column 1 in Figure 2.5), a fairly comprehensive study of the IoM threshold under seepage-face conditions typical of flow-through rockfill dams was undertaken, based on the theoretical framework presented in Hansen *et al*. (2005), *cf*. Stevens and Simons (1979). Three particle diameters, three overflow velocity variations, and a single imposed tailwater level (h_{TW}/H of 0.05, the most severe relative tailwater) were considered, leading to 54 IoM outcomes. The outcomes for the FS for the higher relative tailwater levels of 0.10 and 0.20 were found to be markedly higher and are not presented herein. A rock particle was approximated as a sphere and was assumed to lie in the plane of the downstream face such that it was one-half exposed.

The expression for the Factor of Safety for the moment-based IoM of a single particle is:

$$FS = \frac{W_{sp}\cos\theta}{0.5F_{hyd} + F_{seep}\sin(\theta - \xi)} \qquad [2.19a]$$

$$W_{sp} = (\gamma_P - \gamma_w)\forall_p = (\gamma_P - \gamma_w)\frac{\pi d^3}{6} \qquad [2.19b]$$

$$F_{hyd} = C_D \rho A \frac{U^2}{2} \quad [2.19c]$$

$$F_{seep} = \forall_P (1+e)\gamma_w i \quad [2.19d]$$

where:

W_{sp}= submerged weight,
F_{hyd}= hydraulic force (from drag and shear),
F_{seep}= seepage force,
C_D= drag coefficient (dimensionless), varied according to Re (see Hansen *et al.* 2005),
A= area of forward projection of the object (L^2),
U= velocity of uniform infinite flow field impinging upon object (L/T),
ρ= fluid density,
d= particle diameter (L),
$\forall_P$= volume of the particle (L^3),
e= void ratio (dimensionless),
γ_W = unit weight of water (F/L^3),
γ_P= unit weight of the particle (F/L^3),
i= hydraulic gradient (dimensionless),
θ= angle of the toe of the dam,
ξ = local angle of seepage vector (Figure 2.15).

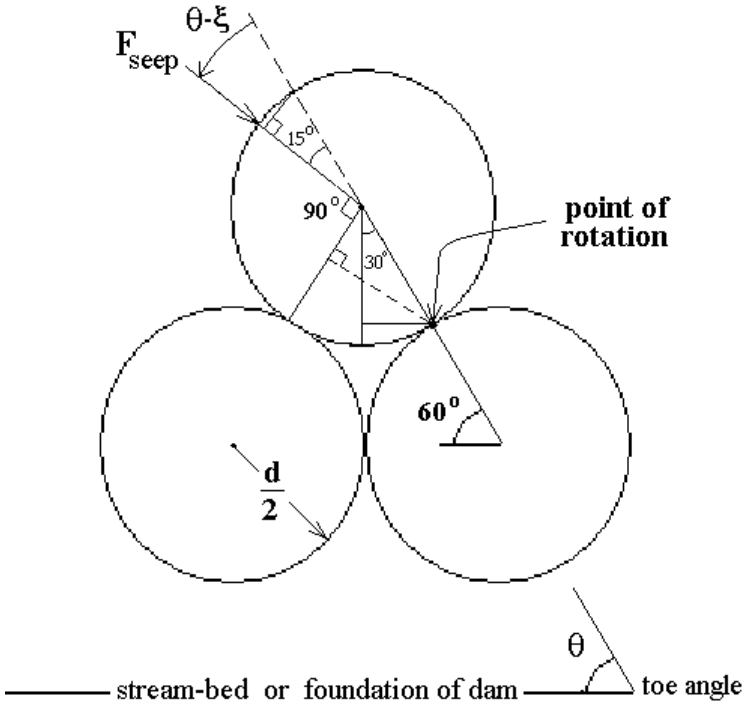

Figure 2.15. Particle position and seepage force direction in the downstream face (adapted from Hansen *et al.* 2005).

Since the hydraulic modeling of SVF, as an open-channel hydraulics problem, was beyond the scope of the work described herein (although it is discussed in Chapter 4), and represents a distinct algorithm, $U(\ell)$ was not modeled for each seepage-face. Rather, a range of likely U values was assumed for use in equation [2.19], so that: **(i)** the relative effect or importance of U could be assessed, and **(ii)** an analyst having $U(\ell)$ from independent SVF outcomes could quantitatively still see its effect for a U of interest. The local velocity U was found from knowledge of h_{TW} and the local depth arising from the assumption of a linear variation from the point-of-emergence (zero depth) to the depth h_{TW} at the toe, as:

$$U(\ell) = \frac{\ell}{\ell_{SF}} U_{at\ h_{TW}} = \frac{b_{ed}}{B_{ed}} U_{at\ h_{TW}} \qquad [2.20a]$$

from which:

$$U_{at\ h_{TW}} = \frac{Q}{h_{TW} \cos\theta} \qquad [2.20b]$$

where:

$U(\ell)$= local mean velocity within seepage-face (L/T),
h_{TW}= tailwater depth at toe of dam (L),
Q= total discharge through dam (L^3/T).

Figures 2.16 through 2.18 show the results of the above initiation-of-motion analyses. The hydraulic gradients under the seepage-face were extracted from part of the parametric study. Figure 2.19 summarizes the variation in the low-end values of the factors of safety for slopes flatter than 1V:1H.

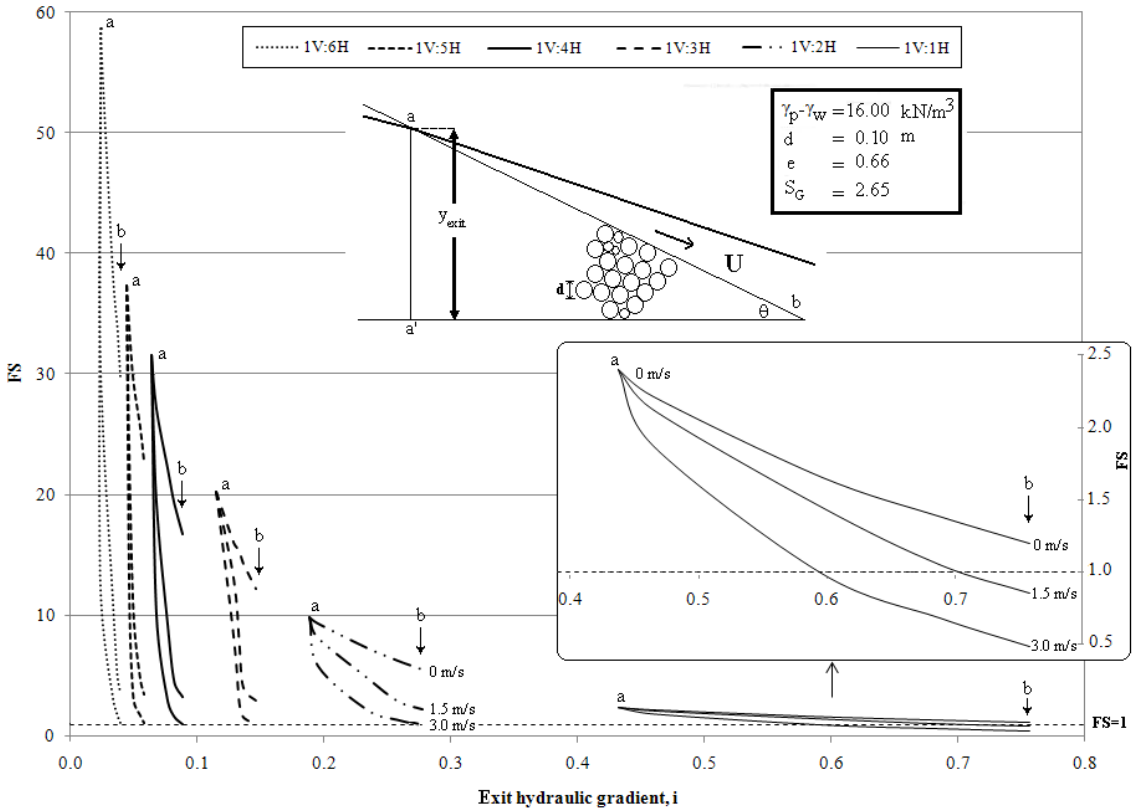

Figure 2.16. Factor of safety as a function of exit gradient for dams with $H/B_C = 0.5$, for three velocities at toe of seepage-face. Particle diameter = 0.1 m. (See also Figure 2.19 for selected low-FS endpoints of 3 m/s cases.)

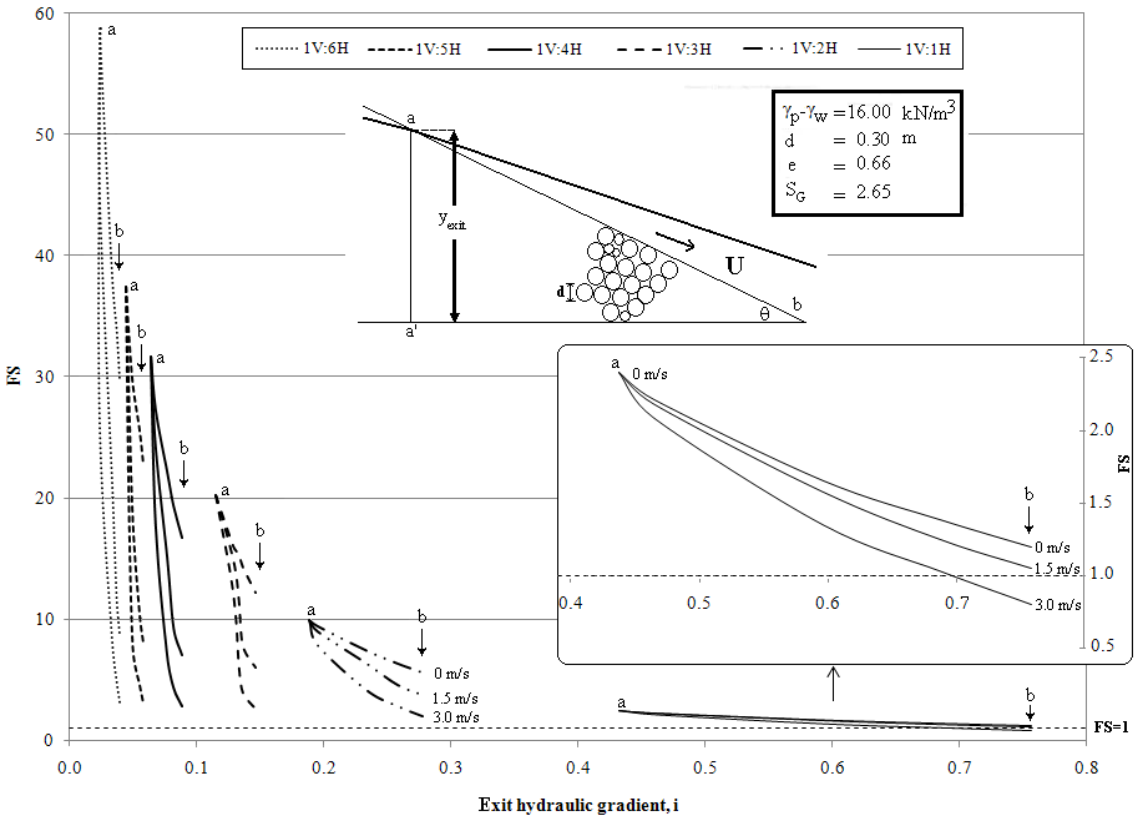

Figure 2.17. Factor of safety as a function of exit gradient for dams with $H/B_C = 0.5$, for three velocities at toe of seepage-face. Particle diameter = 0.3 m. (See also Figure 2.19 for selected low-FS endpoints of 3 m/s cases.)

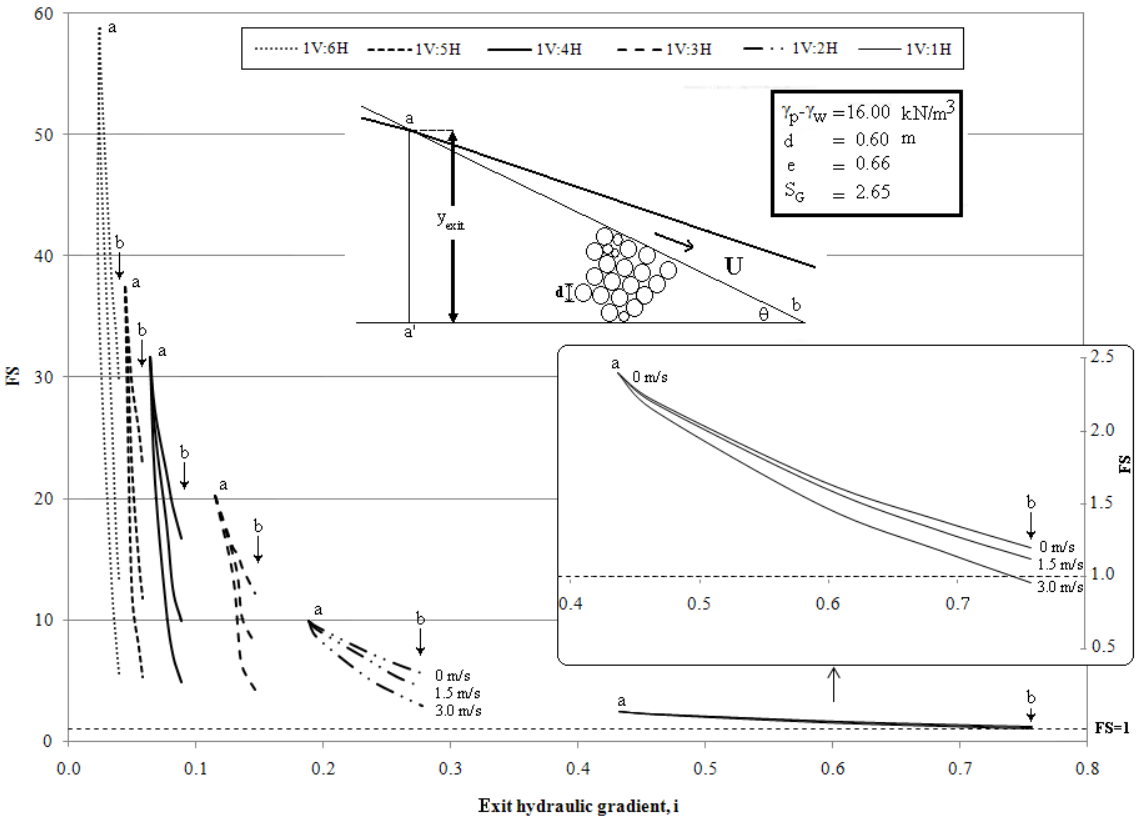

Figure 2.18. Factor of safety as a function of exit gradient for dams in parametric study with $H/B_C = 0.5$, for three velocities at toe of seepage-face. Particle diameter = 0.6 m. (See also Figure 2.19 for selected low-FS endpoints of 3 m/s cases.)

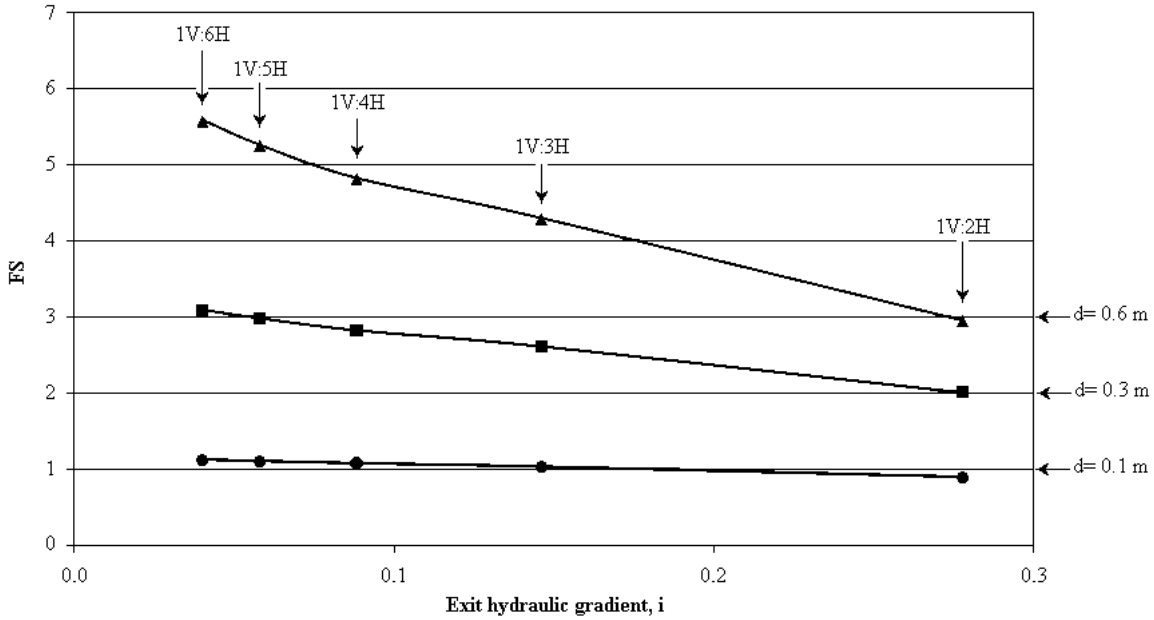

Figure 2.19. Worst case factors of safety as a function of exit gradient for dams in parametric study with $H/B_C = 0.5$ (for three particle diameters and U = 3 m/s).

2.10. SUMMARY AND CONCLUSIONS

It was found that the non-linear flow effect on head is a small effect. The parametric study revealed that the heads associated with fully-developed turbulent flow will never be more than about 10% larger than those associated with laminar flow, and that over most of the 2-D modeling space(s) of interest, the difference is much less than 10%. As an incidental outcome and with regard to studies directed at measuring the magnitude of the head itself, this implies that the physical modeling of flow-through rockfill dams is difficult if not pointless unless the physical model is very large[1].

Starting with an exit height represented by 18 nodes, it was found that quintupling grid density had little effect on the visual smoothness in exit-flowline patterns. It was also found that the direction of these exit flow-lines was little affected by using specialty nodes at regular intervals in the FD molecules.

It was confirmed via the work described herein that the toe of such structures is the primary zone of engineering concern. The particle-based FS was found to decrease very dramatically as the distance to the toe decreased (as ℓ becomes equal to ℓ_{SF} in Figure 2.1). As the velocity of the overflow approached 3 m/s, this caused the FS to drop dramatically and approach unity, regardless of the magnitude of the local hydraulic gradient, as determined where the seepage exits into the seepage-face.

The severity of this overflow effect was greater for flatter slopes, which is perhaps non-intuitive. The reason, however, that the drop in FS with increasing overflow U is greater for flatter slopes is that flatter slopes have inherently smaller exit gradients,

---

[1] The non-linear hydraulic conductivity model outcomes do show a smooth variation in head between the imposed boundary conditions. If the porous medium had been sand and the heads modelled via numerical solution of the LaPlace equation, the general level of confidence with that kind of modeling effort would be high and the resulting internal heads would not be questioned, because that problem is relatively trivial. Since modelled non-Darcy 'flow nets' are little different from Darcian flow nets (PCL 1966, 1967), and the heads modelled herein indeed varied smoothly from the upstream boundary condition to the downstream boundary conditions, a good measure of confidence in the results was implicitly present, especially since the correct non-Darcy phreatic surface was imposed *a priori*.
For a physical model 500 mm high (300 mm herein), the amount of discrepancy between the Darcian and non-Darcian cases would be 2-3 mm in the centre of structure (150 mm to 250 mm above the floor of the flume). Therefore, unless a given piezometer can be positioned to within a millimeter in the vertical and can then clearly resolve heads at the millimeter scale, it will even be quite difficult to distinguish between non-Darcy and Darcian conditions. Such internal head measurement was therefore not attempted in the Dalhousie Hydraulics Laboratory.

tipping the effect of the denominator within the FS expression toward the effect of U and away from i_{exit}. Furthermore, the dams with particle diameters higher than 0.3 m and flat downstream faces flatter than 1V:2H all had worst-case FS values of greater than 2.

An important outcome presented herein is of the strength of the surficial exit gradient that is directly under the seepage-face, as a force destabilizing particles residing on this surface. This gradient was not found to exceed about 0.75, in any of the cases considered. This however is enough to destabilize particles smaller than about 0.3 m in diameter, especially as the toe slope approaches 1V:1H and as the overflow velocity approaches 3 m/s.

Given the fact that equation [2.19] uses certain approximations (such as to the value of C_D), it is recommended that in cases wherein the FS for IoM is less than about two, further and more detailed studies be conducted.

CHAPTER 3 USE OF INDEX GRADIENTS AND DEFAULT TAILWATER DEPTH AS AIDS TO HYDRAULIC MODELING OF FLOW-THROUGH ROCKFILL DAMS[1]

3.1. ABSTRACT

To assess the potential for unraveling failure of flow-through rockfill dams, a systematic study of three aspects of the hydraulic design of these structures was conducted. The first concerned finding that gradient which is most useful in independently computing the height of the point of first flow emergence. The method presented is based on the idea of the angle of the emergent flow field within the toe of the structure. As an outcome, the second presents a method for independently computing the variation in hydraulic head within that vertical which allows the toe of the structure (*i.e.* downstream of the vertical associated with first flow-emergence) to be isolated. It is based in part on a separate parametric study of 24 numerically-simulated flow-through rockfill dams. In the third, the gradient that will allow for the independent estimation of the default tailwater depth is presented and verified, with the help of laboratory results. It is hoped that these three computational tools will facilitate the design and assessment of flow-through rockfill structures, as a particular class of pseudo-hydraulic structure.

Key Words: embankments, barrages of coarse porous media, flow-through rockfill, non-Darcy seepage, unraveling failure, initiation of motion, hydraulic gradients, default tailwater, boundary conditions.

---

[1] With Permission from ASCE (see Appendix C).
Hansen D., and Roshanfekr A. 2012b. Use of index gradients and default tailwater depth as aids to hydraulic modeling of flow-through rockfill dam. ASCE Journal of Hydraulic Engineering, 138(8):726-735.
Note: Numerical and experimental works presented in this chapter were conducted by the second author.

3.2. INTRODUCTION

So-called flow-through rockfill dams and drains have various physical manifestations, often serving to attenuate and delay inflow hydrographs, or simply representing expedient places to deposit mine-waste rock at mountainous mine sites. These structures are not barrages in the ordinary sense, acting more as hydraulic structures made out of very coarse porous media. They have become sufficiently common that matters of safety to be considered in their design are laid out in Section 8.5 of the 2007 Canadian Dam Safety Guidelines (CDA 2007). The quantity of water passing through these 'dams' is much larger than for any true dam, and the mechanism of failure is most often a progressive 'unraveling' of the downstream toe (Wilkins 1956, Parkin *et al.* 1966). This process is due to the large amounts of seepage exiting under high hydraulic gradients. The idea of unraveling failure is that the initiation-of-motion (IoM) of one or perhaps a few stone particles results in impacts on particles further down the seepage-face (Figure 3.1), destabilizing them into motion, and so on (Wilkins 1956, Parkin 1963, Gerodetti 1981). The implied 'domino effect' may be overstated - the simultaneous movement of many particles at the toe (*i.e.* downstream limit of B_d) may be at least as disastrous, especially since there may be nothing to prevent the last 'row' of particles from moving downstream.

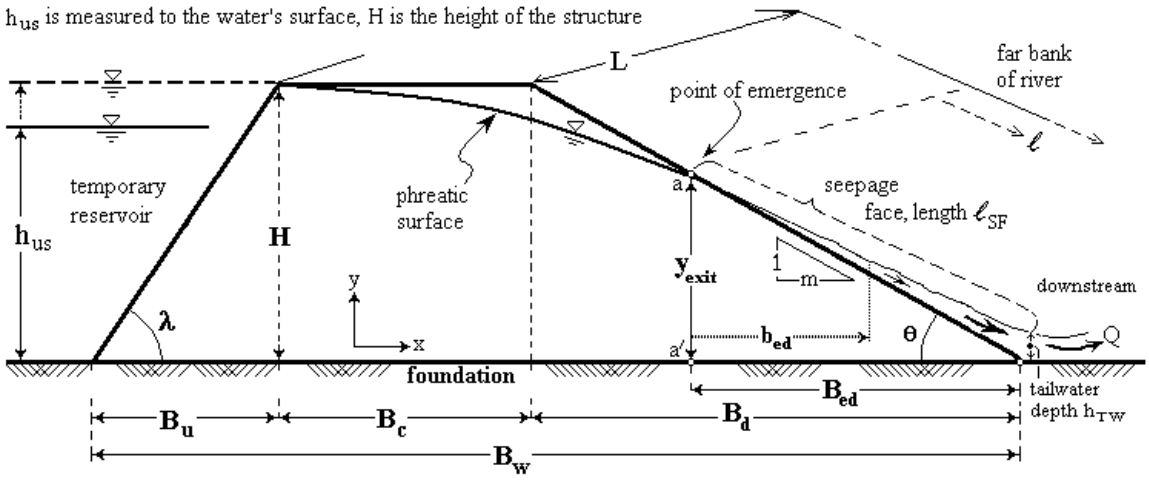

Figure 3.1. Nomenclature for rockfill dam of width B_w with constant flow Q passing through it.

The amount of flow through fine-grained porous media can normally be estimated using Darcy's Law. Darcy's linear law is not valid at medium-to-high Reynolds numbers. It is generally accepted that the transition from linear laminar to non-linear turbulent flow through porous media is a gradual one (Wright 1968, McCorquodale *et al.* 1978, Fand and Thinakaran 1990), although there is no agreement on the value of the Reynolds number at which purely Darcian flow ceases. Due to the nature of turbulent flow in rockfill, the flow must be estimated using a non-linear equation. There are two functional forms that are commonly used to describe the relation between the hydraulic gradient (i) and the bulk velocity (V) for non-Darcy flow, the power function (equation [3.1a]) and the zero-intercept second-order polynomial (equation [3.1b]). The power function was first proposed by de Prony (1804) and has more recently been applied to phreatic surface computation by Hansen *et al*. (2005). The zero-intercept second-order polynomial form was first proposed by Forchheimer (1901). The well-known Ergun equation (Ergun 1952) can be stated in this polynomial form and a form of it has been applied to partially-developed turbulent flows in porous media by Fand and Thinakaran (1990). George and Hansen (1992) have shown how α and N are linked to r and s, and *vice versa*.

$$i = \alpha V^N \qquad [3.1a]$$

$$i = rV + sV^2 \qquad [3.1b]$$

where:

α, r, s= non-Darcy coefficients,
N= turbulent exponent for non-Darcy flow ($1 \leq N \leq 2$).

The toe of flow-through rockfill structures is the primary zone of engineering concern (Hansen *et al.* 2005). It is located under the seepage-face. Three index or representative hydraulic gradients are considered in the context of interest in the hydraulics of the toe: **(i)** The gradient most useful in independently computing the height of the point of first emergence relative to the foundation (denoted y_{exit} in Figure 3.1). This exit height is also the beginning of the seepage-face. In this connection the application of previous research on the angle of the emergent flow field (θ_{ff}) is explained and presented in the next section. **(ii)** A general method for independently computing the

variation in hydraulic head within the vertical that has, as its upper terminus, the point of first flow emergence. Such a method would make possible the hydraulic isolation of that part of the toe of the structure which is downstream of the y_{exit} vertical. This, it will be shown, is associated with the hydraulic gradients within the whole vertical making up y_{exit}. **(iii)** The gradient that will allow independent estimation of the default tailwater depth. It will be shown that this is somewhat related to the previously established concept of the effective hydraulic gradient (Hansen *et al.* 1995), which can be used to quantify the amount of flow that will pass through the structure.

3.3. ESTIMATING HEIGHT OF POINT OF FIRST EMERGENCE

An important fundamental quantity in characterizing a given flow-through rockfill embankment is the height (y_{exit}) of the point of first emergence of the flow on its downstream side, which height also represents the start of the seepage-face. The exit height is fundamental because it can be used to develop a rating curve for the structure, no unraveling occurs above this elevation, and because below it the seepage-face forms the boundary condition. A non-Darcy flow equation such as the Stephenson (1979) equation may be used to help determine the location of this position:

$$V = n\sqrt{\frac{gd}{K_{Steph}}i} \qquad \text{(fully-developed turbulence)} \qquad [3.2a]$$

$$K_{Steph} = \frac{800}{Re} + \kappa_{ang} \qquad [3.2b]$$

$$i = \frac{K_{Steph}}{gdn^2}V^2 \qquad \text{(\textit{i.e.} a form of equation [3.1a])} \qquad [3.2c]$$

$$q = Vy_{exit} \ (\equiv Q/L) \qquad [3.2d]$$

where:

V= bulk velocity (L/T),
Q= total discharge through embankment (L^3/T),
L= length of the embankment (L),
g= gravitational constant (L/T^2),
d= representative particle diameter (L),

n= porosity of the rockfill matrix (dimensionless),
$Re = Vd/(n\nu)$ = Stephenson's particle Reynolds number (dimensionless),
ν = kinematic viscosity (L^2/T),
κ_{ang} = value ranging from 1 for smooth spheres to 4 for angular stones (dimensionless),
q= unit discharge through embankment (L^2/T),
y_{exit}= height (*i.e.* depth, *cf.* Figure 3.1) of point of first emergence (L).

In the current study K_{Steph} was assumed to be its asymptotic value of 4.0, which is associated with a high Reynolds number (fully developed turbulence) and angular stones. The idea that the exit gradient that acts beneath the seepage-face and within the toe may be approximated by the tangent of the toe angle θ has been mentioned by Leps (1973) as a matter of engineering practice. It may be expected, however, that the true angle representative of the emergent seepage field is less than θ, that this effective flow angle θ_{ff} varies with the relative exit height, and that it approaches θ as the relative exit height increases, as in Figure 3.2. The angle θ_{ff} is not the angle with which an extended free surface would arrive at the ground surface. It is an imaginary angle that best represents the exit gradient for the flow emerging from the toe. The hydraulic gradient $\tan\theta_{ff}$ was inferred via hydraulic calculations that were based on knowledge of the exit height and the flow rate (see Hansen *et. al* 2005). For non-Darcy flow in a crushed limestone ($N \cong 2$ in equation [3.1a]), Hansen *et al.* (2005) found that:

$$\frac{\theta_{ff}}{\theta} = 1.41\frac{y_{exit}}{H} + 0.17 \qquad r^2=0.8,\ n_{obs}=33 \quad [3.3]$$

where:
H= height of the dam (L),
θ = angle at the downstream toe,
θ_{ff} = angle of the emergent flow field within the toe.

This equation was found to work best if y_{exit} was less than 0.5H, in keeping with the range of the available raw data. If we assume that, for the toe $i_{exit} = \tan\theta_{ff}$ and substituting θ_{ff} from equation [3.3] into equation [3.2c] to get V, y_{exit} can be simply obtained as:

$$y_{exit} = \frac{q}{V} = \frac{q}{n\sqrt{\frac{gd}{K_{Steph}} i_{exit}}} \qquad [3.4]$$

for the q of interest, where:

i_{exit} = hydraulic gradient most suitable for use in finding y_{exit} (dimensionless).

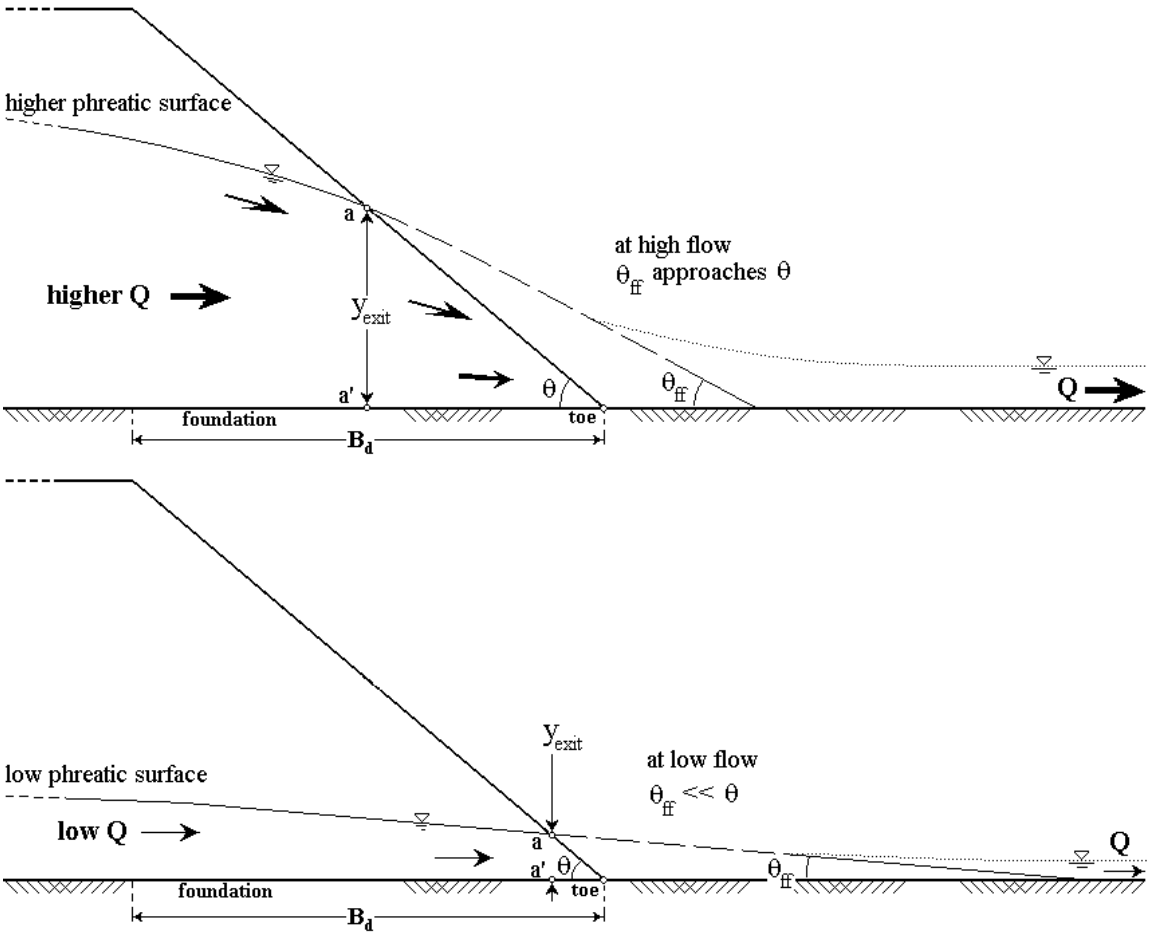

Figure 3.2. Illustration of concept of angle of emergent flow-field, θ_{ff} .

This approach can be used to find the height of the point-of-emergence for the embankment of interest. Although the Stephenson (1979) equation has been suggested and was used in the companion work (Hansen and Roshanfekr 2012a), the same procedure could be followed using any non-Darcy flow equation, of which there are many (*e.g*. review of Hansen *et al.* 1995). Knowing the exit height (y_{exit}) permits

estimation of the hydraulic head beneath the point of emergence and therefore the isolation of the toe, to be described in the next section.

3.4. ISOLATION OF TOE (DOWNSTREAM OF Y_{EXIT} VERTICAL)

There are two main reasons why an analyst might want to isolate the toe of a flow-through rockfill structure (*i.e.* the triangular zone of coarse porous medium between the y_{exit} vertical and the downstream tip of B_{ed} in Figure 3.3a):

i) the face of this zone is probably the most failure-prone (Hansen *et al.* 2005) and deserves the maximum amount of numerical detail (*i.e*. a very fine mesh or grid, in terms of spatial discretization).

ii) this portion of the embankment is a simple triangle that is completely bounded by exterior heads. From a geometric point of view this means that it is easier for the modeler to specify the boundary conditions. By contrast, the phreatic surfaces within these structures, present upstream of the y_{exit} vertical, are always curved. Although these curves can be adequately approximated by a numerical mesh or grid, the more accurate the approximation the more tedious it is to achieve a geometrically precise mesh. Numerical schemes that seek out an appropriate phreatic surface involve relatively complex coding because any given approximation to an assumed phreatic surface (in the iterative sense) requires that the outcome of a given search be checked against the laws governing such surfaces (Cedergren 1989) and against the flow rate within any given vertical implied by the assumed height of the surface. Said discharge is uni-valued if the flow is steady and can be determined by independent means (Hansen *et al*. 1995). In general, it is probably computationally easier to locate the phreatic surface independently using a method such as that described by Hansen *et al.* (2005) and used in Hansen and Roshanfekr (2012a), and then impose it on the mesh, using said rules (Bari and Hansen 2002) as long as an accurate y_{exit} value is in hand. Hansen and Bari (2002) have formally investigated the uncertainty in this algorithm.

Described herein is a way to allow the analysis to efficiently focus on the toe, specifically, the triangular zone downstream of y_{exit}. Large dams, as well as dams

requiring analysis at a high level of detail, may imply the need for very large grids or meshes. Such grids can require orders-of-magnitude more grid relaxations before numerical results can be relied upon. Further, the inclusion of the phreatic surface is a rather involved aspect of a given set-up, in that it is independently calculated and the numerical grid then locally adapted to it. Yet, not all of the dam structure is of equal interest with respect to the failure mode of unraveling. It is the toe, particularly the gradients beneath the seepage-face, which are of prime interest. Highly-detailed modeling might be able to focus only on the toe if the boundary conditions on it, or around it, could be well represented. These conditions have two key planes: the boundary whereby the toe abuts against the rest of the dam (*i.e*. the vertical upstream side of the toe that is directly below the point of first emergence), and the seepage-face. The third plane or boundary, the foundation on which the toe and the dam rest, was assumed to be impermeable.

For the work described herein, the determination of many phreatic surfaces was done as part of the modeling of the hydraulic heads within 24 dams taken in their entirety. The information arising from the parametric study described in Hansen and Roshanfekr (2012a) was then examined and distilled. One of the outcomes of the gross modeling done in the parametric study was a clear pattern of heads through the y_{exit} vertical. This information allowed computational efforts to be focused on the zone inclusive of and downstream of the y_{exit} vertical, *i.e*., the triangular zone where unraveling failure typically begins.

Hansen and Roshanfekr (2012a) have provided details regarding optimal finite difference (FD) modeling strategies, but it may be noted from previous studies of lateral seepage patterns through trapezoidal shapes having a phreatic surface and a point of emergence (*e.g.* Townsend *et al.* 1991, Hansen *et al.* 1995) that the equipotential lines (EPL's) through said surface and then downstream of the terminus of B_C form a series of concentric quarter-ellipses, but with unequal spacing. Clearly, points a and $a^{//}$ in Figure 3.3a have the same hydraulic head because of the existence of the EPL through point a. It was surmised that if the head $h_{a/}$ could be rationally computed, then studies of the

variation in head between points a and a/ would enable the desired isolation to be accurately set up. The hydraulic head at position a// is equal to y_{exit}.

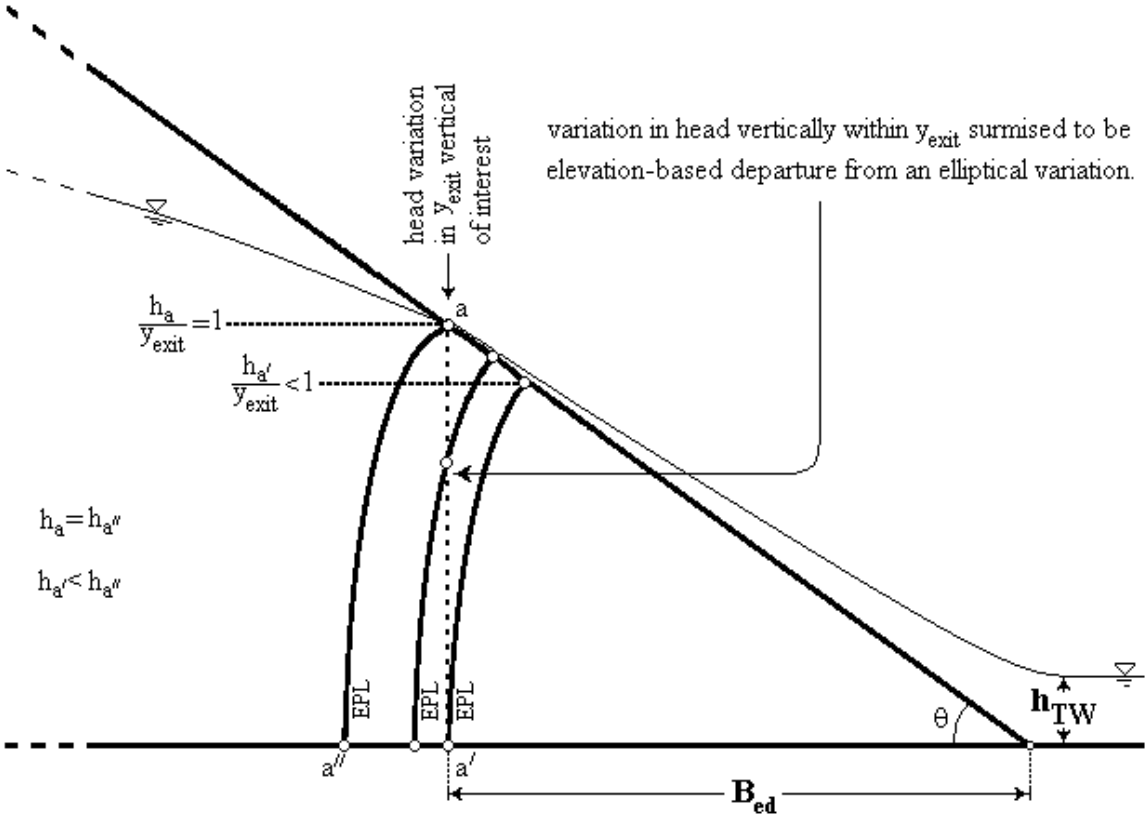

a) EPL's through y_{exit} vertical.

Figure 3.3. Schematic view of the parameters used for toe isolation in y_{exit} vertical.

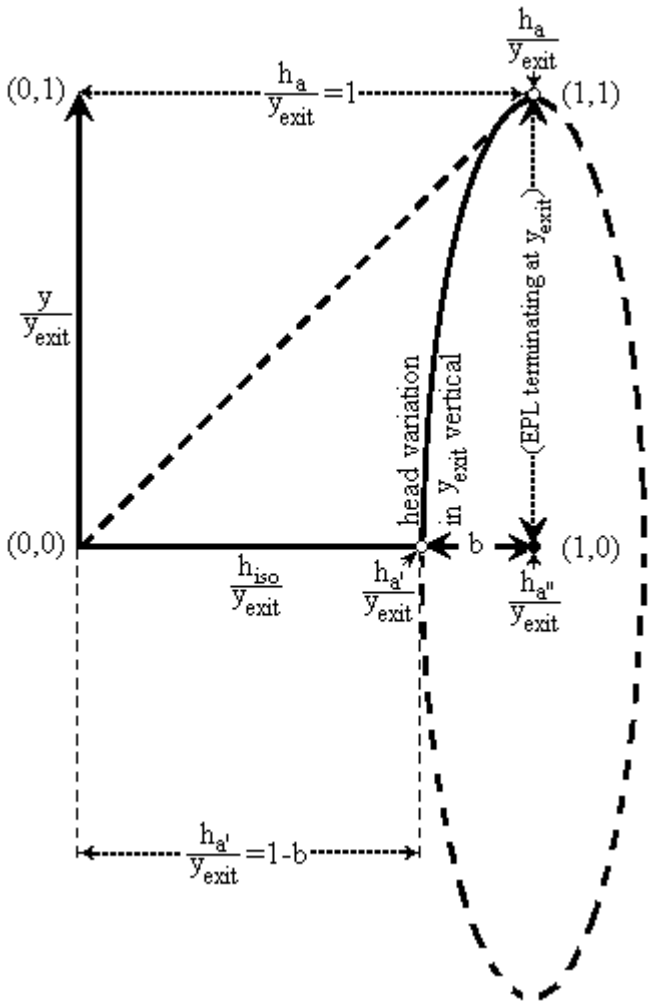

b) head variation in y_{exit} vertical using the quarter of an ellipse approximation.

Figure 3.3 (Cont). Schematic view of the parameters used for toe isolation in y_{exit} vertical.

It was also surmised that a good fit for the variation in head between points a and $a^{/}$ (*i.e.* through the y_{exit} vertical) would be a quarter ellipse (Figure 3.3b). This variation has the advantage that it forces the EPL to be perpendicular to the foundation at $h_{a''}$. Although it does not imply the correct flowline slope at the apex, it is head itself and not its rate of change that is under consideration. In accordance with Figure 3.3b an elliptical equation for the variation in head through the y_{exit} vertical is then:

$$\frac{(X-1)^2}{b^2}+\frac{(Y)^2}{1^2}=1 \qquad [3.5]$$

where:

b = difference in dimensionless heads $h_{a/} / y_{exit}$ and $h_{a//} / y_{exit}$,
$X = h_{iso}/y_{exit}$,
$Y = y/y_{exit}$,
h_{iso}= hydraulic head at any given point within y_{exit} vertical,
y = height of point where hydraulic head (h_{iso}) is calculated.

Under this arrangement, h_{iso}/y_{exit} varies from $h_a^{/}/y_{exit}$ (=1-b) to h_a/y_{exit} (=1). By substitution and rearrangement:

$$\frac{h_{iso}}{y_{exit}} = 1 \pm b\sqrt{1 - \frac{y^2}{y_{exit}^2}} \qquad [3.6]$$

It is expected that for point $a^{/}$ the hydraulic head (h_{iso}) value will be less than y_{exit}, thus excluding the positive sign outcome. If the value of 'b' could be independently determined, equation [3.6] can be used to calculate the heads in the y_{exit} vertical (h_{iso}) for each individual point or nodal location of interest. It was expected that the lower the imposed tailwater depth and the steeper the downstream face, the greater would be the amount of curvature in the head variation through the y_{exit} vertical.

The partial differential equation behind the numerical model used is known as a *p*-LaPlacian (Vazquez 2007). It applies to boundary value problems wherein the relationship between flux and the gradient of the scalar potential is non-linear, as is the case with high-Reynolds-number non-Darcy flow. It was solved using a non-linear hydraulic conductivity adaptation of equation [3.1a] within a five-point FD scheme (*cf.* Hansen and Roshanfekr 2012a). Twenty four numerically-based models (detailed in Hansen and Roshanfekr 2012a) with a range of imposed tailwater levels were developed and the grids for each fully resolved (complete convergence); the resulting 'b' values for these models using different h_{TW}/h ratios are presented in the Tables 3.1 to 3.3. In order to predict the 'b' value, a correlation between several parameters and the observed 'b' values was sought. The best model for the twenty four cases was found to be:

$$b = 0.308\left(\frac{H}{B_c}\right)^{-0.353}(\tan\theta)^{1.220}\left(0.196 - \frac{h_{TW}}{h_{us}}\right)^{0.879} \quad r^2=0.924,\ n_{obs}=72 \qquad [3.7]$$

Equation [3.7] was obtained via ordinary least squares regression of ln-transformed data and included a correction for the bias caused by non-linearity of the transformation. In application, the above equation is constrained to the ranges $0.16 \leq \tan\theta \leq 1$ and $0.5 \leq H/B_c \leq 3$ and to tailwater depths limited to $h_{TW}/h_{us} \leq 0.1$. The model presented in equation [3.7] can be used to calculate a primary value for 'b'. A comparison of calculated versus observed values of this parameter is shown in Figure 3.4.

Table 3.1. Values of 'b' for with h_{TW}/h_{us} = zero (24 embankments).

$\frac{h_{TW}}{h_{us}} = 0.00$	Slope of Toe					
	1V:1H	1V:2H	1V:3H	1V:4H	1V:5H	1V:6H
$H/B_c = 0.5$	0.0900	0.0590	0.0210	0.0140	0.0120	0.0100
$H/B_c = 1.0$	0.0650	0.0400	0.0190	0.0125	0.0100	0.0080
$H/B_c = 2.0$	0.0600	0.0300	0.0150	0.0065	0.0060	0.0055
$H/B_c = 3.0$	0.0520	0.0170	0.0120	0.0050	0.0035	0.0025

Table 3.2. Values of 'b' for with h_{TW}/h_{us} = 0.05 (24 embankments).

$\frac{h_{TW}}{h_{us}} = 0.05$	Slope of Toe					
	1V:1H	1V:2H	1V:3H	1V:4H	1V:5H	1V:6H
$H/B_c = 0.5$	0.0650	0.0490	0.0145	0.0080	0.0070	0.0060
$H/B_c = 1.0$	0.0550	0.0340	0.0125	0.0060	0.0055	0.0050
$H/B_c = 2.0$	0.0500	0.0240	0.0110	0.0030	0.0025	0.0020
$H/B_c = 3.0$	0.0400	0.0120	0.0075	0.0020	0.0010	0.0005

Table 3.3. Values of 'b' for with h_{TW}/h_{us} = 0.10 (24 embankments).

$\frac{h_{TW}}{h_{us}} = 0.10$	Slope of Toe					
	1V:1H	1V:2H	1V:3H	1V:4H	1V:5H	1V:6H
$H/B_c = 0.5$	0.0450	0.0400	0.0080	0.0035	0.0025	0.0015
$H/B_c = 1.0$	0.0380	0.0280	0.0070	0.0030	0.0020	0.0010
$H/B_c = 2.0$	0.0350	0.0180	0.0065	0.0025	0.0010	0.0004
$H/B_c = 3.0$	0.0250	0.0055	0.0040	0.0020	0.0005	0.0002

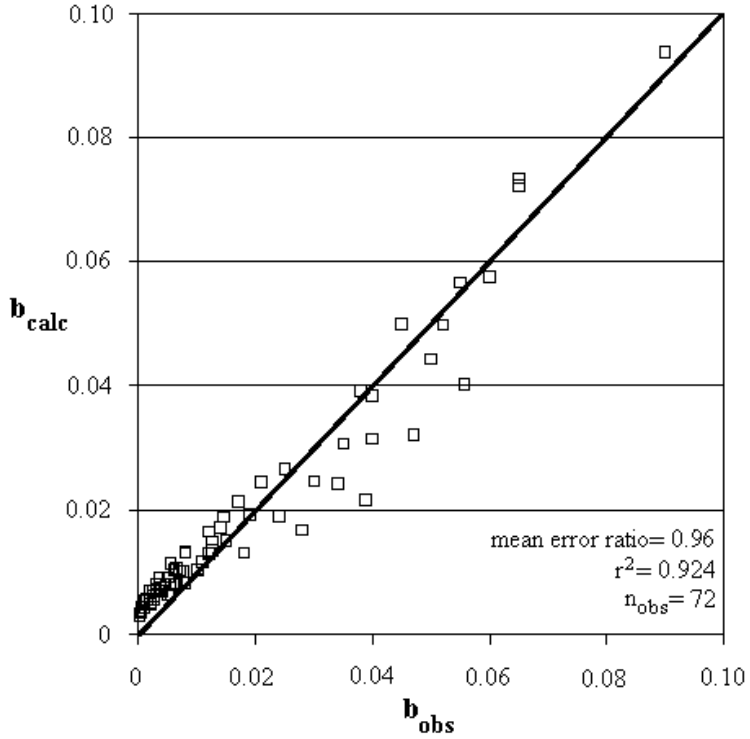

Figure 3.4. Comparison and correlation between the calculated and observed 'b' values.

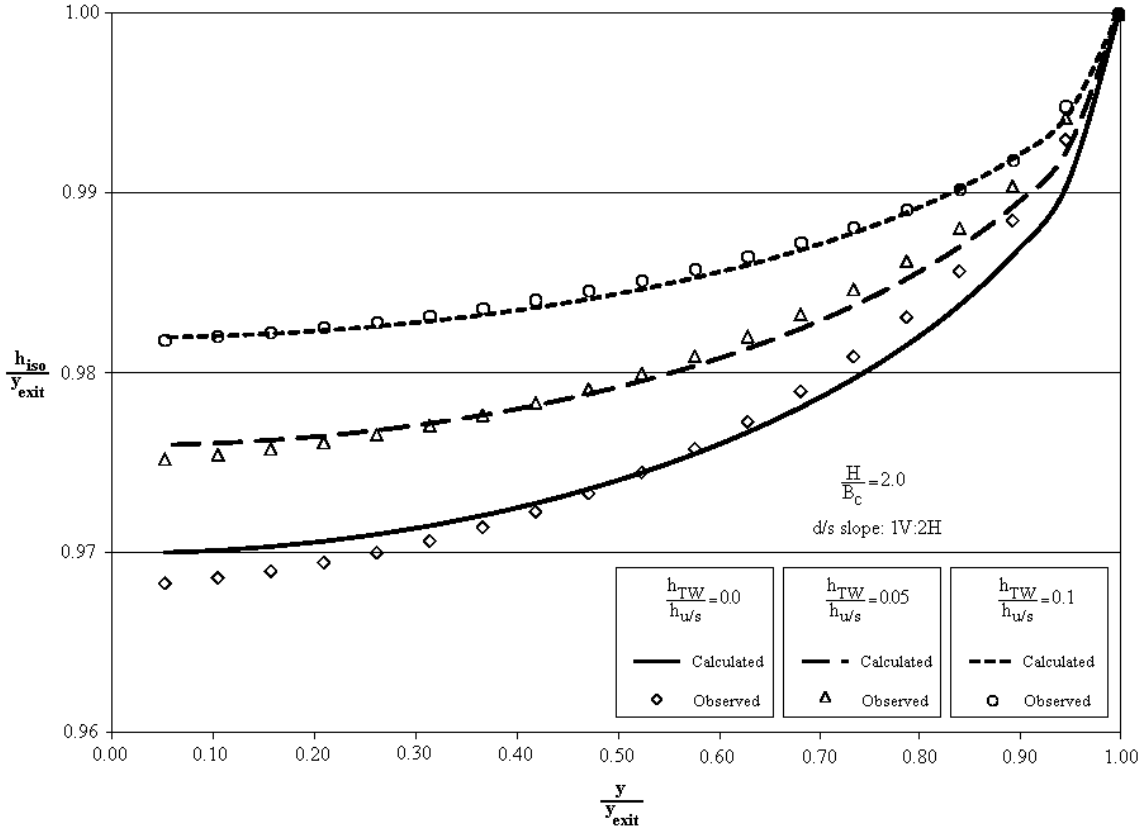

Figure 3.5. Effect of tailwater on the head variation in the y_{exit} vertical for isolation of the toe.

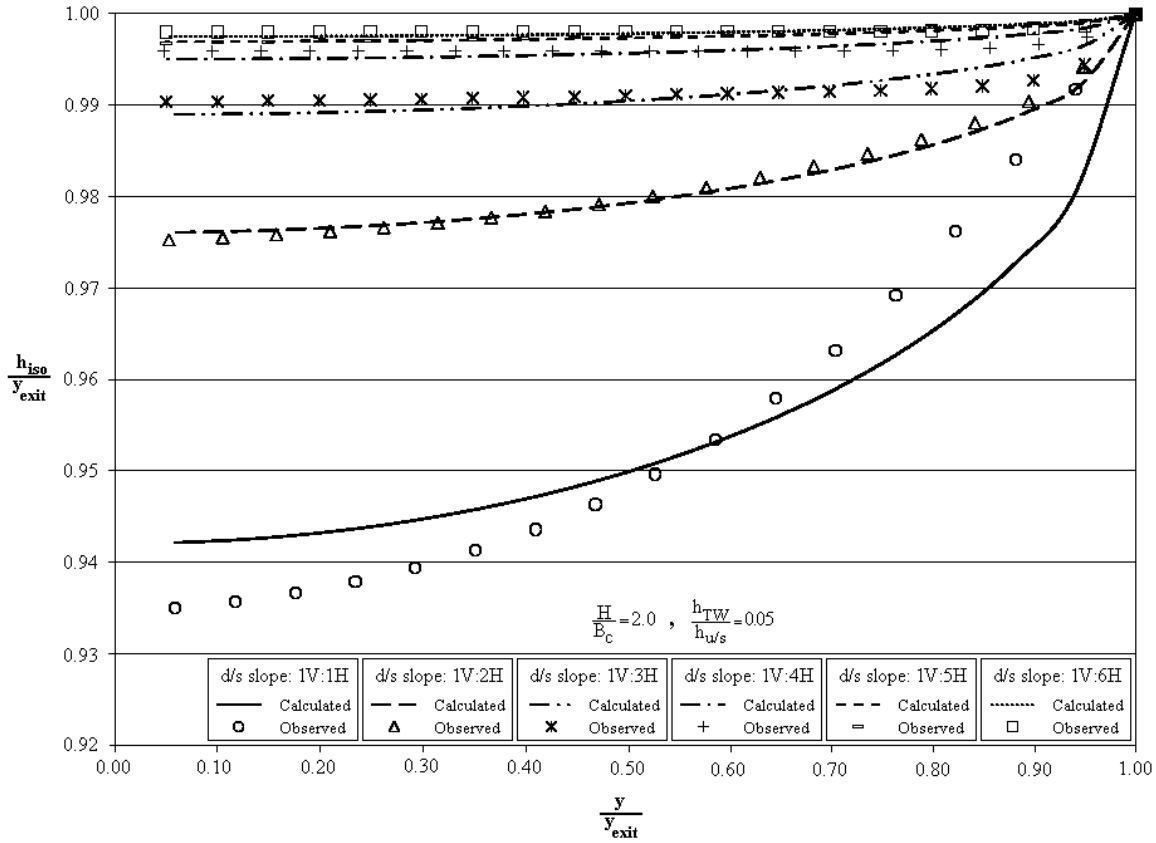

Figure 3.6. Effect of different slopes on the head variation in y_{exit} vertical for isolation of the toe.

Figures 3.5 and 3.6 show that the general level of agreement between those heads predicted using equations [3.6] and [3.7] and numerically simulated hydraulic heads is in fact excellent, in most cases. The level of agreement declines somewhat for dams with small longitudinal extent in the upstream-downstream direction and steep downstream faces. The fitted curves in Figures 3.5 and 3.6 do exhibit what is known as 'lack of fit'. That is, there is a distinct to the residuals and this might have been removed via choice of a better model. Although it is true that a polynomial of (say) 5th order could be fitted very exactly to the points seen in Figures 3.5 and 3.6 (representing hydraulic head) this was not done because:

i) Treatises on seepage, drainage, and flow nets (such as those of Cedergren 1967, 1977, 1989) clearly show that the equipotential 'lines' within the downstream toe resemble quarter-ellipses.

ii) The adjustment of the parameters in a single quarter-ellipse-based equation was considered to be more elegant than simply obtaining a collection of polynomials.

iii) When it was discovered that the discrepancies between the 'true' hydraulic heads presented by the points in Figures 3.5 and 3.6 and the quarter ellipse curves was very small (at most 1% of h_{iso}/y_{exit}), it was decided that this parametric single-equation approach was adequate for engineering purposes.

The worst error in the head ratio was found to be only about 1%. This was for the steepest downstream slope and for the fictitious case of no imposed tailwater depth. A slope as steep as the typical angle of repose of coarse granular material is generally not used in design. This 1% error would be considerably less than the uncertainty associated with the bounding condition that is present on the downstream side of the triangular zone in question, namely, the depth of the flow over the seepage-face. In general it was found that, if the tailwater is relatively high and the downstream face relatively flat, the distribution of head within the y_{exit} vertical is nearly hydrostatic, and easy to approximate. The procedure for isolating the toe is given in Figure 3.7.

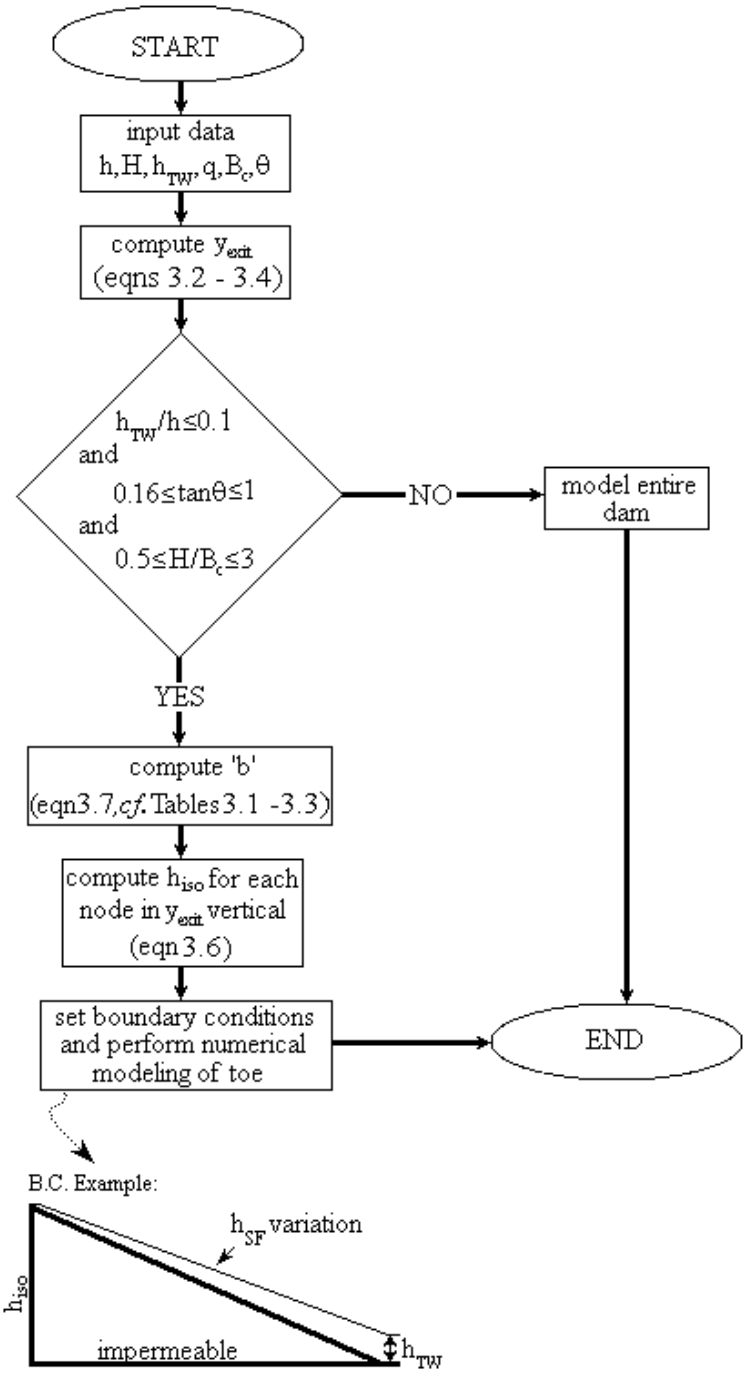

Figure 3.7. Procedure for isolating the toe.

3.5. ESTIMATING DEFAULT TAILWATER DEPTH (H_{TW})

The default tailwater depth refers to the depth that the tailwater reverts to if there is no higher depth imposed on the downstream face from downstream, by the receiving

channel. It can be thought of as being part of the self-generated boundary condition constituting the seepage-face, being the downstream limit of said seepage accumulation. By way of background, Hansen *et al.* (1995) developed the concept of effective hydraulic gradient (i_{eff}) in order to study a representative hydraulic gradient for the entire embankment, using the adaptation of 1-D flow equation to 2-D models and embankments. In order to calculate the hydraulic gradient for use in equations [3.2d] (*i.e.* discharge calculation, see also notes on Table 3.6) the concept of effective hydraulic gradient was applied. It can be written:

$$i_{eff} = 0.8A_R^{-3/2}\left(\frac{h_{us}}{H}\right)^{1.4} \qquad r^2=0.98,\ n_{obs}=48 \quad [3.8a]$$

which

$$A_R = \frac{1}{H}\left(B_u + B_c + 0.5B_d\right) \qquad [3.8b]$$

where:

h_{us}= upstream water level (L),
H= height of the embankment (L),
A_R= aspect ratio of the embankment (dimensionless),
B_u= width of the upstream portion (L),
B_c= width of the crest portion (L),
B_d= width of the downstream portion (L).

In general, the variation in the tailwater depth, especially the default depth h_{DTW}, is small for flow-through structures not subjected to any backwater effects from the downstream receiving channel (Hansen 1992). According to equation [3.8a] the effective hydraulic gradient is largely a function of the shape of the embankment and the upstream depth, relative to the height of the dam, the default downstream water level *per se* does not have much effect on the effective hydraulic gradient (Hansen *et al.* 1995). The concept and practical usefulness of the effective hydraulic gradient has already been established (Hansen *et al.* 1995).

Flow through any porous medium is driven by the boundary conditions. In most cases these conditions are imposed and obvious. In the case of flow-through rockfill structures, the downstream boundary condition is not uni-valued. When the discharge varies significantly in the direction of flow, whether positively or negatively, it is classified as spatially-varied flow (SVF). Sharp and James (1963) were apparently the

first researchers to classify the seepage-face at the toe of a rockfill slope as a case of SVF with increasing discharge. The quantity of flow within it varies from zero at $\ell = 0$ to the total discharge passing through the dam at $\ell = \ell_{SF}$ (see Figure 3.1).

It is also obvious that there is no single flow path. It is suggested that representative values may suffice. Since any hydraulic gradient is the ratio of a difference in boundary conditions (hydraulic heads) to a flow path length, it follows that:

$$i_{DTW} = \frac{h_{us(rep)} - h_{ds(rep)}}{\ell_{rep}} \qquad [3.9]$$

where:

i_{DTW} = hydraulic gradient suitable for finding default tailwater depth (dimensionless),
$h_{us(rep)}$ = representative[1] upstream head (L),
$h_{ds(rep)}$ = representative downstream head (L),
ℓ_{rep} = representative length of mean flow path (L).

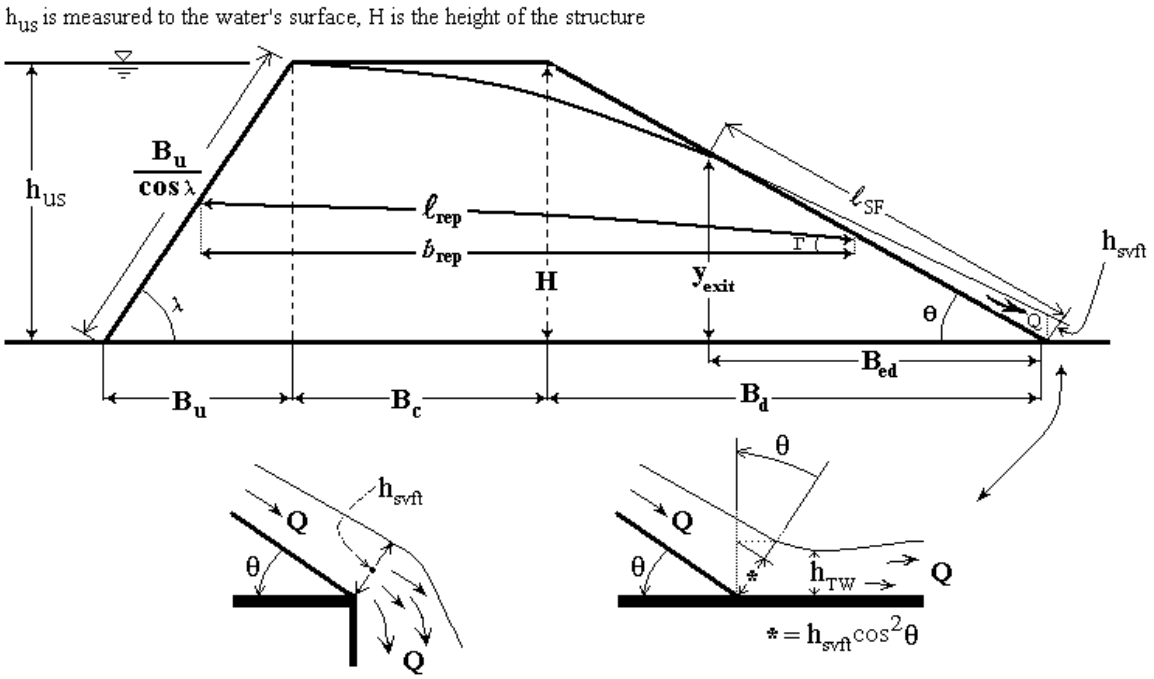

a) free-fall (drop off). **b)** no free-fall but h_{svft} has about same magnitude as (a).

Figure 3.8. Definitions relating $h_{svft}\cos^2\theta$ to y_{exit}.

[1] The question of what head is adequately representative is presented in the theory following.

The quantity h_{svft} is the depth at the termination of the SVF zone (end of the seepage-face, Figures 3.1 and 3.8). Figure 3.8 shows that the depth in the channel just downstream of the terminus of B_{ed} may be comparable to $h_{svft}\cos^2\theta$ at sufficiently low flows.

The situation at the toe can be compared to that present downstream of a hydraulic structure that introduces supercritical flow in a pre-existing hydraulically mild channel. The condition excluded from consideration herein is that of having a tailwater depth that is so high that the hydraulic jump (HJ) is drowned and this level is then able to impinge directly upon the downstream face of the structure. Data associated with very low flows in the receiving channel was also excluded from the default tailwater (DTW) studies. At low flows the exit height was only slightly greater than the default depth over the toe h_{TW} (Figure 3.9), which was in turn only slightly greater than the normal depth (y_n) of the receiving channel. There being no free-fall condition (physical brink) at the toe, the Froude number associated with this h_{TW} was experimentally found to be sub-critical. At small depths the magnitude of h_{TW} relative to the normal depth of the receiving channel (if there is one) therefore becomes important. Data associated with subcritical flow being present over the toe were not considered in the analysis.

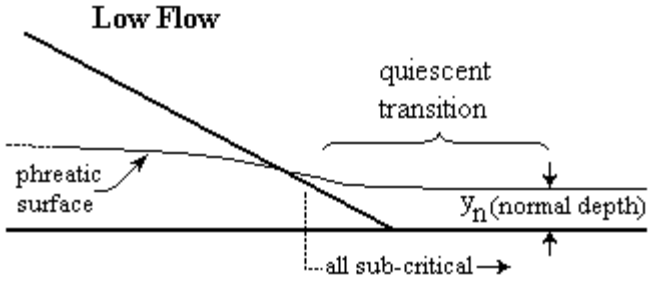

a) tailwater depth less than but comparable to h_{TW} – data excluded.

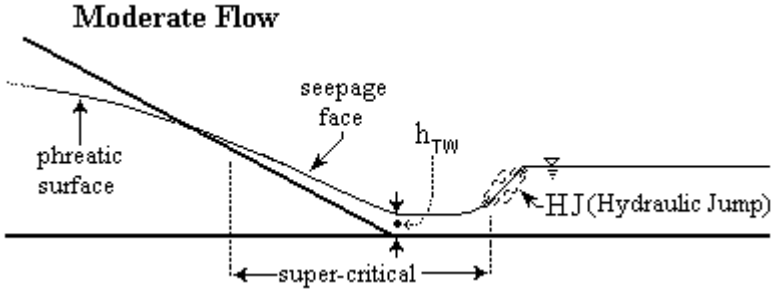

b) tailwater depth at toe governed by (at) default condition – data included (M3 wsp probably forms).

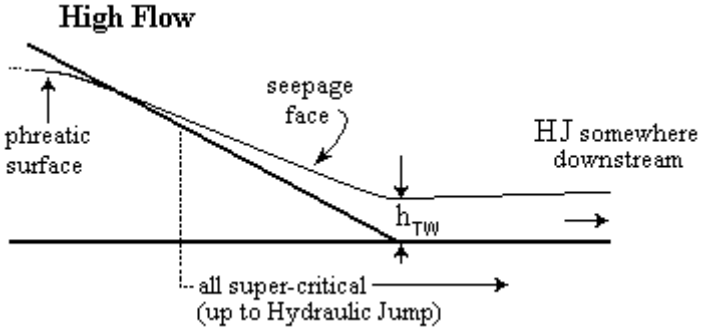

c) tailwater depth at toe also governed by default condition – data included (slope of foundation is very small).

Figure 3.9. Behavior of tailwater with increasing flow.

The representative upstream hydraulic head is obviously h. If $h_{us} = H$, let it be assumed that the 'entry point' of ℓ_{rep} is midway along $B_u/\cos\lambda$ and that the exit point of ℓ_{rep} is midway along ℓ_{SF}. Again for $h_{us} = H$, the representative mean flow path b_{rep} may then be thought of as being comprised of B_u, B_c and B_d components (Figure 3.8):

$$\ell_{rep} = \frac{b_{rep}}{\cos\Gamma} \qquad [3.10a]$$

where:
$$\Gamma = \arctan\left(\frac{h_{us} - y_{exit}}{2b_{rep}}\right) \qquad [3.10b]$$

and where b_{rep} is the straight-line path of flow line, which for a full upstream reservoir (h_{us}=H) can be written:

$$b_{rep} = \frac{B_u}{2} + B_c + \left(B_d - \frac{1}{2}\ell_{SF}\cos\theta\right) \qquad [3.11a]$$

More generally, and for an upstream head h that is less than H, b_{rep} can be written in the following forms:

$$b_{rep} = \left(B_u - \frac{h_{us}}{2\tan\lambda}\right) + B_c + \left(B_d - \frac{1}{2}\left(\frac{y_{exit}}{\sin\theta}\right)\cos\theta\right) \qquad [3.11b]$$

or:
$$b_{rep} = B_w - \frac{1}{2}\left[\frac{h_{us}}{\tan\lambda} + \frac{y_{exit}}{\tan\theta}\right] \qquad [3.11c]$$

The above equations ignore the slight curvature of the ℓ_{rep} path. It might be expected that the depth averaging and other geometric approximations mentioned above will cause the ℓ_{rep} so computed to be slightly shorter than reality, so that:

$$\ell_{rep} = C_{path}\left[\frac{b_{rep}}{\cos\Gamma}\right] \qquad [3.12]$$

The value of C_{path} in [3.12] may be expected to be slightly more than unity. If obtained from experimental observations on model flow-through rockfill structures, the value of C_{path} will be affected by limits on the accuracy of the h_{TW} measurements, made in a turbulent and rather undulating zone of flow.

The seepage-face is an interesting example of a class of open-channel flow known as SVF. An algorithm for handling this class of flow has been presented by Chow (1959) and others. Sharp and James (1963) investigated the particular manifestation considered herein, an investigation which is being continued by these authors. If the terminal water depth arising from the application of such an algorithm is h_{svft}, the boundary condition of interest is the hydraulic head as would be measured at the 'bed' of the 'channel' at the

exact tip of the toe of the dam, $h_{svft}\cos^2\theta$. The distinction between the hydraulic head at the bed and that depth measured at 90° to the bed is immaterial for typical river-bed slopes[1], but this laxitude should not be blindly allowed in this case because θ large. Again, the case under consideration here is the case of zero imposed-backwater, meaning that h_{svft} is allowed to form as part of the self-generated downstream boundary condition which the entire seepage-face represents, and right at the toe of the embankment. The case of some higher imposed depth, such as the normal depth of the receiving river channel, may well also be of interest but is not in view at this point in the analysis.

If an index of the representative downstream head is then $y_{exit}/2 + (h_{svft}\cos^2\theta)/2$, combining [3.12] and [3.9] yields:

$$i_{DTW} = \frac{h_{us} - 0.5\left(y_{exit} + h_{svft}\cos^2\theta\right)}{C_{path}\left[\frac{b_{rep}}{\cos\Gamma}\right]} \qquad [3.13]$$

The above may be termed a path-based effective gradient, as distinct from an aspect-ratio based effective gradient. The latter has been described by Hansen *et al.* (1995), including how actual flow and depth data was used to infer it, for a range of embankment aspect ratios. Both of these effective gradients are more-or-less representative of the hydraulic gradient under which the entire structure appears to be operating, in a gross sense. It follows from [3.13] that:

$$h_{svft}\cos^2\theta = 2\left[h_{us} - C_{path} i_{DTW}\left(\frac{b_{rep}}{\cos\Gamma}\right)\right] - y_{exit} \qquad [3.14]$$

The engineering practitioner may not try to construct a water surface profile for the seepage-face using a formal spatially-varied (supercritical) flow analysis, leading to h_{svft} at the terminus. The shape of the seepage-face is indeed close to being a simple triangle, at least of various model structures (Hansen 1992). If the externally-imposed hydraulic head at the toe is simply denoted h_{TW} by the analyst as:

---

[1] Chow (1959) notes that the correction is less than 1% until θ is nearly 6º (1V:10H).

$$h_{TW} = 2\left[h_{us} - C_{path} i_{DTW} \left(\frac{b_{rep}}{\cos \Gamma} \right) \right] - y_{exit} \qquad [3.15]$$

it was surmised that the distinction between $h_{svft}\cos^2\theta$ and h_{TW} might not be fatal to the usefulness of the available laboratory data nor to the predicted results for tailwater depth. If in fact the receiving waters exert little backwater effect and there is therefore some question about the true condition at the toe in connection with a given value of h_{TW}, then a formal hydraulic analysis of the seepage-face and the receiving channel is indicated. Indeed, a merit of equation [3.15] is that it makes it possible to independently find an approximate value of the depth at the toe, the one that the structure itself will set up if given the freedom to do so (*i.e.* no backwater effects being imposed from downstream). As previously indicated, this should be compared to such depths as the normal depth of the receiving channel for the discharge of interest.

It was found to be difficult for laboratory measurements of tailwater to distinguish between h_{svft} and h_{TW} (see Appendix B). Although the flow was steady, the water surface profile was unsteady at the particle scale, and the spatially-uneven nature of the toe (comprised of gravel particles that always resulted in a rather imperfect wedge shape) resulted in as much lateral variability as longitudinal variability in the depth, right at the toe. It is important to note that the quantities h_{svft} and h_{TW} were found to be small compared to y_{exit}, and yet comparable to each other.

In order to calculate the C_{path} value, a series of model embankment tests were conducted in a glass walled flume at the hydraulics laboratories of Ottawa and Dalhousie Universities (Table 3.4). A framed wire mesh prevented erosion of the toe. This mesh was found to have very little effect on the seepage-face. For each embankment the experimental data were collected and tabulated. The values of α and N in the experiment were determined from packed-column tests performed on the same rockfill material and the porosity (n) of the rockfill material was measured (Table 3.5, also see Appendix B). The downstream depth was made to be a freefall - no downstream backwater condition was imposed. The depth variation in the SVF around the downstream toe of each embankment was measured and the curvature in the water surface profile noted. It was found that the amount of curvature increased with increasing toe angle.

The values of α and N in Table 3.5, together with equations [3.8] and [3.13], were used to calculate Q_{ieff} and Q_{DTW} (see notes on Table 3.6). In order to calculate the best C_{path} value a range of upstream depths (*e.g.* h_{us}= 0.5H, 0.75H, 0.9H and 1H) and discharges were imposed on each embankment and the default tailwater was measured at the downstream terminus of the toe. Table 3.6 shows the various mathematically inferred C_{path} values and the statistical results of a comparison of associated discharges.

Table 3.4. Geometries of model flow-through dams considered for comparison of i_{DTW} and i_{eff}.

Model #	**H** (cm)	**B_u** (cm)	**B_c** (cm)	**B_d** (cm)	$\frac{B_c}{B_w}$ (Figure 3.1)	**Slope of Toe**	**Laboratory**
1	50	50	33.3	50	25.0 %	1V:1H	U. of Ottawa
2	50	50	50.0	100	25.0 %	1V:2H	U. of Ottawa
3	50	50	66.7	150	25.0 %	1V:3H	U. of Ottawa
4	30	30	15.0	30	20.0 %	1V:1H	Dalhousie U.
5	30	30	15.0	60	14.3 %	1V:2H	Dalhousie U.
6	30	30	15.0	90	11.1 %	1V:3H	Dalhousie U.

Table 3.5. Some experimental details (flume sizes and characteristics of gravel), see also Appendix B.

	Flume Width (cm)*	**Slope of Flume**	**α (V in cm/s)**	**N**	**Porosity**
University of Ottawa	38.5	0.0001	0.0088	1.88	0.47
Dalhousie University	31.0	0.0000	0.0213	1.85	0.42

* Channel wall to channel wall, contrary to the sense of "width" in Figure 3.1. In industry, the "length" of an embankment is commonly taken to be the distance from riverbank to riverbank.

Table 3.6. Inferred C_{path} values and statistics of discharge comparisons.

	r^2	Mean Error Ratio[1]	RMSE (L/s)	No. of Data Points (n_{obs})
all discharge data used (C_{path}=1.04)				
Q_{obs}[2] vs Q_{DTW}[3]	0.988	1.04	0.659	22
Q_{obs} vs Q_{ieff}[4]	0.995	0.96	0.568	22
Q_{ieff} vs Q_{DTW}	0.992	0.92	0.673	22
only using discharges for $h_{us}/H>0.6$ (C_{path}=1.02)				
Q_{obs} vs Q_{DTW}	0.980	1.04	0.526	16
Q_{obs} vs Q_{ieff}	0.990	0.95	0.428	16
Q_{ieff} vs Q_{DTW}	0.985	0.91	0.539	16
only using discharges for $h_{us}/H=1$ (C_{path}=1.01)				
Q_{obs} vs Q_{DTW}	0.982	1.03	0.425	6
Q_{obs} vs Q_{ieff}	0.982	0.95	0.357	6
Q_{ieff} vs Q_{DTW}	0.989	0.92	0.467	6

1. based on first quantity divided by second quantity. **2**. Q_{obs} = measured in laboratory.

3. $Q_{DTW} = \left(\frac{1}{\alpha}\right)^{\frac{1}{N}} i_{DTW}^{1/N} h_{us} L$, i_{DTW} via eqn [3.13]. **4**. $Q_{ieff} = \left(\frac{1}{\alpha}\right)^{\frac{1}{N}} i_{ieff}^{\frac{1}{N}} h_{us} L$, i_{eff} from eqn [3.8].

Figure 3.10 shows that the general level of agreement between flows implied by equation [3.13] and observed flow rates is excellent, in most cases. This level of agreement declines somewhat for dams with small longitudinal extent in the upstream-downstream direction and steep downstream faces. In no case is the error ratio greater than 1.09. Due to the good agreement between the Q_{ieff} and Q_{DTW} results, it is suggested that the i_{eff} value can be taken as the i_{DTW} value. By using the i_{eff} instead of i_{DTW} value in equation [3.15] the h_{TW} value can be readily calculated. Due to the limited nature of the range of actual measurements, it is suggested that for C_{path} values associated with i_{eff} values of 0.25 or higher, the procedure not be used. This caveat is included in the flowchart for calculating the h_{TW}, shown in Figure 3.11.

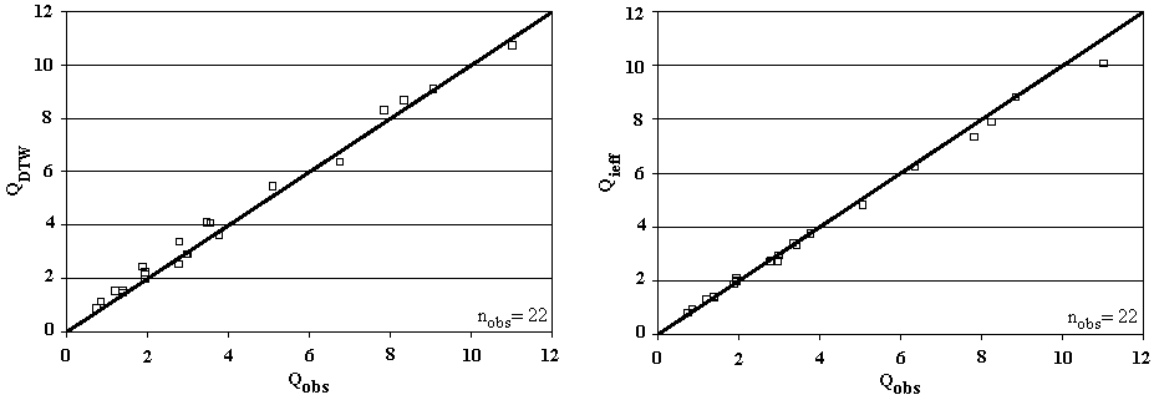

Figure 3.10. Comparison of discharges.

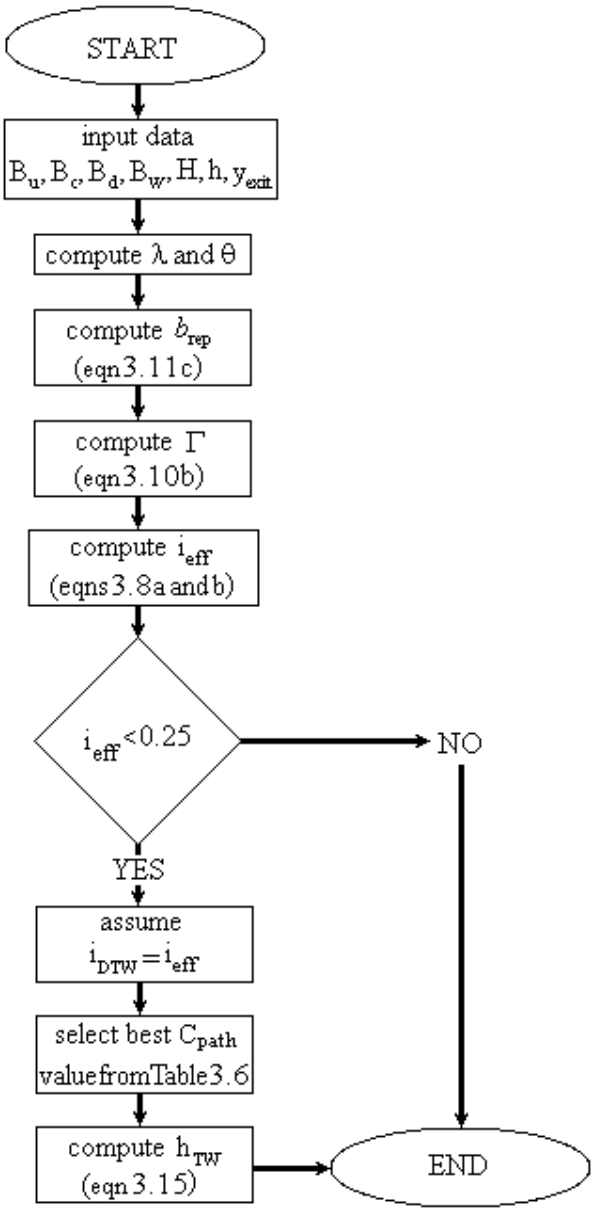

Figure 3.11. Procedure for calculating default tailwater depth.

3.6. SUMMARY AND CONCLUSIONS

1. A method for independently computing the height of the point of first emergence (y_{exit}) relative to the foundation has been presented. This height is important because unraveling failure can only occur below this point. This method is based on the idea of the angle of the emergent flow field at and within the toe of the structure. Although it has been shown how to use the Stephenson (1979) equations in concert with this key computation, it could be executed using any non-Darcy flow equation. It is also the first step toward the hydraulic isolation of the toe, for this class of porous hydraulic structure.

2. A general method for independently computing the variation in hydraulic head within the vertical that has, as its upper terminus, the point of first flow emergence has been presented and verified. It makes possible the hydraulic isolation of that part of the toe of the structure which is downstream of said y_{exit} vertical.

3. A general method for independently computing the default tailwater depth has also been presented and verified. Knowledge of this depth is valuable to the designer because if the default or representative depth of the receiving watercourse (just beyond the toe of the structure), such as its normal depth, is numerically less than this default tailwater condition (h_{TW}), then the h_{TW} value will govern and dictate the nature of the downstream condition, without which more thorough seepage modeling and other hydraulic modeling cannot proceed. It has been shown that the hydraulic gradient needed for this computation is related to the previously established concept of the effective hydraulic gradient (Hansen *et al.* 1995), once again of the structure as a whole.

CHAPTER 4 HYDRAULICS OF FLOW AT THE TOE OF NON-OVERTOPPING ROCKFILL STRUCTURES[1]

4.1. ABSTRACT

So-called flow-through rockfill structures have various physical manifestations. The effect of the water flowing through and out of flow-through rockfill embankments often raises questions about their hydraulic behavior and geotechnical stability, especially of the downstream toe. In order to provide better tools to assess the behavior of these embankments, laboratory and analytical studies were conducted. Firstly, physical models were built to observe boundary conditions and assess the hydraulics associated with the zone of the downstream toe. Secondly, the depth variation along the seepage-face was computationally modeled, and two approaches for solving this spatially varied flow (SVF) problem were undertaken. Under one of the approaches, SVF depths for a given spatial rate of flow emergence were computed and used by the head-based surficial finite difference (FD) nodes. This implied a new spatial rate of flow emergence, then used in the next round of SVF water surface profile modeling. Under the other approach, a layer of flux nodes rather than head-based FD nodes were tied directly to the SVF algorithm. Although there are inherent uncertainties, it was found that these two methods can be made to perform equally well. The difficulty in knowing how Manning's n should be varied was overcome by measuring the flow accumulation at multiple positions down the face. It appears that a dual linear variation in depth can be used to good accuracy and without inducing any unrealistic exit gradients in the zone of primary concern with respect to unraveling. Design guidance on how to describe these two linear variations is provided. It is based on the knowledge of the exit point, the hydraulic control point and the expected depth at the toe, all of which can be estimated *a priori*.

---

[1] Roshanfekr A., and Hansen D. 2014. Hydraulics of flow at the toe of non-overtopping rockfill structures. ASCE Journal of Hydraulic Engineering, HYENG-8269, Partially Accepted, Under 2nd Review.
Note: Numerical and experimental works presented in this chapter were conducted by the first author.

Key Words: hydraulic behavior, rockfill structures, boundary conditions, flow, exit height, spatially varied flow, seepage-face.

4.2. INTRODUCTION

The main application of so-called flow-through rockfill embankments (Figure 4.1) is the reduction of peak flows. Such embankments can be used to reduce the amount of spillage at downstream hydro dams or to control the outflow from stormwater detention basins. There are two different kinds of failure for these structures, massive failure and unraveling failure. According to the CDA (2007) guidelines, flow-through rockfill embankments shall be designed to withstand the combined effects of the action of the seepage emerging from the downstream face, along with any overflow, without local or massive movement of rock particles. In order to analyze the potential for massive failure a limit-equilibrium stability analysis (*e.g.* Bishop's Method) can be used (Garga *et al.* 1995). For unraveling failure a moment-based analysis of the stability of individual particle(s) under the seepage-face can be performed (Hansen *et al.* 2005).

The word "face" in engineering usually refers to a surface of some kind; herein "seepage-face" will refer to a two-dimensional (2-D) surface. This "seepage-face" is therefore distinct from the wedge of water that results from the seepage that comes out of the face. The latter is referred herein as the "seepage-face flow wedge", even though the water surface in question is not exactly planer.

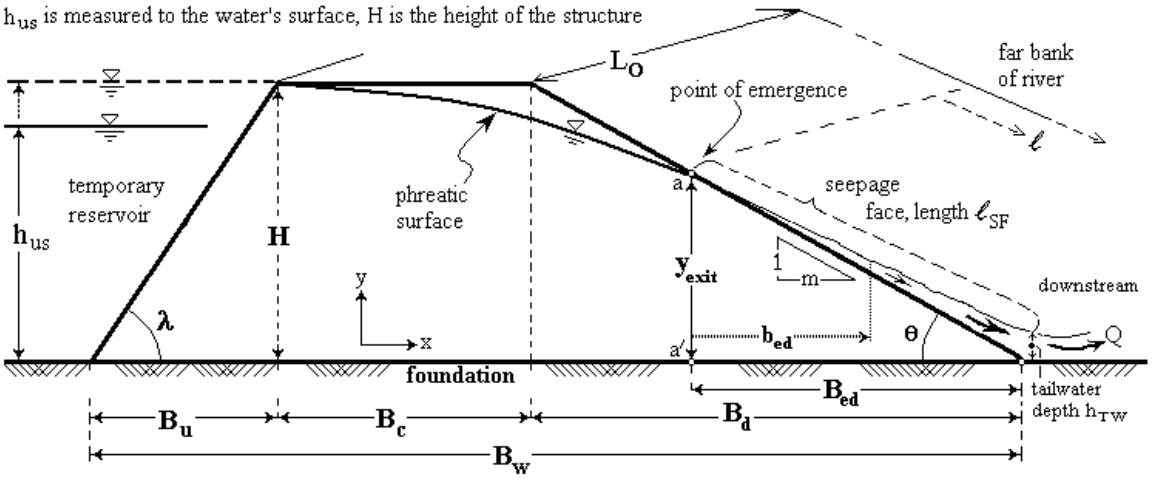

Figure 4.1. Nomenclature for non-overtopping rockfill embankments with constant flow (discharge Q passing through it).

Various researchers (*e.g.* Lane *et al.* 1986, Campbell 1989, Townsend *et al.* 1991, Hansen *et al.* 1995, Bari and Hansen 2002) have discussed the Dupuit-like unconfined non-Darcy flow that occurs through rockfill embankments and mine waste dumps. The toe and downstream face of such structures is the primary zone of engineering concern (Hansen *et al.* 2005). Sharp and James (1963) may be the only published study specifically on the hydraulics of the seepage-face pattern. They presented the 1-D spatially varied flow (SVF) equation for computing the depth variation of this seepage-face and a closed-form expression for finding the distance from the point of first-emergence to the critical depth. No flux nodes were used and no data on the spatial rate of change in depth ($\mathrm{d}d/\mathrm{d}\ell$) as a function of ℓ (Figure 4.1) was presented, but computed discharges were in reasonable agreement with observed discharges. Further work to quantify the hydraulic resistance for this type of emergent flow problem was indicated. Hansen *et al.* (2005) studied the hydraulic performance and stability of coarse rockfill deposits and presented the idea of the flow-field angle for estimating the height of the point of first-emergence. They also stated that the flow field is unusual in the seepage-face because the no-slip condition is absent, due to the emergence of flow (Hansen *et al*. 2005, Figure 11 *loc*. *cit*.). Further, the 'bed' is very steep, and the relative roughness is high (especially around the control section, where depth is small). It is therefore difficult to know how Manning's n should be varied for the SVF algorithm, especially given that the spatial rate of change in discharge ($\mathrm{d}Q/\mathrm{d}\ell$) is also not known *a priori* (see Table 4.2). Hansen and Roshanfekr (2012a and 2012b) did a parametric study of 24 embankments wherein the embankment height and the downstream slope were varied but the upstream slope and crest were kept constant. The potential for unraveling failure was evaluated using a particle-based moment analysis for the material beneath the seepage-face. Results showed that an increase in seepage-face velocity caused the potential for unraveling failure of the downstream toe of such structures to increase but that the strength of the exit gradient played a more important role in this regard.

It appears that little attention has been paid to the SVF hydraulics of the downstream face of non-overtopping rockfill structures. The research described herein was aimed at investigating:

(i) Modeling of the seepage-face over the toe; specifically, the spatial rate of change in

depth ($dd/d\ell$) and discharge ($dQ/d\ell$), and the spatial variation in hydraulic resistance. **(ii)** The value of a simplification of the downstream boundary, namely, a dual linearized variation in depth.

4.3. EXPERIMENTAL SETUP

In order to provide better tools to assess the seepage-face behavior of non-overtopping rockfill structures a number of physical models were built in a glass-walled flume (Figures 4.2 and 4.3).

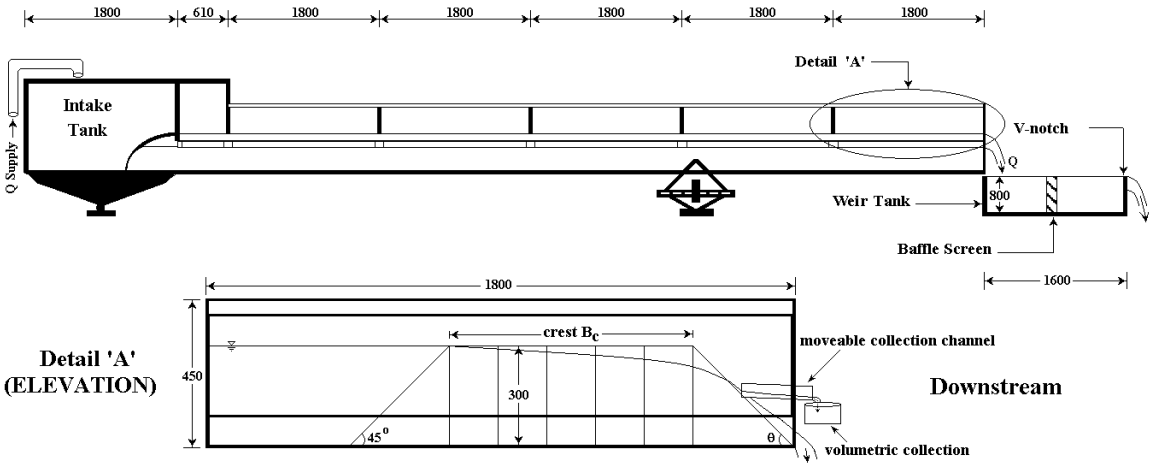

Figure 4.2. Flume in the hydraulics laboratory of Dalhousie University and the experimental setup.

The granular material used for model embankments was restrained in wire baskets, in order to prevent any of it from moving. Use of baskets also increased the speed of assembling any given configuration. These baskets had a ½" mesh size and were filled with a screened crushed limestone of nominal ¾" size (actual D_{50}= 17.2 mm). Packed-column tests were conducted on the same material (results provided in Table 4.1a). The geometries of the model embankments considered are given in Table 4.1b. It was found that a 1V:1H slope had the most curvature in the seepage-face water surface profile (wsp) (Figure 4.3) and is the most extreme case for any stability analysis (Roshanfekr and Hansen 2011). The slope of the flume (S_0) was set to zero and measurements of the upstream water level, phreatic surface, height of point-on-first-emergence and seepage-face were taken for each discharge. Partial discharges at four

positions down ℓ_{SF} were measured volumetrically using a collection channel (Figure 4.2). This was done for three downstream slopes having the same rockfill material, but different discharges. No backwater was present at the toe for any experiment, other than the default tailwater depth (h_{TW}). It is acknowledged that the depths along the seepage-face were of the same order of magnitude as the bed material size.

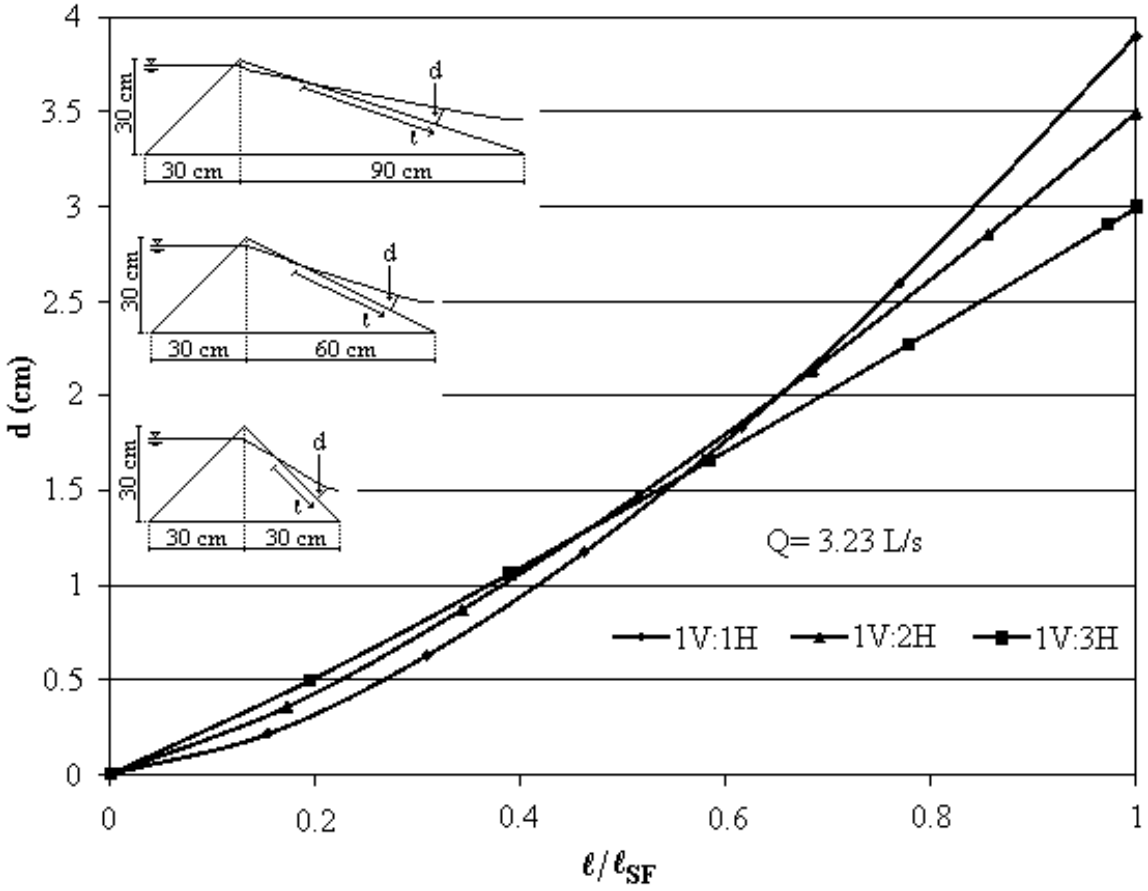

Figure 4.3. Representative water surface profile curvatures for three seepage-faces.

Table 4.1. Some experimental details.

a) Dalhousie University flume size and results of packed-column test on D_{50}=17.2 mm material (see Appendix B for further details).

Flume width * L_O (cm)	**Slope of flume** S_0	Parameters in equation [4.1]		**Porosity** n_p
		α (V_B in cm/s)	**N**	
31.0	0.0000	0.0213	1.85	0.42

* channel-wall to channel-wall, contrary to the sense of "width" in Figure 4.1. For the geotechnical practitioner the "length" of an embankment is commonly taken to be the distance from river-bank to river-bank (hence Figure 4.1).

b) Geometries of model embankments considered.

Model #	**H** (1) (cm)	B_u (2) (cm)	B_c (3) (cm)	B_d (4) (cm)	**Downstream Slope**	**Aspect Ratio,** A_R (5) (dimensionless)
1	30	30	0	30	1V:1H	1.5
2	30	30	15	30	1V:1H	2.0
3	30	30	30	30	1V:1H	2.5
4	30	30	45	30	1V:1H	3.0
5	30	30	60	30	1V:1H	3.5
6	30	30	75	30	1V:1H	4.0
7	30	30	0	60	1V:2H	2.0
8	30	30	0	90	1V:3H	2.5

(1) Height of embankment
(2) Upstream width of embankment
(3) Embankment crest width
(4) Downstream width of embankment
(5) $A_R = (B_u+B_c+0.5B_d)/H$ (Hansen *et al.* 1995)

In connection with the validity of inferences made using data obtained from experiments on small physical models of rockfill structures, the question of the quantity of discharge Q can be handled quite separately from the issue of the gradient. There is virtually no difference in the phreatic surfaces (Parkin *et al*. 1966, Parkin 1971) nor in the associated underlying gradients between the $N \cong 1.8$ cases seen in small models constructed of gravel, and the gradients in full-scale structures comprised of boulders (with N=2). The use of a given gradient in a given non-Darcy flow equation can then yield an estimate of the discharge passing through the structure, which is then essentially stand-alone, as far as questions of scale are concerned. The dependence of Q on ω in

equation [4.2d] (or similar) in the latter calculation presents to the practitioner the opposite effect from the former - strong dependence on particle diameter.

4.4. NON-DARCY FLOW AND EXIT HEIGHT ESTIMATION

A functional form that is commonly used to describe non-Darcy flow is (Parkin *et al.* 1966):

$$i = \alpha V_B^N \qquad [4.1]$$

where:

i= hydraulic gradient (dimensionless),
V_B= bulk velocity (L/T),
α = non-Darcy coefficient (T^N/L^N),
N= turbulent exponent for non-Darcy flow, having a value between 1 (Darcy laminar flow) and 2 (fully turbulent flow) (dimensionless). As the pore size and the void velocity, V_V, become large, N approaches 2.
$V_V = V_B/n_p$= void velocity (L/T),
n_p= porosity (dimensionless).

Equation [4.1] can be written:

$$V_B = \left(\frac{i}{\alpha}\right)^{\frac{1}{N}} = \left(\frac{i^{\frac{1}{N}-1}}{\alpha^{\frac{1}{N}}}\right) i \qquad [4.2a]$$

Darcy's Law may be stated as: $V_B = Ki$ [4.2b]

Comparing equations [4.2a] and [4.2b], a gradient-dependent hydraulic conductivity may be invoked (*cf.* Cedergren 1989):

$$K = \alpha^{-1/N}\, i^{1/N-1} \qquad [4.2c]$$

or: $$K = \omega i^{\psi} \qquad [4.2d]$$

where:

$\omega = \alpha^{-1/N}$ = non-linear hydraulic conductivity coefficient (L/T),
$\psi = 1/N - 1$= non-linear hydraulic conductivity exponent (dimensionless).

In characterizing the seepage-face of flow-through rockfill embankments, the height of the point of first-emergence of the flow on its downstream side is an important

fundamental quantity. Exit height can be used as the starting point of the seepage-face in the downstream direction and for calculation of the phreatic surface in the upstream direction. This exit height (y_{exit}) can also be used to develop a rating curve (see equation [4.3a]) for the structure; also, no unraveling occurs above this elevation. Below this elevation the seepage-face itself forms the downstream boundary condition, which is of interest in the context of pore pressure modeling (Hansen and Roshanfekr 2012a). The y_{exit} of rockfill embankments can be determined using the concept of the angle of the emergent flow-field, θ_{ff} (Hansen *et al.* 2005), in concert with a 1-D non-Darcy flow equation, of which there are many (Hansen *et al.* 1995). For a rectangular channel:

$$Q = V_B A_p = n_p V_V y_{exit} L_O \qquad [4.3a]$$

or:

$$q = V_B y_{exit} = n_p V_V y_{exit} \qquad [4.3b]$$

Since q is uni-valued (= Q/L_O), y_{exit} can be found by substituting equations [4.2b] and [4.2d] into equation [4.3b], and rearranging to:

$$y_{exit} = \frac{q}{\omega i_{exit}^{\psi+1}} \qquad [4.3c]$$

where:

A_p= cross-sectional area of flow in porous media (L^2),
q= Q/L_O= unit-width discharge (L^2/T),
Q= total discharge through embankment (L^3/T),
L_O = length of embankment (L),
i_{exit} = hydraulic gradient most suitable for use in finding y_{exit} (dimensionless).

The quantity of q can independently be determined for a given upstream water level of interest and longitudinal (downstream) width of deposit (Hansen *et al.* 1995).

In Leps' (1973) summary of various geo-hydraulic design methods for this class of structure, it was presented that a practitioner's approximation of the representative hydraulic gradient acting within the toe is simply $i_{exit}=\tan\theta$. This relationship or similar can be used in equation [4.3]. It may be expected, however, that the true angle representative of the emergent seepage field is less than θ, that this effective flow angle θ_{ff} varies with the relative exit height, and that it approaches θ as the relative exit height increases, as in Figure 4.4. This idea of a variable angle, θ_{ff}, for this emergent flow-field

was introduced by Hansen *et al.* (2005) and showed that the following equation performs better than a univalued tanθ:

$$\frac{\theta_{ff}}{\theta} = 1.41\frac{y_{exit}}{H} + 0.17 \qquad [4.4a]$$

For the case of both faces being at the angle of repose for coarse materials, it was surmised that:

$$\frac{\theta_{ff}}{\theta} \cong \sqrt{\frac{h_{us}}{H_{\Delta}}} \qquad [4.4b]$$

where:

y_{exit} = exit height (L),
θ_{ff} = angle of emergent flow-field (see Figure4. 4),
θ = angle of downstream toe (see Figures 4.1 and 4.4),
H= height of embankment (L),
h_{us}= upstream water level (L),
H_{Δ}= measure of longitudinal extent (streamwise) of embankment,
$(= (B_w \tan\lambda \tan\theta)/(\tan\lambda + \tan\theta)$, for mine-waste dumps where 1V:1H it reduces to $= B_w / 2$) (L),
B_w= total length of the embankment (L),
λ= angle of the upstream slope,
θ= angle of the downstream slope.

Such approaches can be used to find the height of the point of first-emergence for flow-through rockfill embankments and mine-waste dumps. The procedure can be invoked using any non-Darcy flow equation, of which there are many (*cf.* review of Hansen *et al.* 1995). Some are in the form of equation [4.1], others are (after algebraic rearrangement – see Hansen *et al.* 1995) second-order polynomials. The two forms are interchangeable (George and Hansen 1992), and the amount of supporting data quite variable from one published equation to the next, so that the choice of non-Darcy flow equation is a matter of engineering judgment (especially in the absence of medium-specific experimental work). It is possible to derive non-Darcy adaptations of the approach of Casagrande (1932) and others; this is beyond the scope of this work.

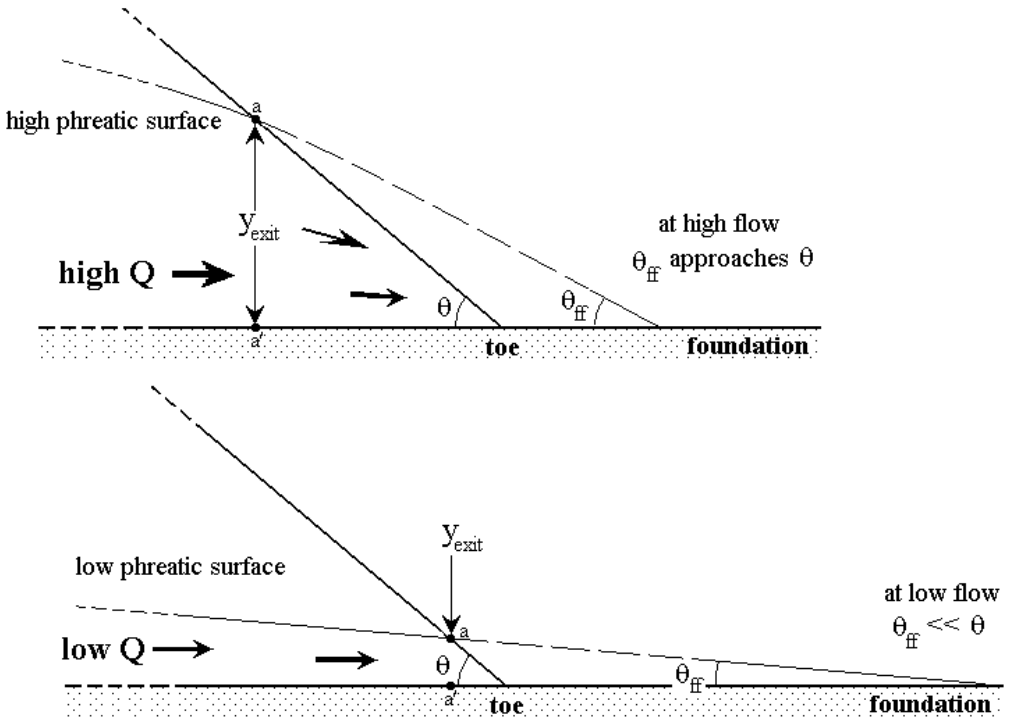

Figure 4.4. Illustration of concept of angle of emergent flow-field, θ_{ff} (adapted from Hansen *et al.* 2005).

4.5. MODELING OF WATER SURFACE PROFILE OF SEEPAGE-FACE

4.5.1. Prerequisites

The seepage-face represents a self-generated boundary condition and as such the depth variation that it represents directly affects the amount of flow that emerges to supply it. Greater depths reduce the rate of flow emergence and lesser depths increase it; a self-adjustment therefore takes place such that the total implied flow is matched to the difference in upstream and downstream heads (*i.e.* depth variation) that drives this flow. The SVF seepage problem has an apparent indeterminacy as a pseudo open-channel hydraulics problem, namely, that neither the variation in flow emergence nor of Manning's n is known beforehand. Ordinarily, the former is not only known, it is often associated with a univalued $dQ/d\ell$; the latter is merely approached by using n values considered to be representative of the surface in question (*e.g.* concrete).

The precise pattern of flow emergence can be thought as being dictated by final surficial heads arising from a very different kind of modeling effort, one sometimes referred to in geotechnical engineering as 'pore pressure' modeling (of the entire embankment). In this case, and in order to dynamically simulate the whole system at once, the hydraulic head model of a given embankment was directly linked to the SVF algorithm for its external water surface profile. We will therefore refer herein to the 'linked model' or 'paired algorithm'.

Two methods were tested: **(a)** SVF depths for a given spatial rate of flow emergence were computed and used by the head-based surficial finite difference (FD) nodes. This implied a revised spatial rate of flow emergence, then used in the next round of SVF water surface profile modeling (Figure 4.7). **(b)** Flux nodes rather than head-based FD nodes were tied directly to the incremental flow requirement of the SVF algorithm (Figure 4.9). Table 4.2 describes the nature of the seepage-face problem and the two modeling approaches used in this research.

Table 4.2. Nature of the seepage-face problem and the parameters involved.

Row	Parameter or Information (i)	Needed as Input? (ii)	Output or Outcome? (iii)	Bounds/Limits (iv)	Notes (v)
1	Average Manning's n.	Yes (as an initialization) Row 2 relevant.	Yes	~10^{-1} to ~10^{-2} for ordinary boundaries, but see Column (v) note →.	No-slip condition not present (so boundary not ordinary). Mean 'n' being too high leads to SVF depths too large and exit gradients too small. The latter is a non-conservative outcome from a design point-of-view.
2	Spatial pattern (down-slope variation) in Manning's n*.	Yes - see equations [4.15], [4.16], and [4.18].	No	Monotonic variation expected.	See Note in Row 5 for consequences of wrong pattern.
3	Total discharge.	No (but is implied by integral of Row 4 input).	Yes (easily integrated)	Expected Q_{total} can be independently estimated using methods described in Hansen *et al*. (1995).	The $dQ/d\ell$ pattern must show monotonic increase in cumulative Q, reaching Q_{total} at the toe ($\ell = \ell_{SF}$).

Table 4.2 (Cont). Nature of the seepage-face problem and the parameters involved.

Row	Parameter or Information (i)	Needed as Input? (ii)	Output or Outcome? (iii)	Bounds/Limits (iv)	Notes (v)
4	Spatial pattern (variation) in discharge.	SVF side uses linear pattern (zero to q from equation [4.3b]) if head-based FD nodes used. Pore pressure side uses linear pattern (zero to q from equation [4.3-b]) if flux FD nodes used.	Yes (inferable) Yes (explicit)	Σ(all incremental Q's) cannot exceed Q_{total}. Monotonically-increasing variation in cumulative Q must occur.	Head-based-node approach requires distinct computation of all incremental flows ** (1). Linked flux-node based algorithm dynamically (automatically) takes care of incremental Q pattern (2).
5	Water surface profile (wsp = variation in seepage-face depth of flow from $\ell = 0$ to $\ell = \ell_{SF}$).	Pore pressure side uses linear pattern (zero to h from equation [4.19]) if head-based FD nodes used. SVF side uses linear pattern (zero to h from equation [4.19]) if flux FD nodes used.	Yes (key outcome)	A given depth (and flow) variation forces a velocity variation. Since the wsp depth is definitely monotonically-increasing, V_{max} cannot exceed Q_{total} / A_{max}, where A_{max} ($=L_O \cdot h_{svft}$) must be at the toe.	If depth pattern is wrong, misplaced maximum gradients result (highly undesirable because of use of gradients in initiation of motion (IoM) estimation). Velocities affect IoM results***.

* In this research the variation in Manning's n could be inferred because of simultaneous knowledge of how the depth varied and how the discharge accumulated. It was inferred by adjusting its mean and its spatial variation until depths and flows matched laboratory observations.

** Iteratively updated. This calculation is part of neither the FD model of the embankment (*per se*) nor of the SVF algorithm.

*** But not as much as exit gradients (Hansen *et al*. 2005).

(1) This method is easier to set up and the exit gradients needed for IoM arise naturally.

(2) Each of side of the paired algorithm is essentially making reference to the same fluxes. The exit gradients needed for IoM must all be calculated after the numerical modeling has been completed.

For modeling the hydraulic heads inside the embankment, equation [4.2] can be substituted into the continuity equation to develop a 2-D non-linear hydraulic conductivity (NLHC) partial differential equation (PDE) (see Hansen and Roshanfekr 2012a and 2012b for details). This NLHC PDE, known as a '*p*-LaPlacian' (Vazquez 2007), was used for modeling the hydraulic head within the model embankments:

$$\left|\frac{\partial h}{\partial x}\right|^{\psi} \frac{\partial^2 h}{\partial x^2} + \left|\frac{\partial h}{\partial y}\right|^{\psi} \frac{\partial^2 h}{\partial y^2} = 0 \qquad [4.5]$$

A finite-difference (FD) version of equation [4.5] with $\Delta=\Delta x=\Delta y$ (also see Figure 4.5) is:

$$h_C = \frac{h_1|h_5 - h_1|^{\psi} + h_3|h_3 - h_7|^{\psi} + h_5|h_5 - h_1|^{\psi} + h_7|h_3 - h_7|^{\psi}}{2|h_5 - h_1|^{\psi} + 2|h_3 - h_7|^{\psi}} \qquad [4.6]$$

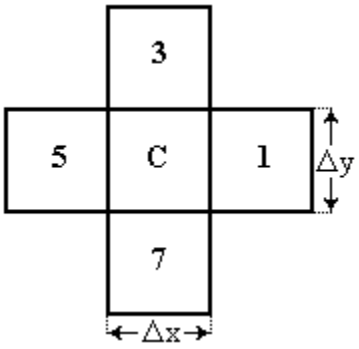

Figure 4.5. Four point body-centered FD molecule used for modeling of hydraulic head inside model embankments.

4.5.2. SVF Water Surface Profile

The downstream slope of these embankments is hydraulically steep (Chow 1959)[1]. In order to calculate the local seepage-face head for such slopes the following equation can be used (Figure 4.6):

[1] That is, the critical depth is greater than the normal depth.

$$h_{SF} = z_{SF(\ell)} + \frac{p_{SF(\ell)}}{\gamma_w} = z_{SF(\ell)} + d_{(\ell)} \cos\theta \qquad [4.7]$$

where:

h_{SF} = local seepage-face head (L),

$z_{SF(\ell)}$ = elevation of seepage-face; varies from zero at $\ell = \ell_{SF}$ to y_{exit} at $\ell = 0$ (L),

$d_{(\ell)}$ = local seepage-face depth normal to bed (L),

$p_{SF(\ell)} / \gamma_w$ = pressure head[1] (also a function of position on face), magnitude varies from zero at $\ell = 0$ to h_{TW} at $\ell = \ell_{SF}$ (L), perhaps nonlinearly,

γ_w = unit weight of water (F/L^3).

When the discharge varies significantly in direction of flow, whether positively or negatively, it is classified as 'spatially varied' flow (SVF). Sharp and James (1963) were apparently the first researchers to classify the seepage-face flow at the toe of a rockfill slope as a case of SVF with increasing discharge. The seepage-face is an unusual example of varied flow in that the standard no-slip condition[2] is not present at the boundary (this should reduce Manning's n), yet the relative roughness is very high, especially (as will be seen) near the control section (this should increase n). Further, the 'bed' slope is unusually steep (being much more than 6º), pushing the control section (*i.e.* transition from subcritical to supercritical) up toward y_{exit} (ℓ=0 in Figure 4.1). Literature on the hydraulic resistance of very rough beds with Fr>1 is itself rather scant (Pagliara *et al.* 2008, Kells 1993). The governing ordinary differential equation (ODE) for steady SVF usually has the following inherent assumptions: flow 1-D, hydrostatic pressure distribution normal to the bed, channel boundary immobile, longitudinal slope small, and air entrainment negligible. The numerical solution of this ODE usually involves the

---

[1] $p_{SF}(\ell)/\gamma_w = y\cos^2\theta$ where y is measure orthogonally to the foundation, also see Figure 4.16.

[2] This no-slip condition might be more accurately referred to as an apparent no-slip condition. The plane of the downstream face of a flow-through rockfill embankment is very rough, relative to the modest depth of water that covers it. However, if it were a smooth surface, one could measure the velocity at regular intervals within a given vertical, right down to this plane itself. The results of such a series of measurements would necessarily result in a non-zero velocity being measured at the plane. Otherwise, the equality between the known local flux rate and the integral of the local velocity distribution could not be satisfied. It is therefore fair to say that although the no-slip condition must be satisfied at a microscopic level (*i.e.* where the fluid is in direct contact with the surface of a given rock particle) it appears not to be satisfied at the macroscopic level, for the spatially-varied flow that occurs within the seepage-face wedges of flow-through rockfill embankments.

Manning equation to assess the friction slope and does not require $dQ/d\ell$ to be single-valued.

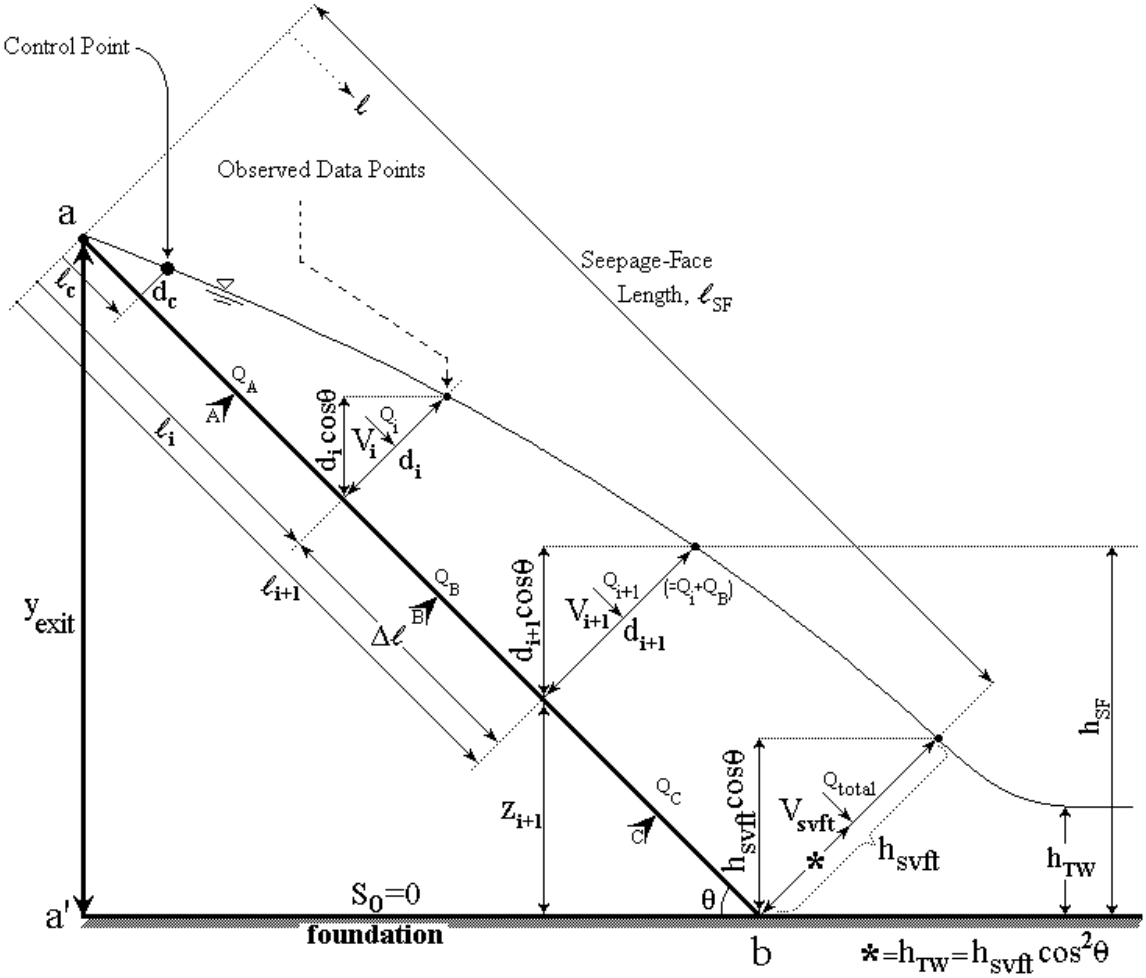

Figure 4.6. Seepage-face in the toe of a rockfill embankment.

The SVF equation applicable to this context (Sharp and James 1963, Hansen 1992, Chow 1959) is:

$$\frac{dd}{d\ell} = \frac{S_\theta - S_f - \alpha' \frac{2Q}{gA^2}\left(\frac{dQ}{d\ell}\right)}{\cos\theta - \alpha' \frac{Q^2}{gA^2 D}} \qquad [4.8]$$

where:

d = depth normal to bed (see Figure 4.6) (L),

$dd/d\ell$ = rate of change of depth (measured normal to the downstream slope) along ℓ, in direction of flow (dimensionless),

S_θ = sinθ= slope[1] of toe of embankment (dimensionless),
S_f = friction slope = $(nV/R^{(2/3)})^2$ (dimensionless),
V = velocity in seepage-face (L/T),
n = Manning's roughness coefficient,
R = hydraulic radius (L),
D = hydraulic depth (L),
Q = total discharge through embankment (L^3/T),
A= cross sectional area of flow in seepage-face normal to embankment slope (L^2),
α' = velocity head correction factor (dimensionless),
g = gravitational acceleration (L/T^2).

The computation of the water surface profile starts from the control section which must therefore be identified first. Due to the variation of the discharge in the streamwise direction, the critical depth (creating the control section) can occur at any point along the channel. It is known the critical section occurs where the specific energy is a minimum, which implies that either Fr = 1 or $dd/d\ell = 0$[2]. In order to determine the position of the control section for a specific geometric and hydraulic condition, the numerator of equation [4.8] should therefore be set to zero (Henderson 1966).

For this study the location of the control point using the methods of Chow (1959) and of Sharp and James (1963) were compared. Chow's (1959) method for determining the downstream location of the control section is numerical. Sharp and James (1963) assumed a single $dQ/d\ell$ value in the downstream direction by using the toe angle to estimate the rate of discharge variation (i= tanθ). The following equation for calculating the distance of the critical depth (ℓ_c), relative to the point of first-emergence, arose:

$$\ell_c = \frac{8\cos^2\theta\, q^{*2}}{g L^2 \sin^3\theta} \qquad [4.9]$$

where:

$q^* = \overline{\frac{dQ}{d\ell}} = \frac{Q_{total}}{\ell_{SF}}$ = average spatial rate of change in discharge (L^2/T).

---

[1] The position occupied by S_θ in equation [4.8] is usually written S_0, the bed slope (meaning the bed of the river or channel).

[2] Normally, the critical depth is univalued (in a prismatic channel through which a given flow is being conveyed) and is greater than the depth of water if the flow is supercritical. Spatially-varied flow has no single value of critical depth and if a transition from subcritical to supercritical flow is present (as here), there will be a unique point where the critical depth coincides with actual depth.

Knowledge of the location of the control point permits computation of the complete water surface profile, which proceeds downstream for supercritical flow and upstream for subcritical flow. Although it is not necessarily the case for SVF (in general), it was found that the inferred Froude number just downstream of the control point was greater than unity in all eight of the cases described herein. For seepage-face SVF cases associated with typical flow-through rockfill dams, (it turns out that) the control section is a short distance downstream of the point of first emergence, meaning that most of the computation and water surface profile is for the supercritical condition, and proceeds downstream from it.

The governing ordinary differential equation of the SVF is non-linear with no closed-form solution even for the prismatic channel case. The following discretization was used to solve equation [4.8] (*cf.* Chow 1959 with $\alpha' = 1$):

$$\Delta d' = \frac{1}{\cos\theta}\left[\underbrace{\frac{Q_i}{g}\frac{(V_i + V_{i+1})}{(Q_i + Q_{i+1})}\left[\Delta V + \frac{V_{i+1}}{Q_i}\Delta Q\right]}_{\text{"Impact" Loss}} + \underbrace{S_f \Delta\ell}_{\substack{\text{Pure}\\ \text{Friction}\\ \text{Loss}}}\right] \qquad [4.10a]$$

$$\Delta d = -\Delta d' + S_\theta \frac{\Delta\ell}{\cos\theta} \qquad [4.10b]$$

where:

$\Delta d'$ = local drop in seepage-face depth relative to bed (L),
Δd = elevation change in surface of seepage wedge (L),
$\Delta V = V_{i+1} - V_i$ = change in seepage-face velocity between sections i and i+1 (L/T),
$\Delta Q = Q_{i+1} - Q_i$ = change in seepage-face discharge between sections i and i+1 (L^3/T),
$\Delta\ell$ = distance between sections i and i+1 along seepage-face (L),
V_i = velocity in section i of seepage-face at ℓ_i (L/T),
Q_i = discharge in section i of seepage-face at ℓ_i (L^3/T).

The two methods used for linking the NLHC-generated heads to the SVF algorithm are described in the following sections.

4.5.3. Linkage to Conventional Nodes

Under the first method, links to SVF depths were merely made to the hydraulic heads of the body (interior) and the flux was calculated separately, using the head outcomes for the conventional surficial head nodes. In this case the Dirichlet boundary condition (Wang and Anderson 1982) was used which, when imposed on a partial differential equation, specify the values that a solution needs to take on at the boundary of the domain. Namely, the heads from equation [4.6] and the fluxes calculated using equation [4.11] were used to get the inputs for equation [4.10]. More specifically, the flux for each conventional node was calculated using (see Figures 4.5, 4.7 and 4.8):

$$Q_C = V_C A_C = \omega(i_C)^{1/N} \cdot L_O \cdot \Delta\ell \qquad [4.11a]$$

$$i_C = i_{C'} \cdot \cos(90 - \theta + \xi) \qquad [4.11b]$$

$$i_{C'} = \sqrt{\left(\frac{h_3 - h_7}{2\Delta y}\right)^2 + \left(\frac{h_5 - h_1}{2\Delta x}\right)^2} \qquad [4.11c]$$

$$\xi = \frac{180}{\pi} \arctan\left(\frac{h_3 - h_7}{h_5 - h_1}\right) \qquad [4.11d]$$

where:

Q_C = flux out of node C (L^3/T),

$V_C = \omega(i_C)^{1/N}$ = velocity of flux out of node C, normal to seepage-face (L/T),

$A_C = L_O \cdot \Delta\ell$ = area through which flux enters seepage-face (L^2),

L_O= length of embankment (L),

i_C = hydraulic gradient at node C, normal to seepage-face (dimensionless) (Figure 4.7),

$i_{C'}$ = absolute magnitude of hydraulic gradient at node C (dimensionless) (Figure 4.7),

ξ = direction of absolute magnitude of hydraulic gradient, as $+\xi$ degrees below horizontal (dimensionless).

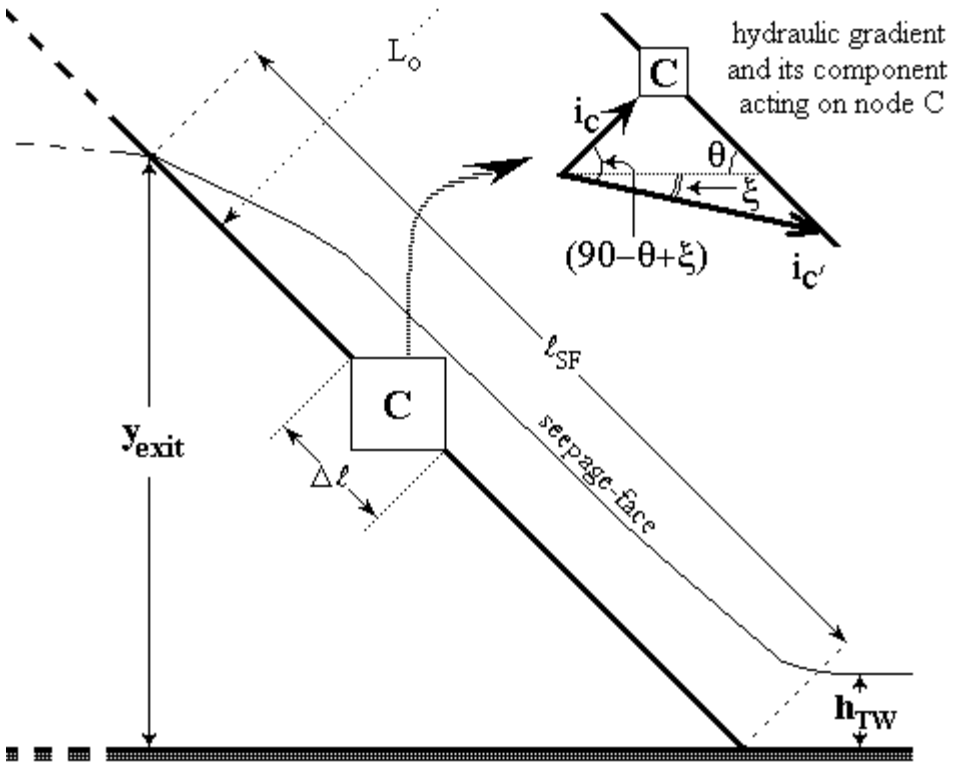

Figure 4.7. Conventional surficial nodes in toe of rockfill embankments (vector i_c is actually centered on node C).

For the linked model in which conventional FD nodes were used on the 'pore pressure' modeling side, the criterion used to halt computations was the successful matching of the down-gradient pattern of discharge exhibited along ℓ_{SF}. Said matching was achieved by revising the water surface profile (patterns of depths) produced by the SVF algorithm, on the basis of the discharge pattern repeatedly handed to it by the pore pressure model. If the resulting depth (handed back to the pore pressure model) was locally greater than that of the previous iteration, this had the effect of lessening the local emergent flow.

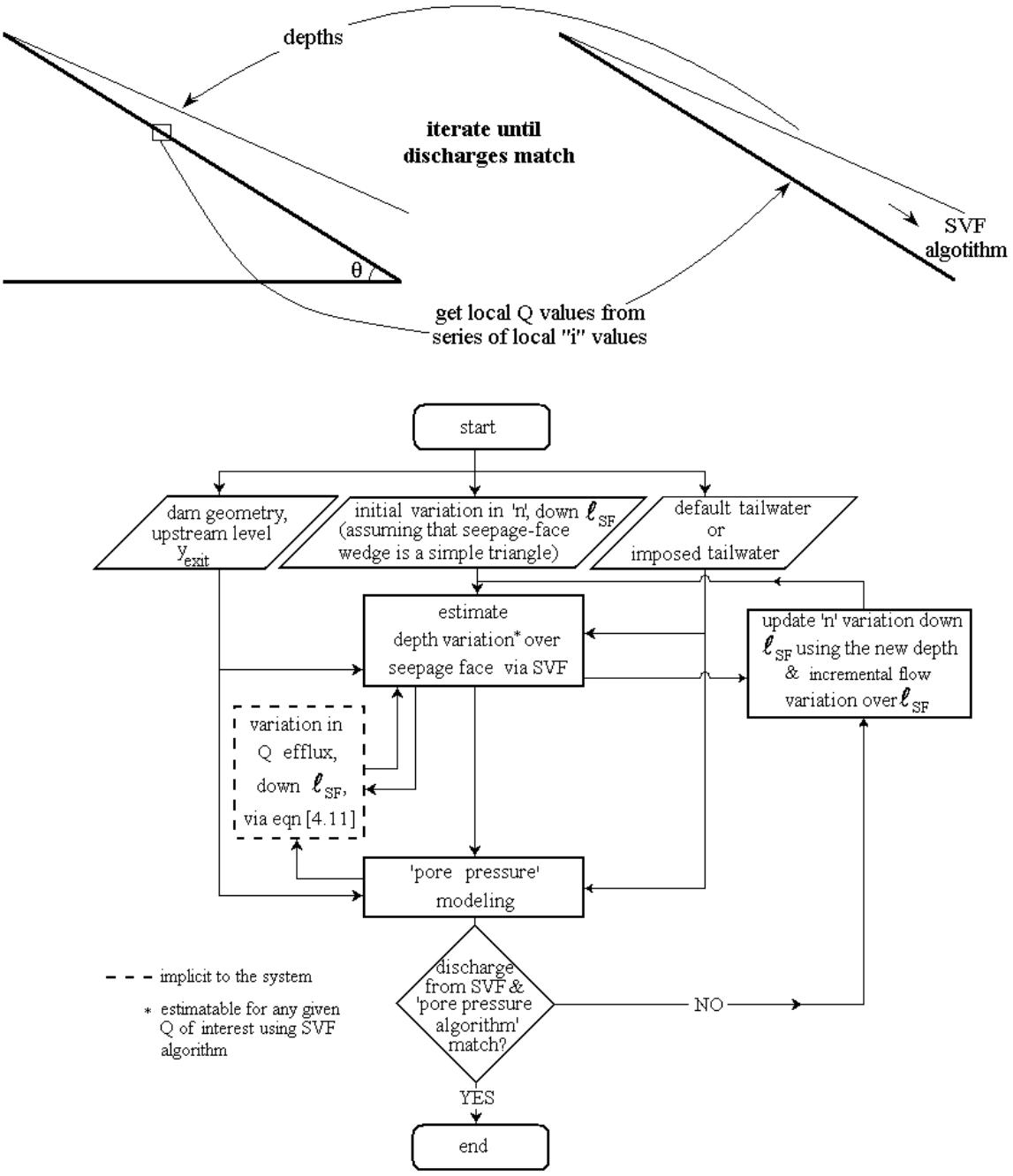

Figure 4.8. Linkage of NLHC hydraulic head model to SVF algorithm via conventional head-based nodes.

4.5.4. Linkage to Flux Nodes

Under the second method, flux nodes rather than head-based FD nodes were tied directly to the SVF algorithm. In this case von-Neumann-like boundary conditions (Wang and Anderson 1982) were used. When imposed on a partial differential equation, these specify that although the system to be simulated has a boundary, the values of the scalar of interest are not fixed. Flux nodes linking the hydraulic heads further 'inside' the body of the rockfill embankment to the SVF algorithm were calculated using the following equation (Hansen and Roshanfekr 2012a and 2012b, Wang and Anderson 1982):

$$\left|\frac{\partial h}{\partial x}\right|^{\psi} \frac{\partial^2 h}{\partial x^2} + \left|\frac{\partial h}{\partial y}\right|^{\psi} \frac{\partial^2 h}{\partial y^2} = -\frac{R(x,y)}{T} \qquad [4.12]$$

where:

$T = (\psi + 1)\omega L_O$ (L^2/T),

$R(x,y) = \frac{-Q(x,y)}{\Delta\ell \cdot L_O}$ = volume of water added per unit time per unit area (L/T),

Q(x,y)= flux node discharge from downstream toe, added to seepage-face (L^3/T).

Equation [4.12] reduces to Poisson's equation when N=1 (recall equation [4.1]). The FD expression for equation [4.12] with $\Delta x=\Delta y=\Delta$ is (see Figures 4.5 and 4.9):

$$h_C = \frac{h_1|h_5 - h_1|^{\psi} + h_3|h_3 - h_7|^{\psi} + h_5|h_5 - h_1|^{\psi} + h_7|h_3 - h_7|^{\psi} + (2\Delta)^{\psi}\Delta^2 R_C / T}{2|h_5 - h_1|^{\psi} + 2|h_3 - h_7|^{\psi}} \qquad [4.13]$$

After making an initial assumption about the spatial variation in the discharge, the discharge for the flux nodes and the SVF algorithm was self-determined (iteratively and interactively - see Figure 4.10).

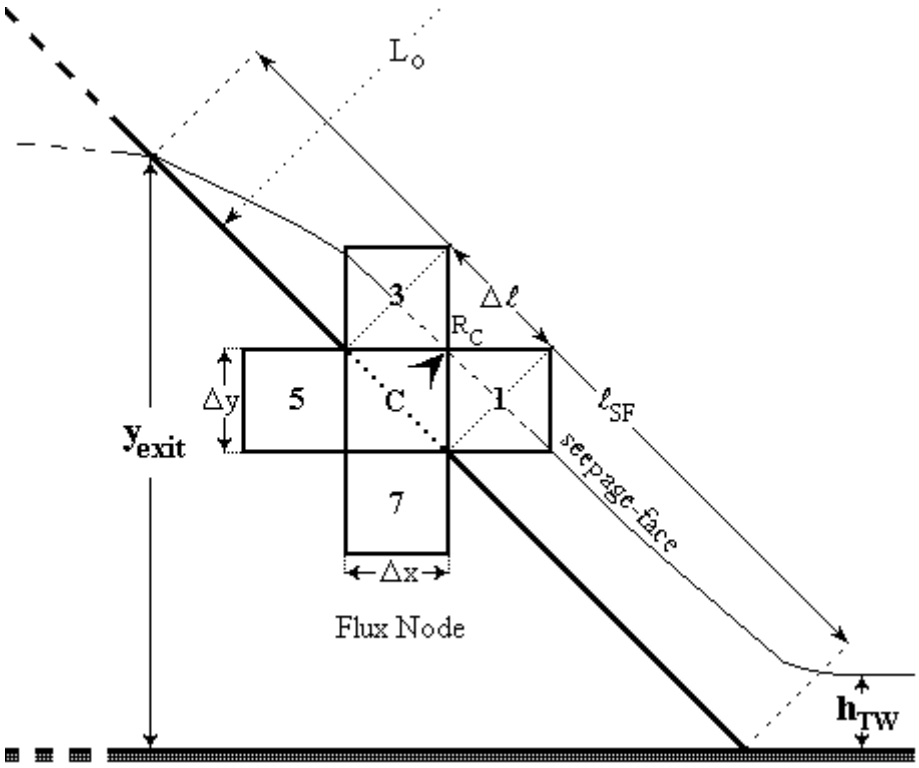

Figure 4.9. Flux nodes in toe of rockfill embankments.

For the linked model in which flux FD nodes were used on the 'pore pressure' modeling side, the criterion used to halt computations was the successful matching of the down-gradient pattern of depth over ℓ_{SF}. Said matching was achieved by the action of the surficial layer of flux nodes, which produced revised flows on the basis of the input depth pattern handed to it by the SVF algorithm. If the resulting flow (*i.e*. nodal efflux, to be handed back to the SVF model) was locally greater than that of the previous iteration, this had the effect of increasing the local depth produced by the SVF algorithm, as expected.

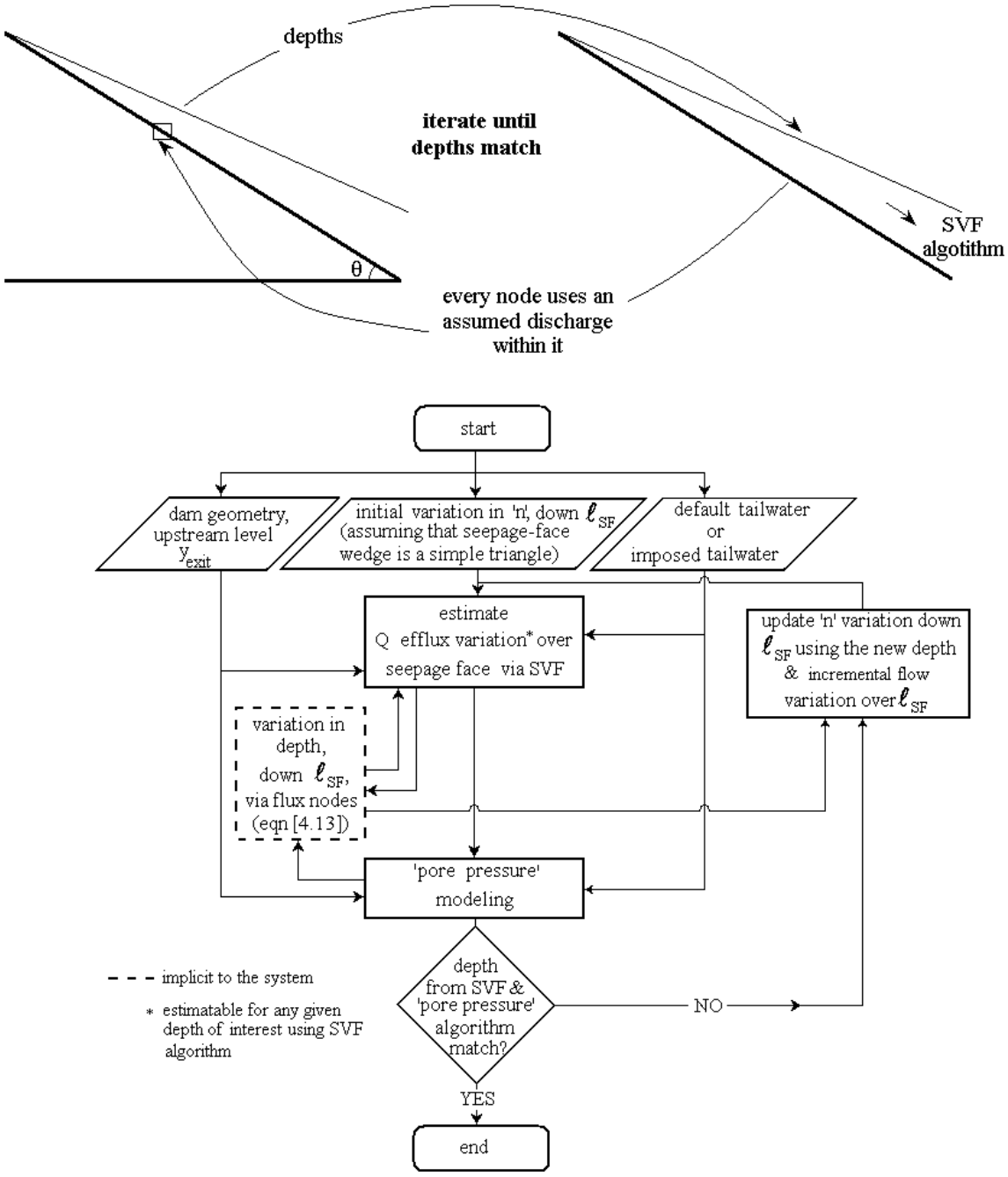

Figure 4.10. Linkage of NLHC hydraulic head model to SVF algorithm via flux nodes.

4.5.5. Role of Roughness

As previously indicated, for the linked-model seepage-face calculation (under either FD method) the downstream variation in Manning's n, incremental flow accumulation, and depth were all unknown *a priori*. Because these quantities themselves are known to interact hydraulically (apart from linkage to another algorithm) they represented an apparent indeterminacy in the SVF 'half' of the linked model. However, it was found that a reasonable set of initial conditions was found to be sufficient information for the linked model to independently arrive at a reasonable final pattern of depths and flows, and of Manning's n values - keeping in mind that any given depth and flow implies a Manning's n through knowledge of the local energy gradient, for a given channel geometry:

$$n_{new} = \left[\frac{S_f^{1/2}}{Q} A R^{2/3} \right]_{previous} \qquad [4.14]$$

It was of interest however to see how the pattern of this important parameter varied over the seepage-face of a given fully-resolved linked model (*i.e.* a given simulated spatially-varied flow water-surface profile). The final pattern of depths and incremental flows was therefore used to infer the 'n' pattern for the final condition of the seepage-face for all eight models, via equation [4.14]. This range of values was compared to the Manning's n values arising from the equations of Strickler and of Keulegan (*cf*. Chow 1959).

Strickler (1923) $$n = 0.047 d_p^{1/6} \qquad [4.15]$$

Keulegan (1952), fully rough case $$n = \frac{R^{1/6}}{21.9 \log_{10}\left(\frac{12.2R}{k_s} \right)} \qquad [4.16]$$

where:

d_p = representative particle diameter (m),
R= hydraulic radius (in),
k_s = Nikuradse's equivalent sand-grained roughness (in).

Eight model embankments with different widths (values of B_w and components, Figure 4.1) and toe angles/slopes were analyzed. Three of these were modeled using additional discharge data and the results were compared against observed depths and in some cases incremental discharges. The observed exit height (y_{exit}), the phreatic surface, and the upstream head (h_{us}) were used as boundary conditions for the numerical modeling. The tailwater level at the toe was set to be the default tailwater depth. This is the tailwater depth that forms in the absence of any backwater effects from the downstream channel. It depends on tanθ, the surface roughness under ℓ_{SF}, and the total Q (Hansen and Roshanfekr 2012b).

Since depths were not measured at every incremental position down ℓ_{SF}, but a given resolution of the imposed conditions did lead to a set of both depths and flows at each such position, and since each paired numerical model did efficiently settle to said pattern of depths and flows - but depth was much easier to measure - there was a disparity between the amount of depth data available versus the amount of incremental flow data available. The preliminary results that follow therefore focus primarily on depth comparisons.

4.5.6. Preliminary Results

The first step was to determine a suitable node size (in this study $\Delta x = \Delta y = \Delta$ for all cases) for each model run, since the number of iterations was known to be non-trivial. A single node represents a finite amount of the porous medium. As more and more nodes are used to represent the same 2-D section of media, the associated mesh or grid becomes finer and the level of detail available in the results becomes greater. However, the computational effort toward full grid-relaxation also increases.

Three node sizes were tested; the optimal size was found to be 0.5 cm (Figure 4.11). The total number of nodes for a given numerical model was around 10^4, and could be relaxed such that each iteration only induced 10^{-6} cm of head change, after a few minutes of processing.

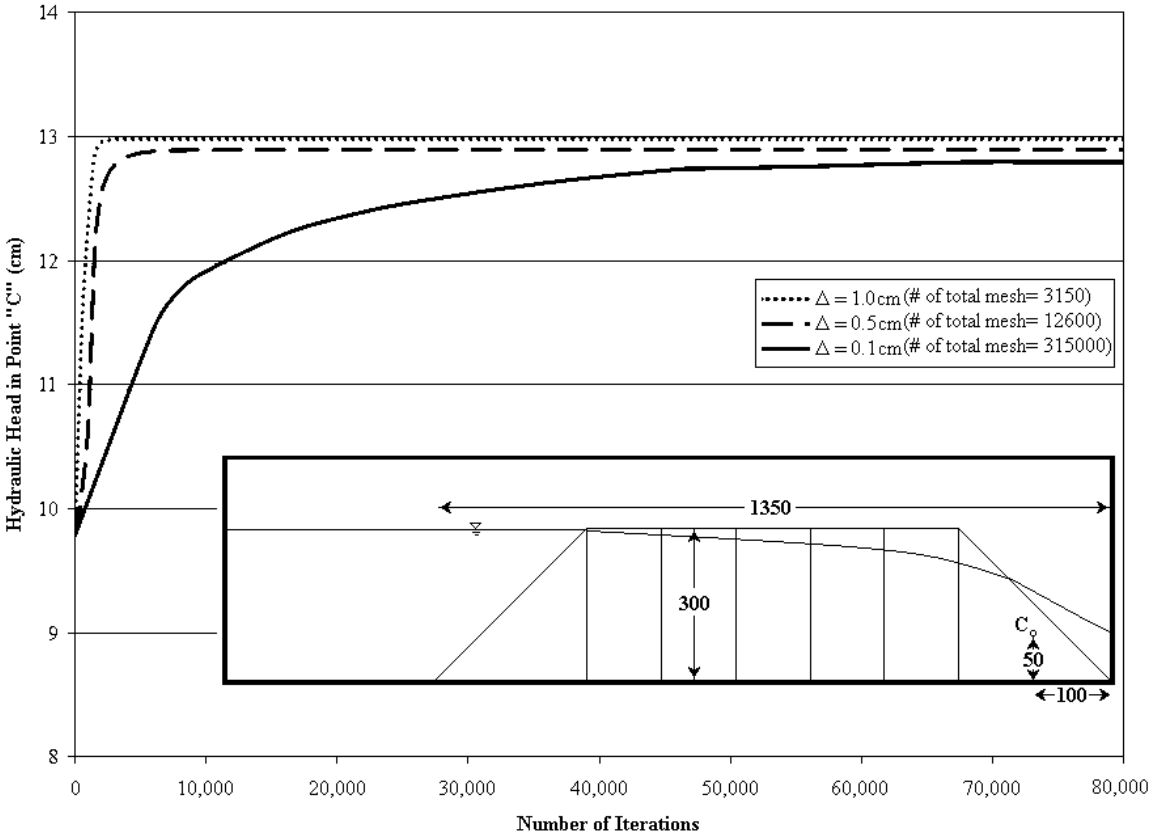

Figure 4.11. Convergence study of NLHC FD scheme for full grid relaxation of Model # 6.

The $\Delta\ell$ within the SVF algorithm was measured along the seepage-face. Since $\Delta\ell = \Delta / \cos\theta$ (in this study $\Delta x = \Delta y = \Delta$ for all cases) the $\Delta\ell$ values were 0.71, 1.12 and 1.58 cm, for the three slopes considered.

An important quantity in SVF considerations is the distance of the critical depth (ℓ_c) from the point of first flow emergence. The methods of Chow (1959) and Sharp and James (1963) were compared for all model embankments; results for the first six cases are shown in Figure 4.12. The average difference between the Chow (1959) and Sharp and James (1963) methods for the ℓ_c calculation was found to be only about 8%. It is suggested that the Sharp and James (1963) equation be used (equation [4.9]) due to its simplicity. In all cases ℓ_c was found to be less than 0.71cm, *i.e.* less than the $\Delta\ell$ values used. The SVF algorithm was therefore started from the first node after the node at the point of first-emergence. The flow downstream of this point (ℓ_c) was found to be

supercritical and was therefore taken as the starting point for all SVF calculations performed.

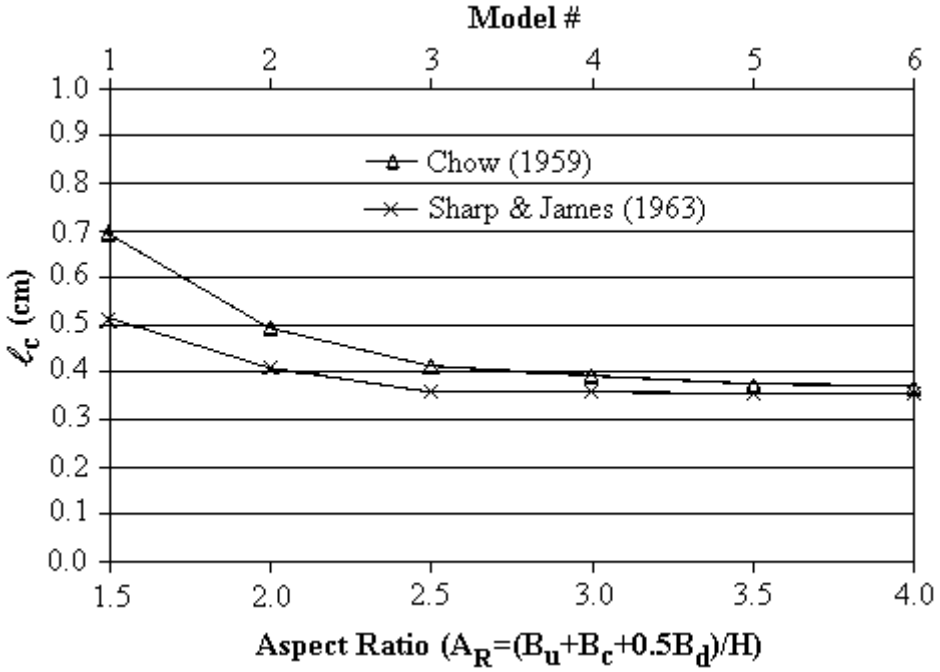

Figure 4.12. Critical depth distance calculation from y_{exit} using Chow (1959) and Sharp and James (1963) for Models 1 to 6 (Q = 3.82 L/s).

After selecting the nodal size and calculating the distance to the critical depth position for all models, the SVF algorithm was set up using both methods (Figures 4.7 and 4.9). It was then linked to the NLHC FD hydraulic head model of each embankment. After setting up the FD model and the SVF algorithm (using one of two methods considered) the initial conditions of depth, local discharge, and Manning's n were imposed (see Table 4.2, especially columns ii and iii). Specifically, the depth variation was made triangular (from zero to the default tailwater value), the discharge variation made linear (in the case of flux node usage) from zero to the value indicated by equation [4.3], and with these two aspects specified, equation [4.16] was used to set up the first pattern of Manning's n values (with $k_s=D_{50}$ and R=d). Table 4.3 provides a statistical comparison of the observed versus the computed seepage-wedge depths and the implied total discharge for all eight embankments. Figure 4.13 shows how the observed vs. the computed local seepage-wedge depths compared, for all eight models.

Table 4.3. Comparison of observed vs. computed seepage-wedge depths and ending flows[1] (total discharge) for all eight models*.

Model #	Observed Total Discharge (L/s)	r^2	Mean Error Ratio (d_{obs}/d_{calc})	RMSE (for depth) (cm)	Error Ratio (Q_{obs}/Q_{calc})
1	3.82	0.980	0.933	0.36	1.06
2	3.82	0.985	0.972	0.31	0.97
3	3.82	0.988	0.979	0.26	0.94
4	3.82	0.988	0.979	0.26	0.94
5	3.82	0.989	0.973	0.22	0.93
6	3.82	0.989	0.966	0.22	0.94
7	3.23	0.982	0.917	0.33	0.98
8	3.23	0.987	0.965	0.20	0.93

* Number of measured depths = 5, in all 8 cases

[1] This is the value of flow at the terminus of B_{ed} in Figure 4.1.

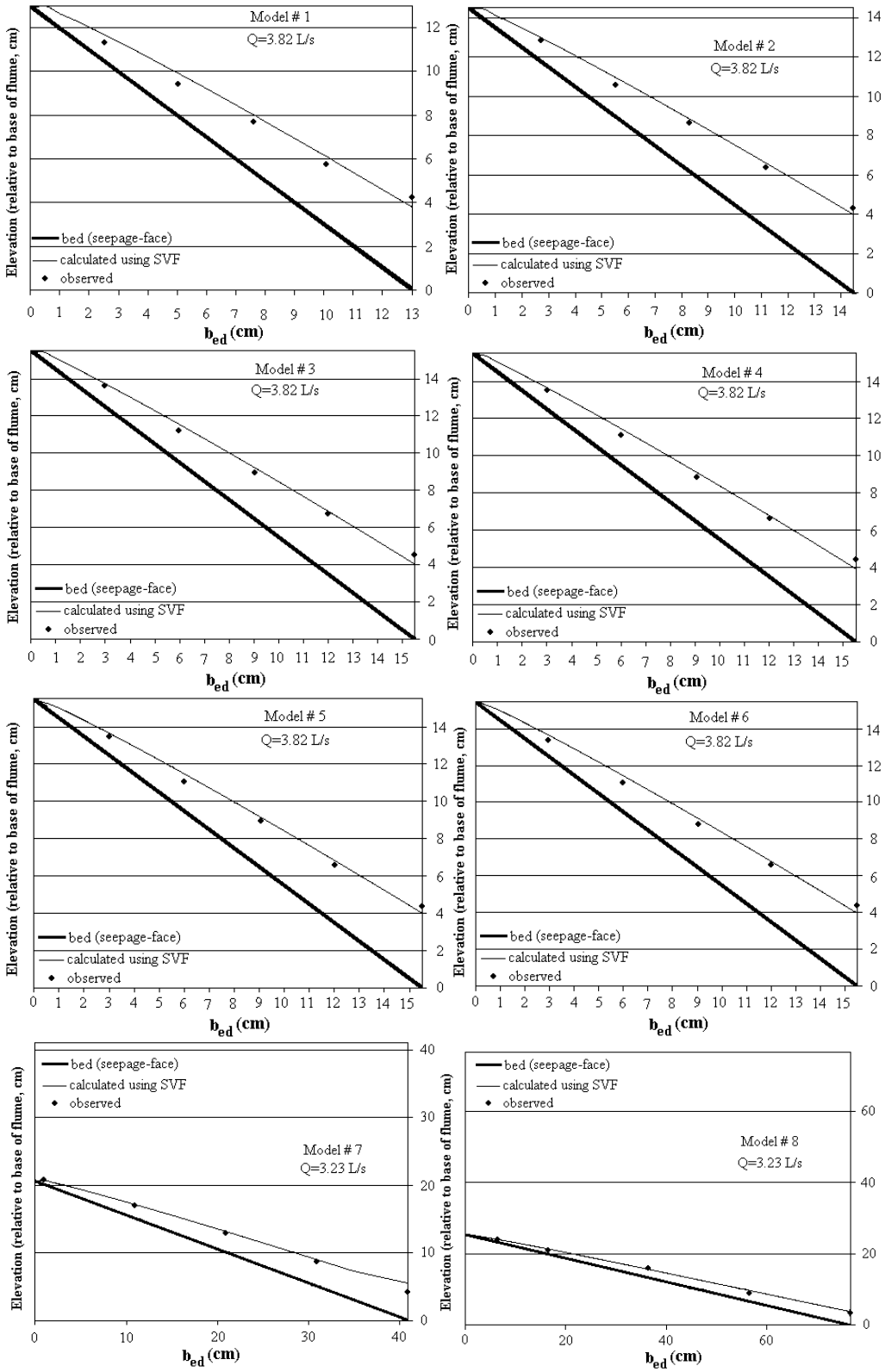

Figure 4.13. Observed vs. computed local seepage-wedge depths along b_{ed} for all eight models (see Appendix B with respect to 'depth').

With respect to the natural manner in which each linked model came to a final condition, it is clear that more depth in the seepage-face would reduce the efflux. Less emergent flow reduces the depth, which then increases the efflux. The nature of the self-correction was essentially no different for the model that did not invoke flux-type FD nodes at the surface of the pore pressure model. The flow merely increased or decreased in accordance with the head corrections and the non-Darcy flow equation specified for the porous medium in question. Overall, this simultaneous self-adjustment of depth and flow is therefore credible for the seepage-face boundary condition described herein.

It is evident that there is a systematic error in the computed flows – most of the summations of flux were found to be too large (total Q_{calc}>total Q_{obs}). The discrepancy is in itself interesting because the emergent fluxes were found using non-Darcy flow parameters (*cf.* equation [4.2d]) arising from packed-column tests done on the same material (see Appendix B), with an effort to maintain the porosity of the porous medium for work done (models built) in the flume. We suggest two possible causes for this systematic error. One is that the relative wall-effect would not have been the same. Although this effect would have been small because D_{50} was less than one-tenth of the inside diameter of the column (Dudgeon 1966) we would in any case expect any wall-effect to be smaller in the flume than in the column, implying a slightly smaller ω to be physically at work in the former context. The other explanation pertains to possible porosity differences between work done in the packed column and that done in the flume. Although the very same particles of rock were used and every effort was made to duplicate the porosity, the porosity of model embankments is in general more difficult to determine than it is for media that are perfectly confined within cylindrical containers. The Wilkins (1956) equation is widely accepted in the open-pit mining industry as a way to describe 1-D flow through linear mine-waste dumps. It may be stated as (Hansen *et al*. 1995):

$$V_V = Wm^{0.5}i^{0.54} \qquad [4.17a]$$

where:

V_v = void velocity (=V_B/n_p), (L/T),
W = 5.243 for hydraulic mean radius in meters and velocity in m/s,
m = hydraulic mean radius (=$(e \cdot d_p)/(6 \cdot r_e)$), (L), e is void ratio, d_p is representative particle diameter and r_e is a particle surface-area-efficiency,
i = hydraulic gradient (dimensionless).

Given that the void ratio is determinable from porosity via $e= n_p/(1-n_p)$, equation [4.17a] can be written:

$$V_B = 5.243 n_p \left(\frac{n_p \, d_p}{6 \, r_e (1 - n_p)} \right)^{0.5} i^{0.54} \qquad [4.17b]$$

By comparison with equation [4.2a], and having the good fortune that the experimental work described herein led to an N of 1.85 (and 1/1.85=0.54), we can write:

$$\left(\frac{1}{\alpha} \right)^{1/N} = 5.243 \, n_p \left(\frac{n_p \, d_p}{6 \, r_e (1 - n_p)} \right)^{0.5} = \omega \qquad [4.17c]$$

It is therefore possible to quantify and adjust for the common problem that packed-column experiments typically have different porosities than model dam experiments done using rock particles with the same average diameter and r_e values:

$$\text{altered } \omega = \frac{(\text{Wilkins } \omega)_{\text{altered } n_p}}{(\text{Wilkins } \omega)_{\text{reference } n_p}} \qquad [4.17d]$$

An analogous argument can be developed with the non-Darcy flow equation of Stephenson (1979). The relative role of porosity within ω for these two equations are therefore presented in Table 4.4, for comparison purposes.

Table 4.4. Effect of porosity on non-Darcy flow coefficient ω in equation [4.2d].

Porosity n_p	Ratio * ω** / 8.01	
	Wilkins Equation	Stephenson Equation
0.38	0.83	0.90
0.40	0.91	0.95
0.42	1	1
0.44	1.09	1.05
0.46	1.19	1.10
0.48	1.29	1.14

* value of ω = 8.01 found experimentally (from packed-column tests, see Appendix B).
** ω = in numerator altered via equation [4.17c] (or its analogue) and equation [4.17d], except for n_p=0.42 entry.

It can be seen from Table 4.4 that only slightly higher porosities in the model dams, as compared to the packed-column porosity of n_p=0.42, could have systematically altered the flow coefficient ω in equation [4.2d], enough to cause the above-noted systematic error in modeled flows.

It was found that it made no difference whether the SVF algorithm was linked to conventional surficial nodes or to flux nodes, the computed depths were virtually identical. The water surface profiles in Figure 4.13 are therefore indistinguishable. The error in the calculated total discharge was found to be less than 7% (Table 4.3). Figure 4.14 shows the down-slope Manning's n variation for all eight models.

As previously mentioned, Manning's n was found from the friction slope and as part of the SVF algorithm. Results indicated that the hydraulic resistance, thus inferred, decayed exponentially down the seepage-face. In the interests of providing guidance to designers with respect to good initial conditions for Manning's n, the following expression was adapted to the problem:

$$\frac{n}{\bar{n}} = a + b \cdot \exp\left(- k_n \frac{\ell}{\ell_{SF}} \right) \qquad [4.18a]$$

$$\frac{\bar{n}}{n_{str}} = C_F \qquad [4.18b]$$

where:

n = local Manning roughness coefficient,
$\bar{n}$ = average (in spatial sense) 'n' value inferred over length ℓ_{SF}.
n_{str} = Manning roughness coefficient calculated using Strickler's equation,
C_F = correction factor for Manning's n variation,
a= empirical constant,
b= empirical coefficient,
k_n = rate-constant,
ℓ = distance down seepage-face (see Figures 4.1 and 4.6).

The mean particle diameter can be used in the Strickler equation. Then the value of the C_F correction factor can be used to estimate the mean n applicable to ℓ_{SF}. The dimensionless 'n' decay equation can then be used to estimate the local 'n' relative to this corrected mean n, for all of ℓ_{SF}. This can be used as an initial pattern for Manning's n, within the SVF algorithm (see Table 4.5).

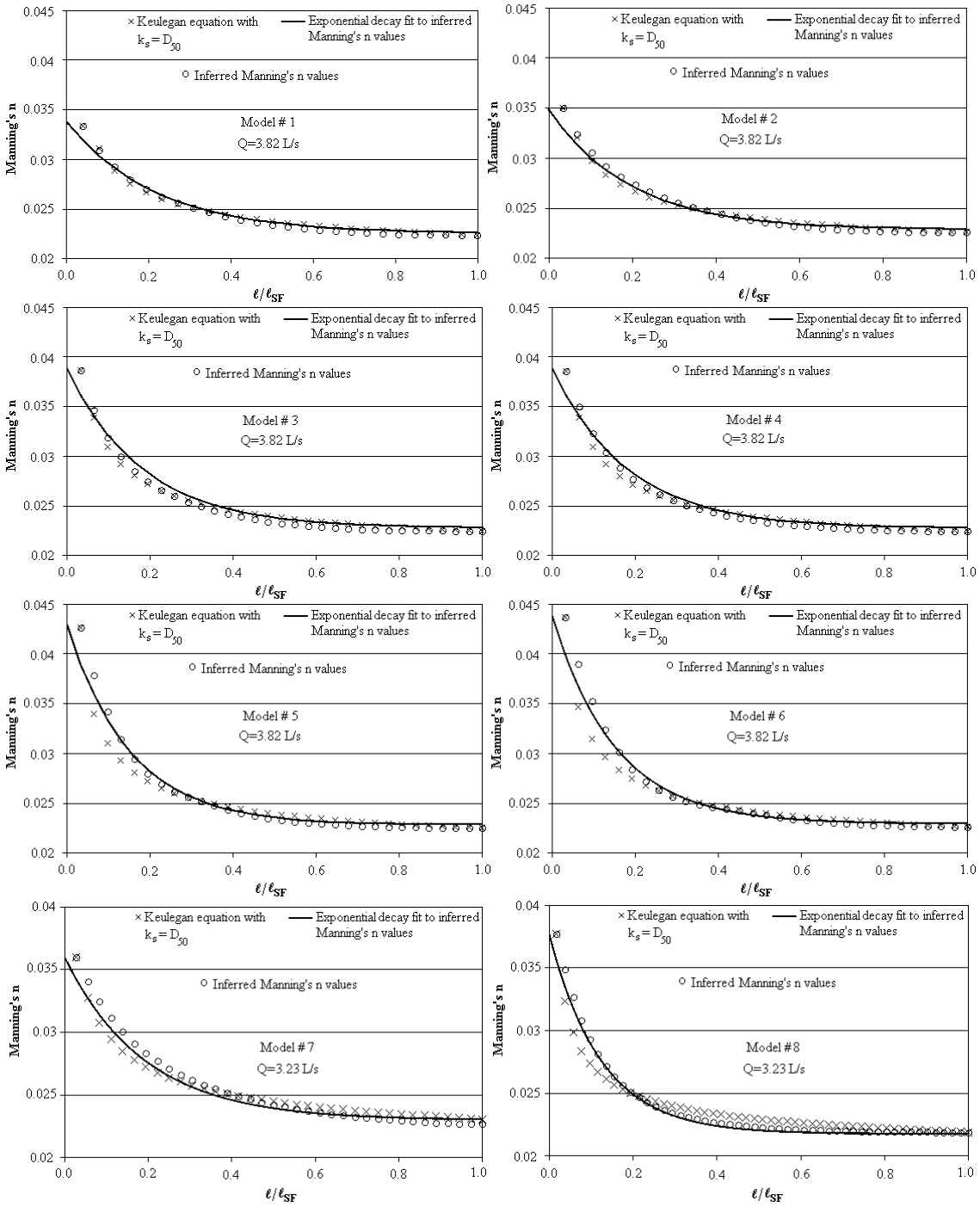

Figure 4.14. Manning's n variation in the seepage-face along ℓ_{SF} for all eight models. Exponential decay curves are Strickler based.

The relative roughness aspect was examined via Keulegan's (1952) equation, with the value of Nikuradse's equivalent sand-grain roughness (k_s) set at the value of the D_{50} of the bed (*i.e.* the toe material).

Table 4.5. Exponential decay parameters in equations [4.18a] and [4.18b] for Strickler-based Manning's n calculation (all eight model embankments).

Model #	Q (L/s)	A_R	Downstream Slope	Parameters in Equations [4.18a] and [4.18b]			
				a	b	k_n	C_F
1	3.82	1.5	1H:1V	0.95	0.46	4.6	1.01
2	3.82	2.0	1H:1V	0.96	0.50	5.1	1.00
3	3.82	2.5	1H:1V	0.96	0.67	5.5	1.01
4	3.82	3.0	1H:1V	0.96	0.67	5.5	1.01
5	3.82	3.5	1H:1V	0.97	0.84	6.6	0.99
6	3.82	4.0	1H:1V	0.97	0.88	6.6	1.00
7	3.23	2.0	2H:1V	0.97	0.62	6	0.95
8	3.23	2.5	3H:1V	0.99	0.72	8.1	0.93

Although the approach taken was made as general as possible, it is admitted that it needs to be verified further using seepage-face data from prototypes. Photographic evidence of seepage-faces (*e.g.* HEC Tasmania 1969, on-line photos by Hydro Quebec of PK85 on the Rupert River) appears to support the general patterns described herein.

4.5.7. Improved Model Verification

Knowing that the depth variations and total flows could be readily generated using the linked model using reasonable initial patterns of Manning's n, it was considered of interest to do a limited study of the $dQ/d\ell$ patterns to see if some of the observed (but much more difficult to measure) incremental flows supported the previously-described work. The results and the statistical analyses are shown in Table 4.6 and Figure 4.15.

Table 4.6. Statistics for limited verification of modeling approach, using incremental discharges.

Model # Toe Slope	Total Discharge (L/s)	Parameter Studied	r^2	Mean Error ratio (obs/calc)	Number of Data Points
1 1V:1H	1.56	Depth	0.984	0.994	5
		Incremental Discharge	0.995	1.074	4
7 1V:2H	2.68	Depth	0.989	1.036	5
		Incremental Discharge	0.994	0.964	4
8 1V:3H	3.04	Depth	0.982	0.947	5
		Incremental Discharge	0.998	0.959	4

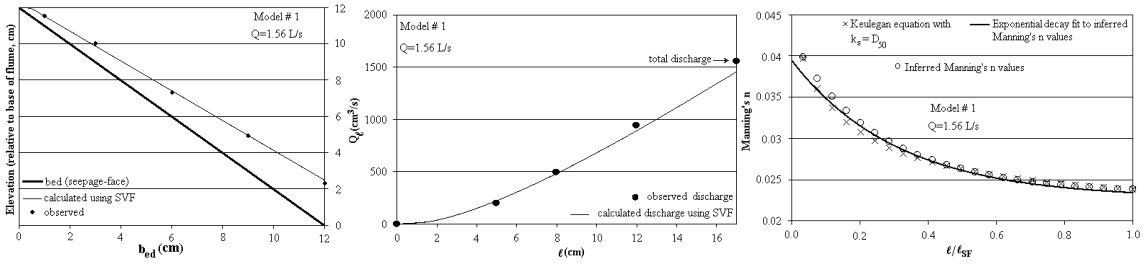

a) Model #1.

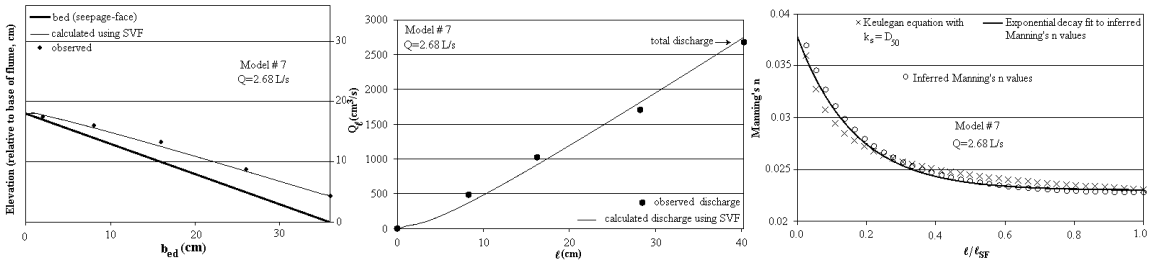

b) Model #7.

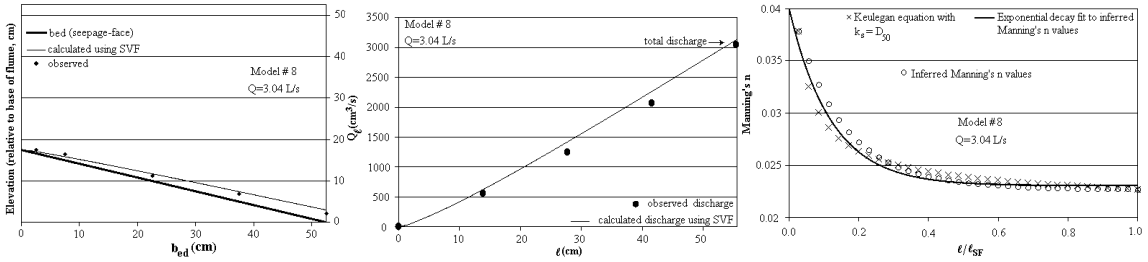

c) Model #8.

Figure 4.15. Results of seepage-face flow wedge modeling.

Figure 4.15 indicates that the growth in discharge down the seepage-face in non-linear. The above results also show that the theoretical basis used to describe SVF hydraulic resistance in this context is reasonable, since the observed depths match, to a reasonable level of agreement. The main disadvantage of doing detailed seepage-face modeling using an SVF algorithm is the increased level of effort. The following section describes the use of linear variation(s) in depth.

4.6. USE OF LINEAR VARIATION(S) IN DEPTH

It was of interest to see whether the water surface profile (wsp) of the seepage-face flow wedge could be simplified. This could be used as a starting point for the initially-imposed depths needed for the SVF algorithm, or if sufficiently accurate, used as-is. Simple linear and bilinear (*i.e.* dual) depth variations were therefore compared to pseudo-observed water surface profiles (*i.e.* numerically generated profiles calibrated to agree with a finite number of location-specific depth observations). Figure 4.16 shows the full geometry and nomenclature for a linearized seepage-face profile using two straight lines.

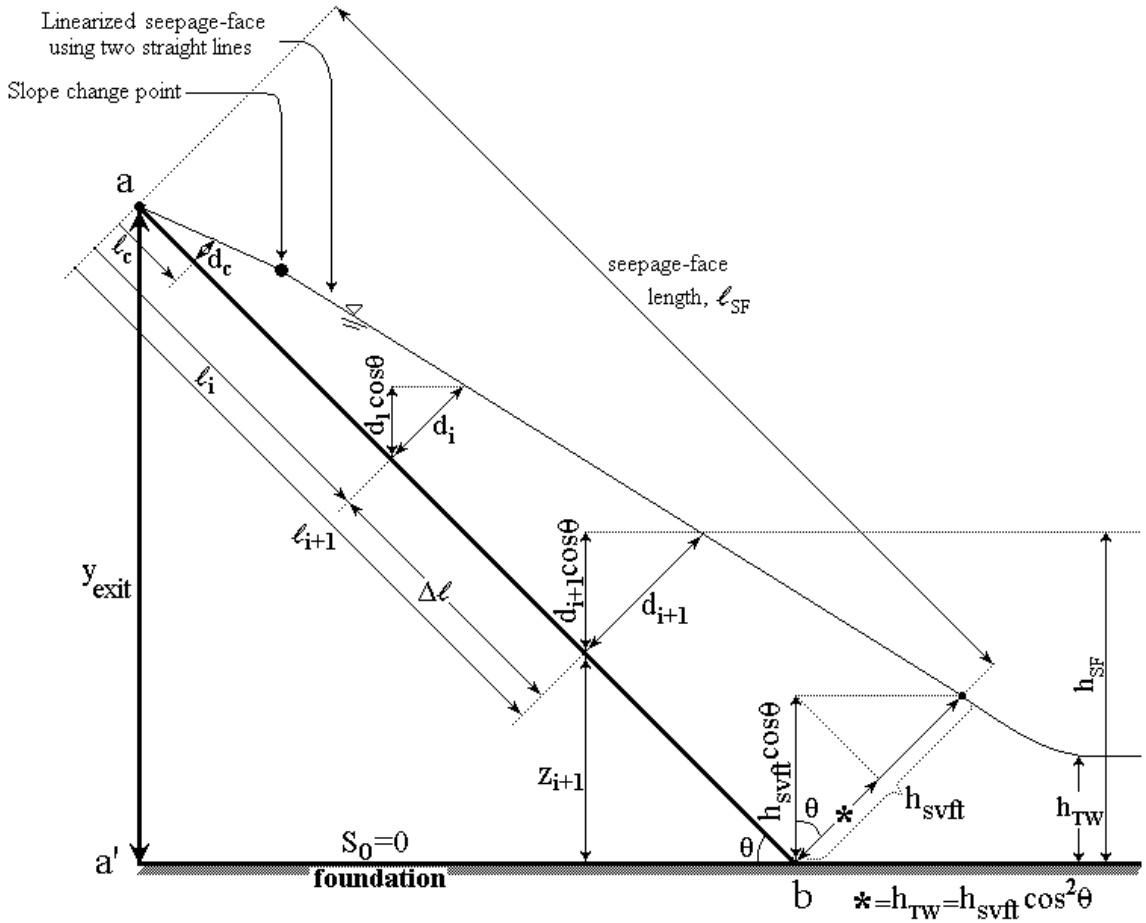

Figure 4.16. Linearized seepage-face depth variation using two straight lines.

From the SVF modeling and the observed data it was noted that the change in the slope of the seepage-face depth occurs near the critical section. It was therefore surmised that the location and height of the point at which the slope of the line changes could be taken to be some multiple of the down-slope distance to this section, for practical purposes. The bilinear variation therefore required the performance of a search for the best location along ℓ_{SF} for the change in slope. Table 4.7 summarizes the results.

Table 4.7. Accuracy of mono vs. bilinear water surface profiles.

WSP variation/approximation	**Error** (Mean and Maximum)	**Notes**
One straight line	3% and 5%	maximum error ratio occurs at $\ell = 12 \cdot \ell_c$
Two straight lines	1% and 2.5%	best slope change at $\ell = 12 \cdot \ell_c$ and $d = 3 \cdot d_c$

As can be seen in Table 4.7 by comparing the results of all models, the best location of the slope change was found to occur at $12 \cdot \ell_c$, at a depth of $3 \cdot d_c$ (see footnote 2 below Figure 4.8). In addition, the results of the two straight line linearized seepage-face depths was compared with the seepage-face depth pattern calculated using the SVF algorithm for Models 1 to 6, along b_{ed} (see Figure 4.17).

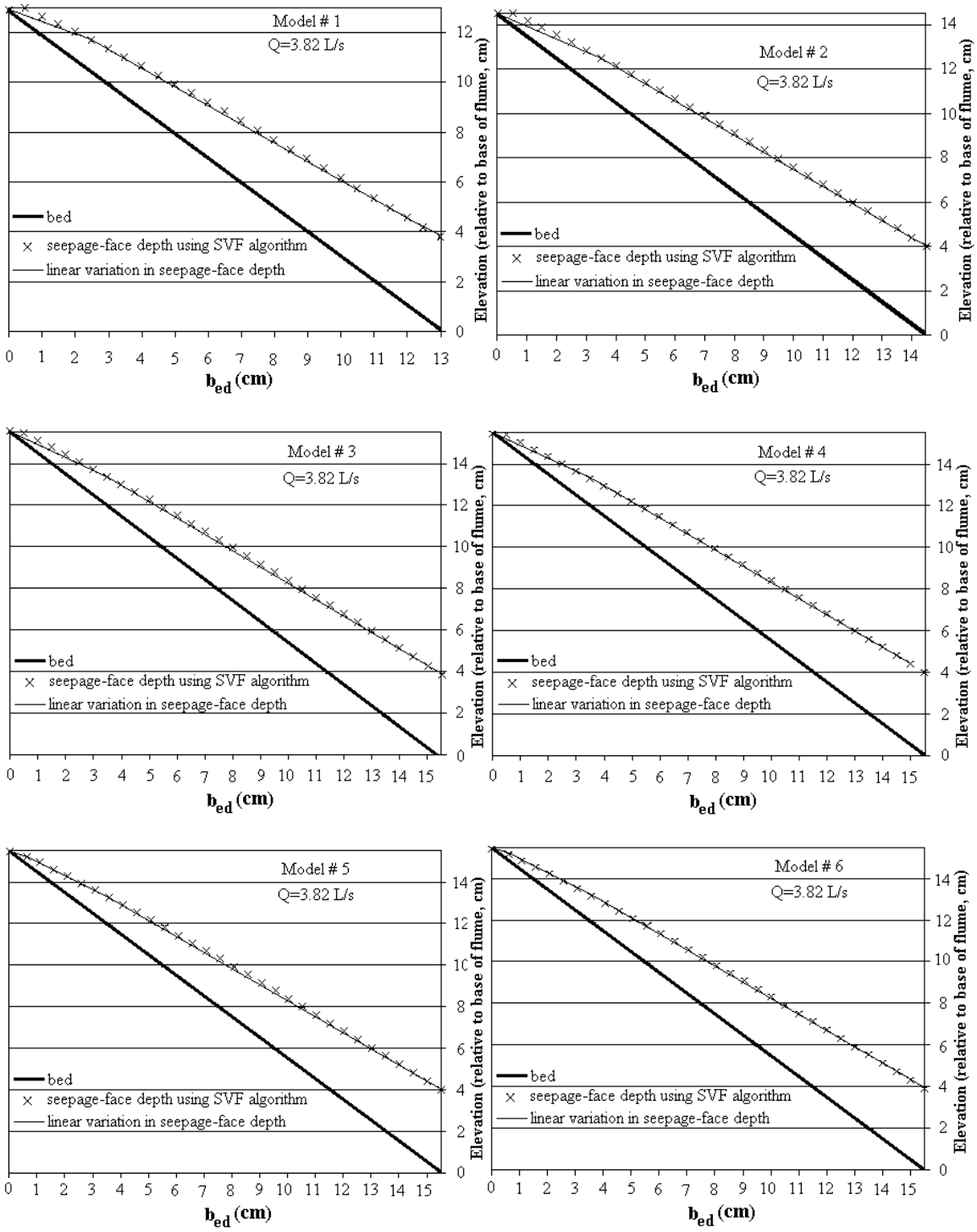

Figure 4.17. Two straight line linearized seepage-face depths compared with seepage-face depth pattern calculated using SVF algorithm for Models 1 to 6, along b_{ed} (Q= 3.82 L/s).

Figure 4.17 shows that the difference in depths is small. The results of Figure 4.17 also show that using two straight lines for seepage-face depth variation is more realistic than a single straight line. This indicates that, by simply using a dual linear variation in depth instead of the complex SVF algorithm, the accuracy will be adequate, from a practical point of view (*e.g.* error in depth of less than 5%). Doing so greatly reduces the time needed for solving the NLHC FD grid and obviates the need for additional iterations in the hydraulic head calculation while calculating each node in the SVF algorithm.

4.6.1. Depth at Toe

The procedures described herein implies the need for guidance for the depth at the toe of a prototype. Hansen and Roshanfekr (2012b) have presented the following equation in this regard:

$$h_{svft}\cos^2\theta = 2\left[h_{us} - C_{path} i_{DTW}\left(\frac{b_{rep}}{\cos\Gamma}\right)\right] - y_{exit} \qquad [4.19]$$

where:

h_{svft}= the depth at the termination of the SVF zone (end of the seepage-face),
i_{DTW}= hydraulic gradient suitable for finding default tailwater depth (dimensionless),
b_{rep} = straight-line path of flow line (L),
Γ = angle of the straight-line path of flow line,
C_{path}= correction factor, slightly larger than unity (*cf.* Hansen and Roshanfekr 2012b),

The above equation can be applied to prototype situations.

4.7. SUMMARY AND CONCLUSIONS

Flow within the seepage-face can be classified as a case of SVF with increasing discharge. In order to handle the interaction between the non-linear hydraulic head 'pore pressure' model and the SVF wsp algorithm, two numerical schemes were considered: one invoking flux nodes and one using ordinary head-based nodes. The former is slightly

more complex but both were found to be effective in modeling the entire system. It was found that discharge increased non-linearly within the seepage-face wedge but that Manning's n decreased exponentially, in the downstream (down-gradient) direction, over the toe of the embankment. The hydraulic resistance outcomes presented are used to provide guidance as to how to independently set up viable initial patterns of Manning's n values. A dual linear variation was found to adequately describe observed depth variations, with the most suitable break point being located at $12 \cdot \ell_c$ and $3 \cdot d_c$. Imposition of said dual linear variation dramatically decreases the number of iterations required to relax the NLHC finite-difference grid, and even single linear variations represent wsp's that are not far off the truth, for most of the down-gradient length of the seepage-face.

CHAPTER 5 SUMMARY AND CONCLUSIONS

5.1. SUMMARY

As stated earlier, flow-through rockfill structures are river engineering structures often used to attenuate and delay inflow hydrographs. It was also highlighted that in such structures, the most common form of failure is an unraveling failure.

Little attention has been given to the simplification of the design of the internal and downstream face hydraulics of these barrages. The main purpose of this research was therefore to study the hydraulics of flow-through rockfill embankments and provide additional guidance on the design and safety of these structures. In this regard, the non-linear nature of flow within these structures was studied using a *p*-LaPlacian-like partial differential equation. The factor of safety against the unraveling failure was presented for a range of downstream slopes, thus showing the unsafe combinations of slope and particle size. It was shown that the factor of safety tends to drop below unity under the seepage-face primarily because of the strength of the exit gradient near the toe of the structure, and secondarily because of the overflow velocity.

Also, in order to assess the potential of an unraveling failure in flow-through rockfill dams, three different aspects of the hydraulic design of such structures were systematically studied. The first concerned finding the gradient most useful in the independent computation of the height of the first flow emergence point. The second involved a method for independently computing variations in the hydraulic head within the y_{exit} vertical which allows the toe of the structure to be isolated for purposes of stability analysis. The third was the study of the gradient that will allow for the independent estimation of the default tailwater depth, the results of which were confirmed by experimental data. In order to provide better tools to assess the hydraulics associated with the zone of the downstream toe, laboratory and analytical studies were conducted. The depth variation of the seepage-face was computationally modeled, and two approaches for solving this spatially varied flow (SVF) problem were undertaken. The results showed that a dual linear variation in depth can be used to good accuracy and

without inducing any unrealistic exit gradients in the zone of primary concern with respect to unraveling.

It is hoped that the findings of this study will result in more scientifically based designs and therefore improved safety evaluations of such structures, whether new or existing.

5.2. CONCLUSIONS

The observations resulting from the modeling and experimental work presented herein is summarized as follows:

- The non-linear flow effect on the head was found to be small.
- The heads associated with fully-developed turbulent flows was found to be no more than about 10% larger than those associated with laminar flows, and that this difference is much less than 10% over most of the 2-D modeling space(s) / region(s) of interest.
- The physical modeling of flow-through rockfill dams with regards to studies on the magnitude of the head itself was found to be difficult, if not pointless, unless the physical model is large.
- Quintupling grid density was found to have little effect on the visual smoothness in exit-flowline patterns, as compared to grids of the toe having an exit height represented by only 18 nodes.
- The effects on the exit flow-lines were found to be minor when specialty nodes at regular intervals in FD molecules were used.
- The particle-based FS was found to decrease dramatically as the distance to the toe decreased (as ℓ becomes equal to ℓ_{SF} in Figure 2.1).
- The FS dropped dramatically and approached unity as the velocity of the overflow approached relatively high value of 3 m/s.

- The severity of this overflow effect was found to be greater for smaller slopes, which is perhaps non-intuitive. The reason, however, that the drop in FS with increasing overflow U is greater for smaller slopes is that smaller slopes have inherently smaller exit gradients, tipping the effect of the denominator within the FS expression towards the effect of U and away from i_{exit}. Furthermore, the dams with particle diameters larger than 0.3 m and flat downstream faces (flatter than 1V:2H) all had worse-case FS values of greater than 2.
- The strength of the surficial exit gradient, under the seepage-face, was found to act as a destabilizing force for particles residing on this surface. This gradient was not found to exceed about 0.75, in any of the cases considered. This however is enough to destabilize particles smaller than about 0.3 m in diameter, especially as the toe slope approaches 1V:1H and the overflow velocity approaches 3 m/s.
- The need for further and more detailed studies in cases where the FS for IoM is less than two were identified, given the fact that certain approximations (such as the value of C_D) was used for FS estimation.
- The independent computation of the height of the point of first emergence (y_{exit}) relative to the foundation was done using a new method. The method is based on the angle of the emergent flow field at and within the toe of the structure. It is also the first step toward the hydraulic isolation of the toe for this class of porous hydraulic structure. It should be noted here that although the Stephenson (1979) equations have been used for this key computation, any non-Darcy flow equation may also be utilized for the same purpose.
- The independent computation of the variation in the hydraulic head within the vertical that has, as its upper terminus, the point of first flow emergence using a new general method has been presented and verified. This makes the hydraulic isolation of that part of the toe of the structure, which is downstream of the said y_{exit} vertical, possible.
- The independent computation of the default tailwater depth using a new general method has also been presented and verified. Knowledge of this depth is valuable to

the designer because if the default or representative depth of the receiving watercourse (just beyond the toe of the structure), such as its normal depth, is numerically less than this default tailwater condition (h_{TW}), then the h_{TW} value will govern and dictate the nature of the downstream condition, without which more thorough seepage modeling and other hydraulic modeling cannot proceed. It has been shown that the hydraulic gradient needed for this computation is related to the previously established concept of the effective hydraulic gradient (Hansen *et al.* 1995), once again of the structure as a whole.

- The classification of the flow within the seepage-face as a case of SVF with increasing discharge was demonstrated. In order to handle the interaction between the non-linear hydraulic head 'pore pressure' model and the SVF wsp algorithm, two numerical schemes were considered: one invoking flux nodes and one using ordinary head-based nodes. The former is slightly more complex but both were found to be effective in modeling the entire system.
- The discharge within the seepage-face was found to increase non-linearly even though Manning's n decreased exponentially, in the downstream (down-gradient) direction, over the toe of the embankment. The hydraulic resistance outcomes presented are used to provide guidance as to how to independently set up viable initial patterns of Manning's n values.
- The observed depth variations within the seepage-face were found to be adequately described using a dual linear variation with the most suitable break point being located at $12 \cdot \ell_c$ and $3 \cdot d_c$. The imposition of the said dual linear variation dramatically decreases the number of iterations required to relax the NLHC finite-difference grid. Even single linear variations represent wsp's that are not far off the reality, for most of the down-gradient length of the seepage-face.

5.3. FUTURE WORK

Based on a comprehensive review of the pertinent literature and the results of the studies conducted for this thesis, the following work is currently being undertaken:

- Studies of the linear growth of mine-waste dumps, specifically: **(i)** the quantification of the discharge and the height of the point of first-emergence; especially the applicability of the flow-field angle and the effective hydraulic gradient theories; **(ii)** the exploration of the effects of the linear growth in crest length on the upstream water level and the downstream point of first-emergence of the flow.

  Existing theories and equations for exit height estimation (such as Schaffernak 1917, Casagrande 1932 and flow-field angle theory) for mine-waste dumps are to be modified and compared with experimental data. Also it was surmised that the height of this point of first-emergence would not increase indefinitely for a given non-overtopping upstream water level, but that it would asymptotically reach some limiting length.

- The internal and downstream face of the hydraulics of flow-through rockfill spurs as a function of the upstream water level; specifically: **(i)** the quantity of flow moving through the spur, **(ii)** the nature of the three-dimensional phreatic surface within the structure, **(iii)** the pattern of the seepage-face on the downstream side of the structure, **(iv)** the nature of the three-dimensional seepage pattern inside the structure, and **(v)** the theoretical stability of particles residing under the seepage-face.

  In this regard 36 rockfill spurs have been built in the hydraulics laboratory of Dalhousie University and a *p*-Boussinesq-like equation is used for phreatic surface modeling within the rockfill spurs. Also a partially-linked numerical model has been developed. The model developed to address the above objectives consists of a 2-D and a 3-D component. Each will run individually but will be linked externally. The 2-D component of the model will be used to provide key boundary conditions for the 3-D component. The output results of the 3-D model will then used for FS estimation for those particles on the downstream toe of the rockfill spurs.

REFERENCES

Bari R., and Hansen D. 2002. Application of gradually-varied flow profiles to simulate buried streams. IAHR Journal of Hydraulic Research, 40(5):674-683.

Basak P. 1977. Non-Darcy flow and its implications to seepage problems. ASCE Journal of the Irrigation and Drainage Division,103(IR4):459-473.

Budd C.J., and Collins G.J. 1998. An invariant moving mesh scheme for the non-linear diffusion equation. Applied Numerical Mathematics, 26:23-39.

Campbell D.B. 1989. Some observations relative to the performance of flow-through rock drains. 13th Annual B.C. Mine Reclamation Symposium, 7-9 June, BiTech, Vancouver, pp. 119-128.

Casagrande L. 1932. Naeherungsmethoden zur bestimmung von art und menge der sickerung durch geschuettete daemme. thesis, Technische Hochschule, Vienna. Translated by U.S. Corps of Engineers, Waterways Exp. Sta., Vicksburg, Miss.

CDA (Canadian Dam Association). 2007. Technical Bulletin on Dam Safety. Geotechnical Considerations, sub-section 8.5 "Flow-through Rockfill Dams". Coordinator for Geotechnical Considerations: B. Touileb, Hydro Quebec.

Cedergren H.R. 1989. Seepage, Drainage, and Flow Nets. Wiley & Sons, NY, 3rd ed., 465 pp. (1st ed. 1967, 2nd ed. 1977)

Chow V.T. 1959. Open-Channel Hydraulics. McGraw-Hill Inc., Kogakusha, 680 pp.

Curtis R.P., and Lawson J.D. 1967. Flow over and through rockfill banks. Journal of the Hydraulic Division, 93(HY5):1-21.

Dake J.M.K. 1972. Essentials of Engineering Hydraulics. Macmillan Publishers Limited, 392 pp.

de Prony R .1804. Recherches Physico-Mathématiques sur la Théorie des Eaux Courantes. Imperial Press, Paris, 130 pp. (see Rouse and Ince, 1957).

DeLillo S., Lupo G., and Sanchini G. 2006. A Cauchy problem in non-linear heat conduction. J. of Physics A: Mathematics Gen., 39:7299-7303.

Desai C.S., and Sherman W.C. 1971. Unconfined transient seepage in sloping banks. ASCE Journal of Soil Mechanics and Foundation Division, 97(SM2):357-373.

Desai C.S. 1972. Seepage analysis of earth banks under drawdown. ASCE Journal of Soil Mechanics and Foundation Division, 98(SM11):1143-1162.

Desai C.S. 1973. An approximate solution for unconfined seepage. ASCE Journal of Irrigation and Drainage Division, 99(IR1):71-87.

Dudgeon C.R., 1966. Wall effects in permeameters. ASCE Journal of the Hydraulics Division, 93(HY5):137-148.

Ergun S. 1952. Fluid through packed columns. Chemical Eng. Progress, 48(2):89-94.

Esteban J.R., Rodriguez A., and Vazquez J.L. 1988. A non-linear heat equation with singular diffusivity. Communications in Partial Differential Equations, 13(8):985-1039.

Fand R. M., and Thinakaran R. 1990. The influence of the wall on flow through pipes packed with spheres. ASME Journal of Fluid Engineering, 112:84-88.

Forchheimer P. 1901. Wasserbewegung durch Boden, Zeits. V. deutsch. Ing., 45: 1782-1788.

Freeze R.A., and Cherry J.A. 1979. Groundwater. Prentice-Hall, Englewood Cliffs, NJ, 604 pp.

Gao L., and Li Z. 1996. Non-linear thermal conductivity of granular composite medium. Solid State Communications, 100(1):53-56.

Garga V.K., Hansen D., and Townsend R.D. 1995. Mechanisms of massive failure for flowthrough rockfill embankments. Canadian Geotechnical Journal, 32(6):927-938.

Garga V.K., Townsend D.R., and Hansen D. 1991. A method for determining the surface area of quarried rocks. ASTM Geotechnical Testing Journal, 14(1):35-45.

George G., and Hansen D. 1992. Conversion between quadratic and power law for non-Darcy flow. ASCE Journal of Hydraulic Engineering 118(5):792-797.

Gerodetti M. 1981. Model studies of an overtopped rockfill dam. Water Power and Dam Construction, Sept., p. 25-31.

Hansen D. 2004. Discussion of: On the use of the Kozeny-Carman equation to predict the hydraulic conductivity of soils. Canadian Geotechnical Journal, 41: 990–993.

Hansen D. 2003. A review of terminology pertaining to Darcy's Law and flow through porous media. Journal of Porous Media, 6(2):83-97.

Hansen D. 1992. The Behavior of Flowthrough Rockfill Dams. PhD thesis, University of Ottawa, Department of Civil Engineering, 355 pp.

Hansen D., and Bari R. 2002. Uncertainty in the water surface profile of a buried stream flowing under coarse material. ASCE Journal of Hydraulic Engineering, 128(8):761-773.

Hansen D., and Roshanfekr A. 2012a. Assessment of potential for seepage-induced unraveling failure of flow-through rockfill dams. ASCE International Journal of Geomechanics, 12(5):560-573.

Hansen D., and Roshanfekr A. 2012b. Use of index gradients and default tailwater depth as aids to hydraulic modeling of flow-through rockfill dam. ASCE Journal of Hydraulic Engineering, 138(8):726-735.

Hansen D., Garga V.K., and Townsend D.R. 1995. Selection and application of one-dimensional non-Darcy flow equation for two-dimensional flow through rockfill embankments. Canadian Geotechnical Journal, 32(2):223-232.

Hansen D., Zhao W.Z., and Han S.Y. 2005. Hydraulic performance and stability of coarse rockfill deposits. Institution of Civil Engineers (UK): Water Manag't, 158(4):163-175.

Harr M.E. 1962. Groundwater and seepage. McGraw-Hill, NY, 315 pp.

Hydro-Electric Commission, Tasmania, 1969. Failure of Cethana Dam, flood breach of a partly completed rockfill dam. Australian National Committee of the International Commission on Large Dams Bulletin, no.28, Hobart Tasmania, p.23-36.

Henderson F.M. 1966. Open Channel Flow. Macmillan Publishing Co., New York, 522 pp.

Jardin S.C., Bateman G., Hammett G.W., and Ku L.P. 2008. On 1-D diffusion problems with a gradient-dependent diffusion coefficient. J. of Computational Physics 227:8769-8775.

Kells J.A. 1993. Spatially varied flow over rockfill embankment. Canadian Journal of Civil Engineering, 20, 820-827.

Kells J.A. 1994. Reply: Spatially varied flow over rockfill embankments. Canadian Journal of Civil Engineering, 21(1):163-166.

Kells J.A. 1995. The Analysis of Flow Through and Over a Gabion Dam. PhD thesis, Dept. of Civil Engineering, University of Saskatchewan, 360 p.

Keulegan G.H. 1952. Determination of critical depth in spatially variable flow. Proceedings of 2nd Midwestern Conference on Fluid Mechanics, Bulletin 149, Ohio State University, Engineering Experiment Station, Columbus, Ohio, 67-80.

Kleiner D.E. 1985. Engineering with spreadsheets. ASCE Civil Engineering Magazine, October, p. 55-57.

Lane D., Berdusco R., and Jones R. 1986. Five years experience with the Swift Creek rock drain at Fording Coal Limited. Proceedings of the International Symposium

on Flowthrough Rock Drains, Cranbrook, British Columbia, 8-11 September, p. 7-11.

Leps T.M. 1973. Flow through Rockfill, in "Embankment-Dam Engineering", R.C. Hirschfeld Ed., John Wiley and Sons, pp. 87-107.

Martins R. 1991. "Principles of Rockfill Hydraulics". Chapter 17 in: Advances in Rockfill Structures, Kluwer Pub., pp. 523-570.

McCorquodale J.A., Hannoura A.A., and Nasser M.S. 1978. Hydraulic conductivity of rockfill. IAHR Journal of Hydraulic Research, 16(2):123-137.

Munier A., Burgan J.R., Gutierrez J., Fijalknow E. and Feix M.R. 1981. Group transformations and the non-linear heat diffusion equation. Society for Industrial and Applied Mathematics, 40(2):191-207.

Olsthoorn T.N. 1985. Modelling without special programs. Groundwater, May-June, p. 381-390.

Özisik M.N. 1993. Heat Conduction. 2nd ed., John Wiley & Sons Inc., New York, 692 pp.

Pagliara S., Das R., and Carnacina I. 2008. Flow resistance in large-scale roughness condition. Canadian Journal of Civil Engineering, 35:1285-1293.

Parkin A.K. 1991. "Rockfill Modelling". Chapter 3 in: Advances in Rockfill Structures, Kluwer Pub., pp. 35-51.

Parkin A.K. 1971. Field solutions for turbulent seepage flow. ASCE Journal of the Soil Mechanics and Foundations Division 97(SM1):209-218.

Parkin A.K. 1963. Rockfill dams with inbuilt spillways I-hydraulic characteristics. Bulletin 6, University of Melbourne and Water Research Foundation of Australia, Melbourne.

Parkin A.K., Trollope D.H., and Lawson J.D. 1966. Rockfill structures subject to water flow. ASCE Journal of the Soil Mechanics and Foundations Division 92(SM6):135-151.

Polyanin A.D., and Zaitsev V.F. 2004. Handbook of Non-linear Partial Differential Equations. Chapman & Hall/CRC Press, Boca Raton, 848 pp.

Roshanfekr A., and Hansen D. 2011. Procedures for assessing flow capacity and seepage-face patterns of linear deposits of mine waste. CIM Mines without Borders Conference, Montréal, Canada (22-25 May 2011).

Sabin G.C.W., and Hansen D. 1994. The effects of particle shape and surface roughness on the hydraulic mean radius of a porous medium consisting of quarried rock. ASTM Geotechnical Testing Journal, 17(1):43-49, March.

Schaffernak F. 1917. Uber die standsicherheit durchlaessiger geschuettetter damme. ZAMM, vol. 11.

Sharp B.B., and James J.P. 1963. Spatially varied flow at the toe of a rock-fill slope. Proceedings of 1st Australasian Conference on Hydraulics and Fluid Mechanics, Perth, Australia.

Sissom L.E., and Pitts D.R. 1972. Elements of Transport Phenomenon. McGraw-Hill, New York.

Smith G.D. 1978. Numerical Solution of Partial Differential Equations: Finite Difference Methods. 2nd ed., Clarendon Press, Oxford, UK, 304 pp.

Souplet P., and Weissler F.B. 2003. Regular self-similar solutions of the non-linear heat equations with internal data above the singular steady state. Ann. I. H. Poincare, 20(2):213-235.

Southwell R.V. 1946. Relaxation Methods in Theoretical Physics. Oxford University Press, England, 240 pp.

Stephenson D. 1979. Rockfill in Hydraulic Engineering. Elsevier Scientific, Amsterdam, Netherlands, 215 pp.

Stevens M.A., and Simons D.B. 1971. "Stability analysis for coarse granular material on slopes", Chapter 17 in River Mechanics, publ. by H.W. Shen, ed., Fort Collins, Colorado.

Strickler A. 1923. Beiträge zur Frage der Geschwindigkeitsformel und der Rauhigkeitszahlen für Ströme, Kanäle und geschlossene Leitungen. Mitteilungen des Amtes für Wasserwirtschaft, Eidgenössisches Departement des Innern, Bern, Switzerland, n. 16 (in German).

Sturm T.W. 2001. Open Channel Hydraulics. McGraw-Hill Higher Education Pub., 512 pp.

Tanigawa Y., Akai T., Kawamura R. and Oka N. 1996. Transient heat conduction and thermal stress problems of a nonhomogeneous plate with temperature-dependent material properties. Journal of Thermal Stresses, 19(1):77-102.

Taylor D.M. 1948. Fundamentals of Soil Mechanics. John Wiley & Sons Inc., New York.

Townsend R.D., Garga V.K., and Hansen D. 1991. Finite difference modelling of the variation in piezometric head within a rockfill embankment. Canadian Journal of Civil Engineering, 18(2):254-263.

Vazquez J.L. 2007. The Porous Medium Equation: Mathematical Theory. Oxford University Press, New York, 624 pp.

Volker R.E. 1969. Non-linear flow in porous media by finite elements. ASCE J. of the Hydraulics Division, 95(HY6):2093-2114.

Wang H.F., and Anderson W.P. 1982. Introduction to Groundwater Modeling - Finite Difference and Finite Element Methods. Freeman and Co., USA, 237pp.

Wilkins J.K. 1963. The stability of overtopped rockfill dams. Proc. of 4nd Australia-New Zealand Conference on Soil Mechanics and Foundation Engineering, Aug. 19-23, p.1-7.

Wilkins J.K. 1956. The flow of water through rockfill and its application to the design of dams. Proc. 2nd Australia-New Zealand Conference on Soil Mechanics and Foundation Engineering.

Wright D.E. 1968. Nonlinear flow through granular media. ASCE Journal of the Hydraulics Division, 94(4):851-872.

Zingg T. 1935. Beitrag zur Schotteranalyse. Schweizerische Mineralogische und Petrographische Mitteilungen, vol.15, p.39-140.

APPENDIX A - DERIVATION OF THE NON-LINEAR HYDRAULIC CONDUCTIVITY EQUATION

A.1. THE RELATIONSHIP BETWEEN EMPIRICAL QUANTITIES: NON-LINEAR HYDRAULIC CONDUCTIVITY APPROACH

Darcy's Law is stated as:

$$V = K\,i \qquad [A.1]$$

A gradient-dependent non-linear hydraulic conductivity relation may be stated as:

$$K = \omega\, i^{\psi} \qquad [A.2]$$

where:

ω= coefficient,

ψ= exponent having a value between 0 (laminar flow) and -0.5 (fully turbulent flow).

then:

$$V = \omega\, i^{(\psi+1)} \qquad [A.3]$$

A common power-function form of non-Darcy flow equation is:

$$i = \alpha V^{N} \qquad [A.4]$$

or:

$$V = \left(\frac{1}{\alpha}\right)^{\frac{1}{N}} i^{\frac{1}{N}} \qquad [A.5]$$

Equating [A.3] and [A.5]:

$$\omega i^{(\psi+1)} = \left(\frac{1}{\alpha}\right)^{\frac{1}{N}} i^{\frac{1}{N}} \qquad [A.6]$$

therefore:

$$\omega = \left(\frac{1}{\alpha}\right)^{\frac{1}{N}} \qquad [A.7]$$

and:

$$\psi = \frac{1}{N} - 1 \qquad [A.8]$$

A.2. Derivation of the Non-Linear Hydraulic Conductivity Partial Differential Equation

This section describes the derivation of the Non-Linear Hydraulic Conductivity PDE using the equivalent value of the hydraulic conductivity (non-linear hydraulic conductivity).

It is known *a priori* that the general direction of flow for the configuration shown in Figure 1.1 is from left-to-right, and with a downward component. Also, the hydraulic conductivity (K) is greater than zero. Different researchers have used the magnitude of the hydraulic gradient (i) for gradient dependent hydraulic conductivity calculations (*e.g.* Curtis and Lawson 1967, Kells 1994), and therefore it may reasonably be assumed that the gradient dependency of the hydraulic conductivity in the x and y-direction is related to the x and y-direction gradient at a given point. The value of K in the x and y-directions can be expressed as:

$$K_x = \omega i_x^{\psi} = \omega \left|\frac{\partial h}{\partial x}\right|^{\psi} = \omega \left[\left(\frac{\partial h}{\partial x}\right)^2\right]^{\frac{\psi}{2}} \qquad [A.9]$$

and:

$$K_y = \omega i_y^{\psi} = \omega \left|\frac{\partial h}{\partial y}\right|^{\psi} = \omega \left[\left(\frac{\partial h}{\partial y}\right)^2\right]^{\frac{\psi}{2}} \qquad [A.10]$$

which the hydraulic head is given by:

$$h = \frac{p}{\gamma_w} + z \qquad [A.11]$$

where:

h= hydraulic head,

$\partial h / \partial x$ and $\partial h / \partial y$ = gradient components in the x and y directions, respectively,

p/γ_w = pressure head,

z= elevation head,

p =pressure,

γ_w = unit weight of water.

Equations [A.9] and [A.10] show that for a Darcian flow, for which $\psi = 0$ and therefore N = 1, the values of K_x and K_y, are equal to ω. For turbulent flows however, N>1 and therefore $\psi < 0$ and K_x and K_y are a function of the flow gradient. Applying Darcy's law the velocity components in the x- and y-direction can be expressed as:

$$V_x = K_x \frac{\partial h}{\partial x} \qquad [A.12]$$

and:

$$V_y = K_y \frac{\partial h}{\partial y} \qquad [A.13]$$

Substituting the velocity components into the steady-state, two-dimensional continuity equation expressed as:

$$\frac{\partial V_x}{\partial x} + \frac{\partial V_y}{\partial y} = 0 \qquad [A.14]$$

one obtains a partial differential equation for steady, two-dimensional, non-Darcy flow, viz.

$$\frac{\partial}{\partial x}\left(K_x \frac{\partial h}{\partial x}\right) + \frac{\partial}{\partial y}\left(K_y \frac{\partial h}{\partial y}\right) = 0 \qquad [A.15]$$

Equation [A.15] is the governing equation for steady-state flow through porous media, and it can be applied to both Darcian and non-Darcian flow regimes alike provided that the K_x and K_y, term are properly described. Substituting equations [A.9] and [A.10] into equation [A.15] gives:

$$\frac{\partial}{\partial x}\left\{\omega\left[\left(\frac{\partial h}{\partial x}\right)^2\right]^{\frac{\psi}{2}}\frac{\partial h}{\partial x}\right\}+\frac{\partial}{\partial y}\left\{\omega\left[\left(\frac{\partial h}{\partial y}\right)^2\right]^{\frac{\psi}{2}}\frac{\partial h}{\partial y}\right\}=0 \qquad [A.16]$$

Assuming the coefficient ω to be constant and applying the chain rule for differentiation to equation [A.16] results in:

$$\left[\frac{\psi}{2}\left[\left(\frac{\partial h}{\partial x}\right)^2\right]^{\frac{\psi}{2}-1}2\frac{\partial h}{\partial x}\frac{\partial^2 h}{\partial x^2}\frac{\partial h}{\partial x}+\left[\left(\frac{\partial h}{\partial x}\right)^2\right]^{\frac{\psi}{2}}\frac{\partial^2 h}{\partial x^2}\right]+$$
$$\left[\frac{\psi}{2}\left[\left(\frac{\partial h}{\partial y}\right)^2\right]^{\frac{\psi}{2}-1}2\frac{\partial h}{\partial x}\frac{\partial^2 h}{\partial x^2}\frac{\partial h}{\partial x}+\left[\left(\frac{\partial h}{\partial y}\right)^2\right]^{\frac{\psi}{2}}\frac{\partial^2 h}{\partial y^2}\right]=0 \qquad [A.17]$$

Also by rearranging and dividing equation [A.17] by the term (ψ+1), the simplification of the above expression yields the following equation:

$$\left|\frac{\partial h}{\partial x}\right|^{\psi}\frac{\partial^2 h}{\partial x^2}+\left|\frac{\partial h}{\partial y}\right|^{\psi}\frac{\partial^2 h}{\partial y^2}=0 \qquad [A.18]$$

It is emphasized that for turbulent flows ψ<0, and therefore equation [A.18] is used in its entirety in deriving a solution to a given problem. For Darcian flows, ψ=0 and equation [A.18] is reduced to the familiar LaPlace equation which is applicable to seepage analysis in homogeneous, isotropic soils.

APPENDIX B - OBSERVED DATA

B.1. OVERVIEW

In keeping with the main objectives of the thesis, various experiments were conducted:

A. Characteristics tests (*i.e.* size, shape, distributions and porosity) on selected porous media.

B. Column tests on the porous media, carefully-characterized in Item A, in order to permit a limited investigation of the relationship between hydraulically-determined 1-D non-Darcy flow parameters and parameters not determined hydraulically (such as porosity).

C. A series of tests in the glass flume of the hydraulics lab of Dalhousie University. These provided data on 2-D flow-through rockfill structures which were then used to compare various computational techniques.

Because water sediment effects on rockfill were not part of the anticipated scope of this thesis research, clear water was used for the experiments. Hence all the supply tanks in the hydraulic laboratory were cleaned and re-filled with clear water.

After cleaning the tanks and refilling them with clear water, the rock materials were selected. The next step of the test was to select and sieve the rock material in order to remove fines and dirt and to achieve the desired size fraction. In this regard ½ m^3 of ¾" crushed limestone called 'clear blue' (similar to that used in previous research including Parkin *et al.* 1966, Wilkins 1963, Hansen 1992) was selected for this research. A sample of the materials used in this study is shown in Figure B.1. The same materials used here were also used for the column test and the model rockfill embankments.

Figure B.1. Sample of rockfill materials used in this study.

B.2. CHARACTERISTICS OF THE POROUS MEDIA

As sample or a control volume of rockfill (as a porous media) can be defined if the following is known:

i. gradation (typical via sieve analysis), particle type(s) (see Zingg diagram), an particle rugosity.

ii. porosity and hydraulic mean radius (Taylor 1948).

iii. specific gravity (which is governed by lithology).

As stated earlier, in this study ¾" (nominal) crushed limestone was used. The first step was to conduct different experiments on the characteristics of the porous media. The observations and the experiments conducted on the porous media material were as follow:

B.2.1. Porosity of the Model Embankments

The porosity is an important parameter that characterizes rockfill deposits. It depends on the shape of the rockfill particles, the gradation, and the degree of compaction. From a rockfill hydraulics perspective, porosity does not vary greatly and is rather high (Martins 1991). In this research, porosity was measured for the model embankments and for the column test, both before and after each experiment. The results are shown in Tables B.1 and B.5.

Table B.1. Porosity estimates for model embankments (C=cube, T=triangle).

Wire Mesh Module	Mesh Weight	Total Weight	Total Weight	Porosity (n)	Porosity (n)
		Before Experiments	***After*** Experiments	***Before*** Experiments	***After*** Experiments
#	(kg)	(kg)	(kg)	(dimensionless)	(dimensionless)
C1	0.17	10.30	11.04	0.49	0.45
C2	0.17	10.86	11.49	0.46	0.42
C3	0.17	10.54	11.26	0.47	0.44
C4	0.17	12.59	13.44	0.41	0.37
C5	0.17	10.46	11.15	0.48	0.44
C6	0.17	10.35	11.06	0.48	0.45
C7	0.17	10.76	11.41	0.46	0.43
C8	0.17	11.46	12.21	0.46	0.43
C9	0.17	11.45	12.07	0.46	0.43
C10	0.17	10.64	11.40	0.47	0.43
C11	0.17	11.19	11.97	0.44	0.40
C12	0.17	10.94	11.64	0.45	0.42
C13	0.17	12.11	12.86	0.43	0.40
C14	0.17	11.12	11.97	0.44	0.40
C15	0.17	11.70	12.53	0.45	0.41
C16	0.17	11.85	12.78	0.44	0.40
C17	0.17	10.95	11.66	0.45	0.42
C18	0.17	11.68	12.33	0.45	0.42
C19	0.17	10.93	11.62	0.45	0.42
C20	0.17	12.45	13.02	0.42	0.39
C21	0.17	10.12	10.99	0.49	0.45
C22	0.17	10.45	11.13	0.48	0.44
C23	0.17	10.60	11.30	0.47	0.43
C24	0.17	10.35	11.10	0.48	0.44
C25	0.17	11.66	12.27	0.45	0.42
C26	0.17	10.60	11.30	0.47	0.43
C27	0.17	11.98	12.82	0.44	0.40
C28	0.17	10.42	11.12	0.48	0.44
C29	0.17	10.85	11.44	0.46	0.43
C30	0.17	10.99	11.94	0.45	0.40

Table B.1 (Cont). Porosity estimates for model embankments (C=cube, T=triangle).

Wire Mesh Module	Mesh Weight	Total Weight Before Experiments	Total Weight After Experiments	Porosity (n) Before Experiments	Porosity (n) After Experiments
#	(kg)	(kg)	(kg)	(dimensionless)	(dimensionless)
C31	0.17	10.80	11.43	0.46	0.43
C32	0.17	11.83	12.78	0.44	0.40
C33	0.17	11.81	12.62	0.45	0.41
C34	0.17	11.44	11.98	0.46	0.44
C35	0.17	10.95	11.85	0.45	0.41
C36	0.17	11.67	12.29	0.45	0.42
T1	0.21	11.12	11.93	0.43	0.39
T2	0.21	10.96	11.80	0.44	0.39
T3	0.21	12.45	13.47	0.40	0.35
T4	0.21	11.79	13.35	0.39	0.31
T5	0.21	11.83	13.42	0.39	0.31
T6	0.21	11.71	13.33	0.40	0.31
T7	0.21	10.52	11.73	0.46	0.40
T8	0.21	11.17	12.04	0.43	0.38
T9	0.21	10.31	11.51	0.47	0.41
T10	0.21	11.55	13.09	0.41	0.32
T11	0.21	11.21	12.07	0.42	0.38
T12	0.21	11.09	11.92	0.43	0.39
T13	0.21	12.29	13.43	0.41	0.35
T14	0.21	12.55	13.65	0.39	0.34
T15	0.21	11.31	12.09	0.42	0.38
T16	0.21	11.36	12.98	0.42	0.33
			Average Porosity:	**0.44**	**0.40**

B.2.2. Rock Particles: Dimensions and Shape

Zingg (1935) presented the four possible gross shapes that a single particle may have; spheroid, disk, rod, blade. His perspective was geological, so artificial particles with reentrant surfaces (such as raschig rings) was not in view. Figures B.2 and B.3 shows how the three relevant orthogonal particle axes are defined and used. The mean value ‘b’ is a good measure of the particle ‘size’ (see Table B.2).

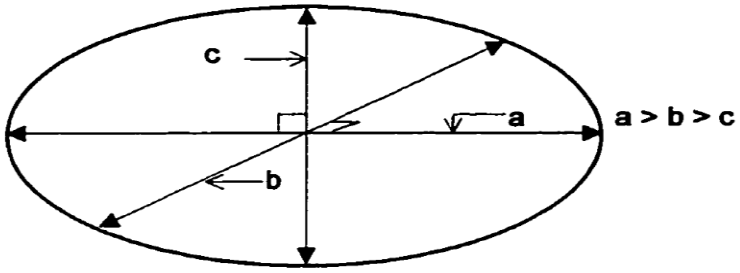

Figure B.2. Definition of "a", "b" and "c" for the Zingg diagram (Hansen 1992).

Table B.2. Zingg diagram observations.

Number	a (long axis)	b (intermediate axis)	c (short axis)	Zingg Shape
#	(mm)	(mm)	(mm)	
1	22.5	12.8	10.2	Rod
2	22.1	12.9	12.9	Rod
3	19.9	12.9	11.6	Rod
4	28.6	13	12.1	Rod
5	26.3	13	12.8	Rod
6	13.7	13	9	Spheroid
7	24.2	13.1	12.2	Rod
8	23.2	13.3	12.9	Rod
9	19.8	13.5	10	Spheroid
10	17.7	13.8	10.6	Spheroid
11	24.4	13.9	14.5	Rod
12	19.7	13.9	13.1	Spheroid
13	14.5	13.9	12.3	Spheroid
14	15.6	14.1	8.2	Disk
15	28.4	14.5	8.6	Blade
16	23.3	14.5	8.7	Blade
17	16.9	14.5	8.8	Disk
18	31.6	14.7	13.6	Rod
19	21.8	14.8	10.5	Spheroid
20	19.7	14.9	12.5	Spheroid
21	21.9	15	8.9	Disk
22	23.2	15.2	8.1	Blade

Table B.2 (Cont). Zingg diagram observations.

Number	a (long axis)	b (intermediate axis)	c (short axis)	Zingg Shape
#	(mm)	(mm)	(mm)	
23	22.7	15.3	12.2	Spheroid
24	26.3	15.7	8.1	Blade
25	34.9	15.7	15.3	Rod
26	21.8	15.9	11.1	Spheroid
27	23.8	15.9	8.7	Disk
28	19.9	15.9	9.4	Disk
29	16.8	15.9	7.9	Disk
30	22.1	16	15.2	Spheroid
31	25.1	16.3	14.1	Rod
32	20.3	16.3	13.1	Spheroid
33	21.5	16.3	11.4	Spheroid
34	20.6	16.4	11.2	Spheroid
35	23.7	16.4	8.9	Disk
36	31.1	16.4	11.4	Rod
37	25.8	16.4	16	Rod
38	22.2	16.5	8.8	Disk
39	25.1	16.6	9.7	Blade
40	22.5	16.6	11.3	Spheroid
41	23.9	16.7	9.2	Disk
42	22.5	16.8	16	Spheroid
43	36.3	16.9	17.4	Rod
44	18	17	13.1	Spheroid
45	23.8	17	15.8	Spheroid
46	23.7	17.1	10	Disk
47	21.3	17.1	10.8	Disk
48	23.3	17.1	11.7	Spheroid
49	19.9	17.3	9.9	Disk
50	24.2	17.5	11.1	Disk
51	19.9	17.8	13.5	Spheroid
52	29.1	17.8	15.2	Rod
53	34.6	17.9	12.7	Rod
54	21.6	17.9	13.8	Spheroid
55	18.8	17.9	12.6	Spheroid
56	23.4	18	11.1	Disk

Table B.2 (Cont). Zingg diagram observations.

Number	a (long axis)	B (intermediate axis)	c (short axis)	Zingg Shape
#	(mm)	(mm)	(mm)	
57	30.1	18	14.2	Rod
58	35.3	18.2	11.9	Blade
59	25.3	18.4	15.1	Spheroid
60	26.2	18.4	12.2	Disk
61	22.1	18.4	10.9	Disk
62	22.5	18.4	13.8	Spheroid
63	28.7	18.6	11.9	Blade
64	34.6	18.6	16.1	Rod
65	18.9	18.6	14.1	Spheroid
66	32.9	18.7	11.9	Blade
67	19.8	18.7	14.4	Spheroid
68	21.5	18.8	8.9	Disk
69	23.6	18.8	15.2	Spheroid
70	24.8	18.9	14.9	Spheroid
71	19.9	18.9	13.5	Spheroid
72	39.7	18.9	15.6	Rod
73	24.9	18.9	16.6	Spheroid
74	24.1	19	10.9	Disk
75	26.3	19.2	18	Spheroid
76	24.5	19.5	17.4	Spheroid
77	26.4	19.5	8.9	Disk
78	21.2	19.6	13.9	Spheroid
79	24.1	19.7	10.9	Disk
80	22.4	19.8	18.6	Spheroid
81	20.1	19.8	14	Spheroid
82	26.3	20	10.7	Disk
83	24.2	20	11.9	Disk
84	21.7	20	12.1	Disk
85	37.3	20.1	16.2	Rod
86	28.7	20.1	11.5	Disk
87	44.2	20.7	14.4	Rod
88	34.6	20.9	16.7	Rod
89	28	20.9	19.9	Spheroid
90	25.7	20.9	20.2	Spheroid

Table B.2 (Cont). Zingg diagram observations.

Number	a (long axis)	B (intermediate axis)	c (short axis)	Zingg Shape
#	(mm)	(mm)	(mm)	
91	25.4	21	11.6	Disk
92	43.7	21.1	16.4	Rod
93	22.3	21.4	13.1	Disk
94	27.3	21.7	11.9	Disk
95	34.6	21.7	14.6	Rod
96	34.9	21.8	19.7	Rod
97	24.9	21.8	19.9	Spheroid
98	28.8	22.1	13.2	Disk
99	24.3	22.2	15.1	Spheroid
100	41.6	22.3	16.1	Rod
101	32.2	22.3	11.4	Disk
102	25.9	22.4	11.6	Disk
103	34.1	23.1	14.5	Disk
104	29.9	23.1	12.2	Disk
105	27.3	23.2	12.4	Disk
106	27.5	23.4	13.2	Disk
107	28.4	23.5	13.4	Disk
108	29.9	24.5	18.5	Spheroid
109	29.8	24.6	11.3	Disk
110	28.4	26.5	12.3	Disk

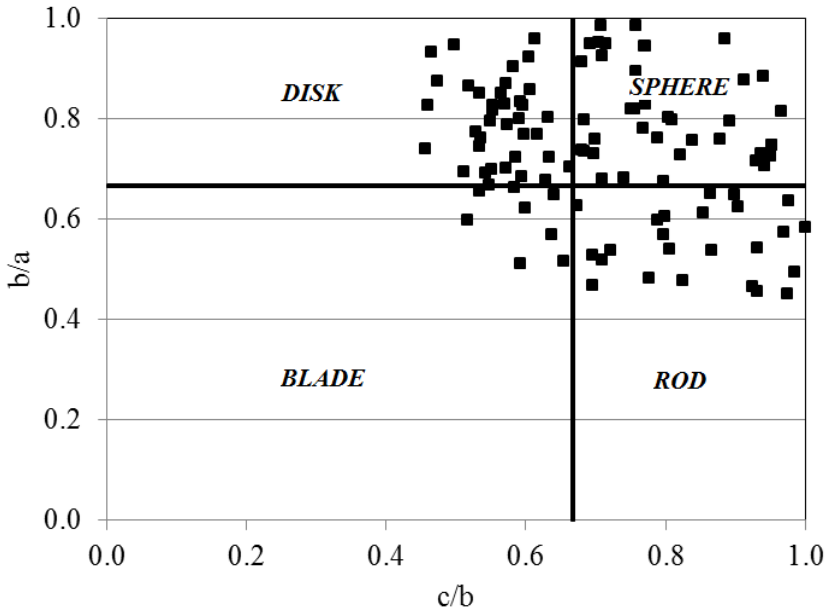

Figure B.3. Zingg diagram for the rocks studied in this research.

B.2.3. Grain Size Analysis

A common way of characterizing a sample (large number) of particles is classical sieve analysis. In this regard a sieve analysis was carried out on a selected sample of the rockfill material. In this study sieves with openings 25.4 mm (1”), 19.0 mm (¾”), 15.9 mm (0.625”) and 12.7 mm (½”) were selected. After sieving, the rock particles were washed and particles larger than 1” and smaller than ½” were removed, yielding a fairly uniform material for use in the model embankments. Figure B.4 shows the equipment used. Table B.3 and Figure B.5 show the results of the sieving work.

Figure B.4. Sieve analysis experimental setup.

Table B.3. Observation for the particle size distribution.

a) Sieve analysis

Particle Size (mm)	Particle Size (inch)	Weight Lower (kg)	% Weight Lower
25.4	1	9.962	100.00
19.0	0.75	7.181	72.08
15.9	0.625	3.359	33.72
12.7	0.5	0.000	0.00

b) D_{60}, D_{50} and D_{10} of the rock particles used.

D_{60}:	0.71	Inch	18.05	Mm
D_{50}:	0.68	Inch	17.22	Mm
D_{10}:	0.54	Inch	13.64	Mm

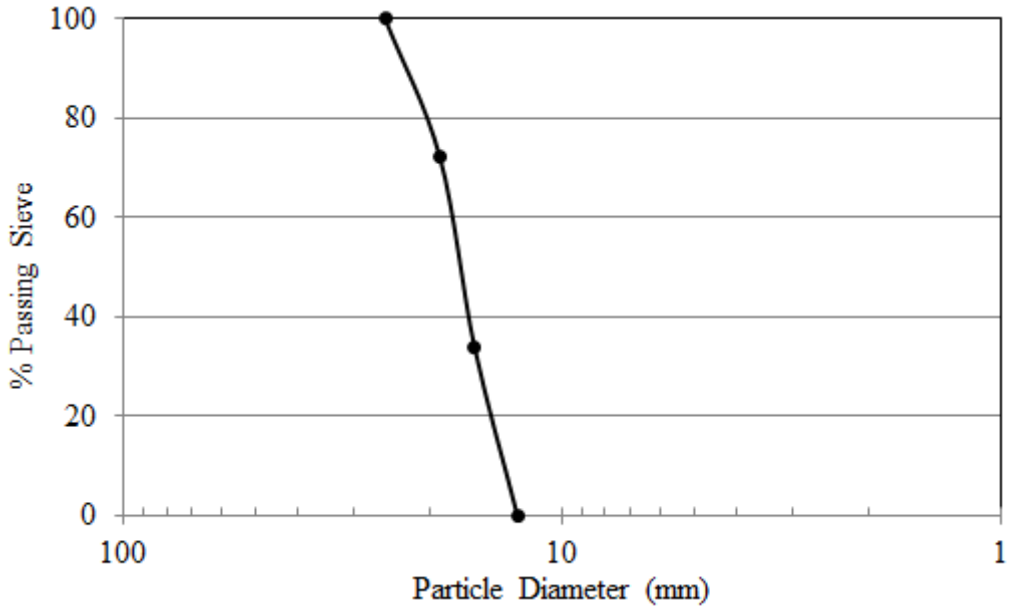

Figure B.5. Particle size distribution.

B.2.4. Hydraulic Mean Radius

The quantity is a measure of pore size (Taylor 1948) and was used by Wilkins (1956) and others to characterize the 'permeability' of rockfill. For a porous medium consisting entirely of spheres od diameter 'd' it may be shown that (Sissom and Pitts 1972, Hansen 2004):

$$m = \frac{ed}{6} \qquad [B.1]$$

For control volume filled with non-spherical particles this has been modified to:

$$m = \frac{ed}{6r_e} \qquad [B.2]$$

where:

e= void ration (dimensionless),
r_e= surface area efficiency (Garga *et al.* 1991, Sabin and Hansen 1994) (dimensionless),
d= representative particle diameter (L).

In this study d was taken to be D_{50}. In this study, crushed limestone was used, as was used by Garga *et al.* (1991) and Sabin and Hansen (1994). This lithology, together with comparisons of Zingg diagrams (similar) and photographs of particles in the source literature (Hansen 1992) led to an estimate of r_e of 1.84.

B.2.5. Specific Gravity

This was found by:

i. weighting particles (submerged and unsubmerged) repeated four times,

ii. weighting a control volume of porous medium (submerged and unsubmerged) repeated twice,

and according to ASTM procedures D127 and D6743. The average value was found to be 2.65 (for both methods).

B.3. PACKED-COLUMN TESTS

The following summary describes the details of the data collection for packed-column tests which allowed for the calculation of the non-Darcy parameters of the rockfill used in this study. The column used is shown in Figure B.6.

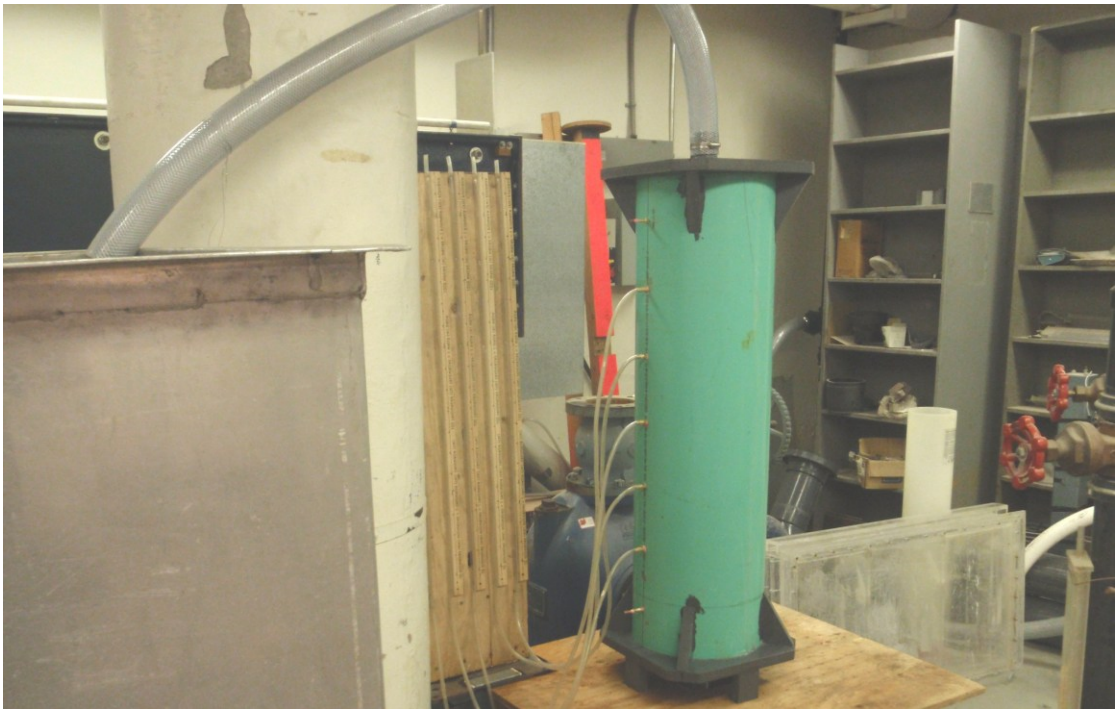

Figure B.6. Packed-column test setup (length: 1100 mm, inside diameter: 297 mm, volume: 76.9 L).

Flow occurred upwards through the rock matrix in the column and passed unrestricted into a weighing tank. Flow was controlled by a valve in the base of the column. The hydraulic head was measured at equally-spaced locations 150 mm apart. In order to avoid the influence of the kinetic head and to facilitate determining the exact location of each tap, the tips of the piezometers were pointed directly upwards (they extended in the centre axis of the column). Table B.4 gives the results from column test.

Table B.4. Packed-column test results.

Run	Head at Tapping Point					Elapsed Time	$\forall_{water}$	Q
	1	2	3	4	5			
#	(cm)	(cm)	(cm)	(cm)	(cm)	(s)	(cm^3)	(cm^3/s)
1	150	150	150	150	150	0	0.0	0.0
2	199.2	199	198.9	198.7	198.6	478	211493	442.5
3	205.2	204.6	204.4	204.2	204	714	507583	710.9
4	178.8	177.8	176.7	176	175	456	613330	1345.0
5	204.3	202	199.5	198.5	196	293	549882	1876.7
6	228.2	225	221.8	218.8	215.6	268	634479	2367.5
7	285.2	280	274.8	270	265.2	205	634479	3095.0
8	274	268.2	263.1	258.3	254	219	697927	3186.9
9	293.9	287.1	281.6	276.3	270.2	170	571031	3359.0
10	294.7	282.9	278.6	272.3	265.2	164	634479	3868.8
11	302.8	292.3	282.8	276.1	266.3	173	761375	4401.0
12	316.2	304.7	292.5	278.2	264.1	149	782524	5251.8

Figure B.7 shows that the best fit line to the data using $i=\alpha V^N$ fromation, as follows:

$$\alpha = 0.0213 \text{ (V in cm/s)}$$

$$N = 1.85$$

$$r^2 = 0.99$$

The porosity of the packed-column was also determined. Table B.5 shows the observations for the porosity measurements in the packed-column.

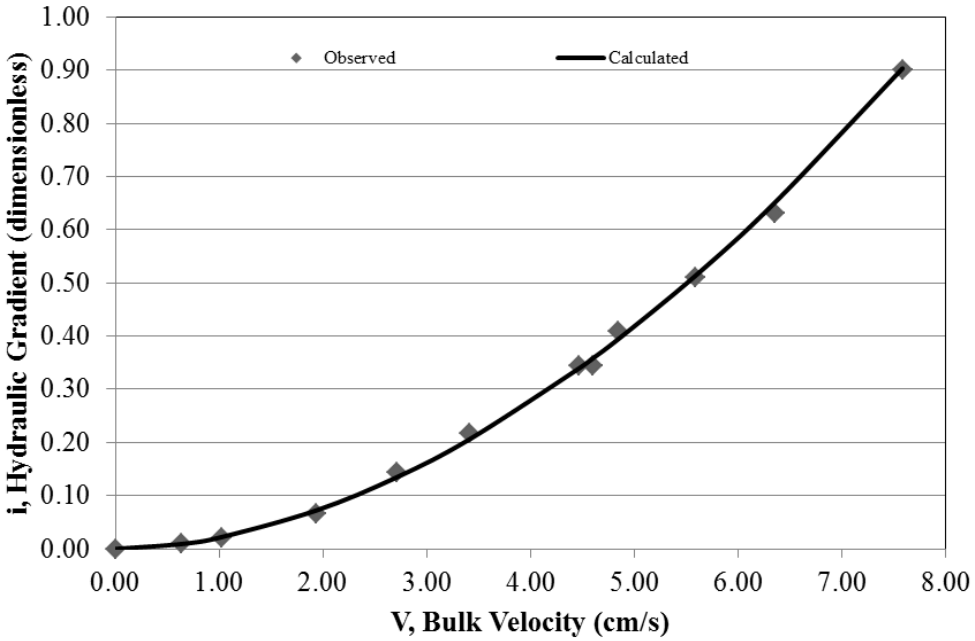

Figure B.7. Packed-Column test results.

Table B.5. Observations for the porosity measurements in the packed-column.

	Rock	Column	Total
Weight	118 (kg)	26.67 (kg)	144.67 (kg)
Volume	44.6 (L)	76.9 (L)	
Porosity	**0.42**		

Fortunately the same porosity was achieved for the model embankments.

B.4. Studies in the Dalhousie University Hydraulics Laboratory Glass-Walled Flume

Figure 4.2 shows the glass-walled flume of the hydraulics laboratory at the Department of Civil and Resource Engineering, Dalhousie University. Placing a clean-grid scale on the glass permitted the position of the phreatic surface, the location of the point of first emergence, and the seepage-face to be recorded. In addition, individual photographs were taken for each experiment to better record and observe the data. Also due to the turbulent nature of the flow through the rockfill, all data were measured three times and an average value was recorded in all cases.

Furthermore, photos from different sides of each model embankment were taken in order to enable a more accurate study of the head and the flow through the model rockfill embankments (see Figure B.9).

The total discharge was measured with an electromagnetic field distortion meter and was checked with a 90^{o} V-notch weir located at the collection tank downstream of the glass-walled flume. Upstream and downstream water levels were measured with a point gauge or a measuring tape on the glass. The 'bed' (surface of the downstream toe) was delineated using a permanent marker, such that it passed through the mean position of the bed, roughly through the mid-point of the particles under the seepage-face. The thickness of the seepage-face wedge was measured using a 1 cm by 1 cm grid that fixed of the glass, followed by the application of a ruler having 1 mm divisions. The tailwater depth downstream was set as the default tailwater depth and no special adjustments were made. The glass-walled flume was leveled using a laser leveler.

Also in-order to prevent the washout of the rockfill material, a modular model setup was used (see Figure B.8). In this regard different wire mesh boxes with ½" openings (13 mm by 13 mm) were built to allow for simple movement and fast installation. The boxes were filled with the same materials used in the column test. The rectangular wire mesh box sizes were approximately 150L×150W×300H and the triangular wire mesh boxes were 300L×150W×300H (see Figure B.8).

Each box was restrained with wire to prevent bulging. Wire and wire tie-wraps were used to tightly hold the modules together, such that no gaps were present and the particles in neighbouring modules were touching (through 13 mm square mesh holes). The porosity at these interfaces might have been slightly higher but this was not quantified because the phreatic surface exhibited no discontinuities. The very low position of the mesh relative to the bulk of the flow (wherein the higher velocities of the wedge were present), the small diameter of the wires relative to their spacing, and the very rough nature of the surface relative to the diameter of the mesh wires all heuristically indicated that the mesh probably played a minor role in the seepage face hydraulics. The 'points' of many of the crushed limestone particles under the seepage-face protruded or nearly protruded out of the 13 mm by 13 mm holes in the mesh. The

diameter of the mesh wire itself was about 1 mm. Since the experiments simply could not be conducted without some sort of restraints on the particles making up the surface of the downstream toe, the work had to be done under conditions which did have a slight degree of 'interference' in the downgradient direction, as has also been present in previous studies of this kind (*e.g.* Kells 1995, Gerodetti 1981).

In order to calculate the porosity of the each box, the boxes were numbered and the weight and volume of each box was recorded before and after the experiments were completed. It should be noted that at the end of each experiment, the boxes were emptied and spread out to air dry for a few days before being weighed. The porosity for each box was calculated individually and in the end, the average porosity was calculated for all of the boxes (see Section B.2.1 on porosity, for the observed data).

Figure B.9 are simplified renditions of photos of the linear growth of model embankment, showing how water levels varied for a fixed rate of inflow.

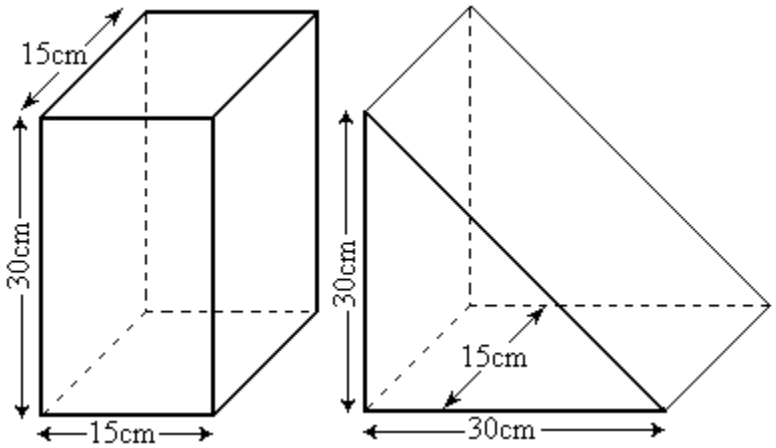

Figure B.8. Modular orientation of the wire mesh boxes for the mode embankments.

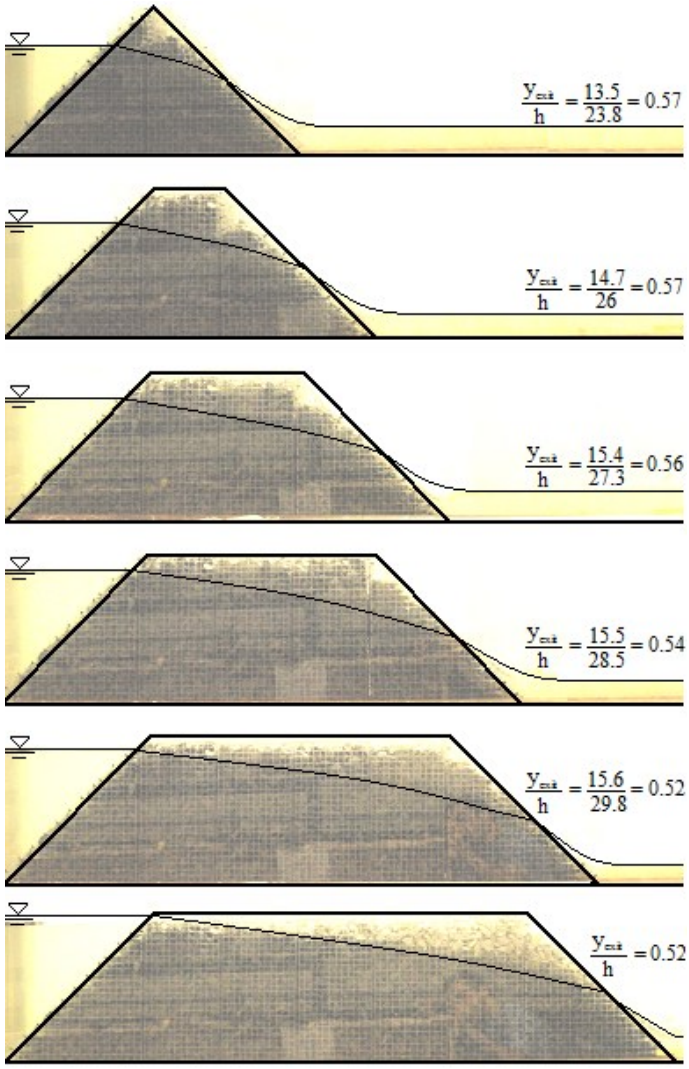

a) Laboratory experiments conducted at the hydraulics laboratory of Dalhousie University for linear growth of model embankment. All slopes 1V:1H. Q=3.82 L/s (adapted from 2011 photographs), H= 30 cm.

Figure B.9. Observations and simplified renditions of photos of the linear growth of model embankment.

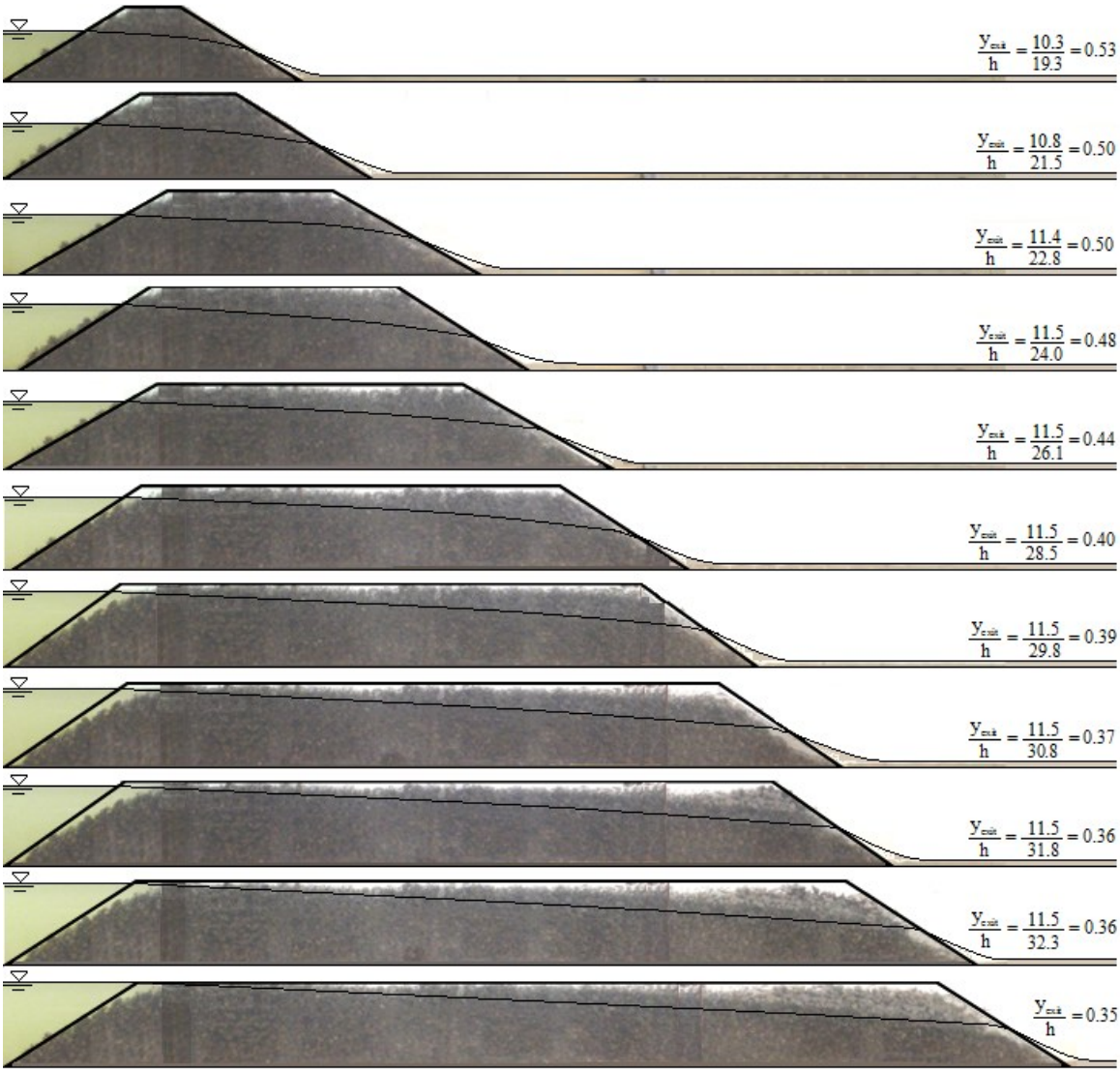

b) Laboratory experiments conducted at the hydraulics laboratory of Dalhousie University for linear growth of model embankment. All slopes 1V:1H. Q=2.50 L/s (adapted from 2012 photographs), H= 32.5 cm.

Figure B.9 (Cont). Observations and simplified renditions of photos of the linear growth of model embankment.

For these experiments the rockfill material was added to the downstream face without turning off the flow.

APPENDIX C - COPYRIGHT PERMISSION LETTERS

Title: Assessment of Potential for Seepage-Induced Unraveling Failure of Flow-Through Rockfill Dams

Author: Hansen, D. and Roshanfekr, A.

Publication: International Journal of Geomechanics

Publisher: American Society of Civil Engineers

Date: 10/01/2012

Permissions Request

As an ASCE author, you are permitted to reuse you own content for another ASCE or non-ASCE publication.

Please add the full credit line "With permission from ASCE" to your source citation.

Please print this page for your records.

Type of use: Dissertation/Thesis

Portion: full article

Format: print and electronic

Use of this content will make up more than 25% of the new work: no

Author of this ASCE work or ASCE will publish the new work: yes